

Anna-Kristin Trummer, BSc

Metabolite dynamics following the switch from aerobic to anaerobic fermentation of xylose by natural and recombinant yeasts

MASTER'S THESIS

to achieve the university degree of

Diplom-Ingenieurin

Master's degree programme: Biotechnology

submitted to

Graz University of Technology

Supervisor

Dipl.-Ing. Dr.nat.techn. Univ.-Doz Mario Klimacek

Institute of Biotechnology and Biochemical Engineering

AFFIDAVIT

I declare that I have authored this thesis independently, that I have not used other than the declared sources/resources, and that I have explicitly indicated all material which has been quoted either literally or by content from the sources used. The text document uploaded to TUGRAZonline is identical to the present master's thesis dissertation.

Date

Signature

Acknowledgement

First of all I want to thank my advisor Dipl.-Ing. Dr.nat.techn. Univ.-Doz. Mario Klimacek for providing this topic, supporting and revision. In addition, I would like to thank Univ.-Prof. Dipl.-Ing. Dr.techn. Bernd Nidetzky for enabling this work at the Institute of Biotechnology and Biochemical Engineering at Graz University of Technology.

Special thanks goes also to Mag. Dr. Christoph Magnes and Dipl.-Ing. Gert Trausinger, Bakk.techn. for metabolite analysis at the HEALTH department of JOANNEUM RESEARCH Forschungsgesellschaft mbH.

Furthermore I would like to thank all members of the institute for the great working atmosphere and their support, but especially Karin Longus, Ing. Margaretha Schiller and Natascha Loppitsch for their helpful laboratory assistance.

Last but not least, I would like to express my eternal gratitude to my parents Eva-Maria and Wolfgang and to Jürgen Kollegger, who supported me throughout my whole university education.

Content

1	Summary.....	1
1.1	Background.....	1
1.2	Results.....	1
1.3	Conclusion.....	2
2	Zusammenfassung.....	3
2.1	Hintergrund.....	3
2.2	Ergebnisse.....	3
2.3	Schlussfolgerung.....	4
3	Introduction.....	5
3.1	Xylose fermentation.....	5
3.1.1	Composition of lignocellulose.....	5
3.1.2	Potential products from xylose.....	5
3.1.3	<i>Saccharomyces cerevisiae</i> as organism of choice for xylose fermentation.....	6
3.2	Xylose assimilation pathways.....	7
3.2.1	Oxido-reductive pathway.....	7
3.2.2	Isomerization pathway.....	7
3.2.3	Oxidative pathway.....	7
3.2.4	Comparison of the oxido-reductive pathway with the isomerization pathway.....	8
3.3	History of the recombinant <i>S. cerevisiae</i> strain IBB10B05.....	8
3.4	Native xylose-utilizing yeasts.....	9
3.4.1	<i>Scheffersomyces stipitis</i> and <i>Candida tenuis</i>	9
3.5	Metabolite Profiling.....	11
3.5.1	Sample-workup.....	11
3.5.2	LC-MS analysis.....	12
3.6	Yeast strains investigated in this work.....	13
4	Aim of work.....	15
5	Materials.....	16
5.1	Chemicals.....	16
5.2	Instruments.....	19
5.3	Yeast strains.....	21
5.4	Media.....	21
5.4.1	Yeast peptone dextrose medium.....	21
5.4.2	Mineral medium.....	22
6	Methods.....	23
6.1	Fermentation.....	23

6.1.1	Preculture	23
6.1.2	Mainculture in shake flasks	24
6.1.3	Mainculture in bioreactor	24
6.1.4	Sampling	25
6.2	Analytics	25
6.2.1	Determination of cell density (OD ₆₀₀)	25
6.2.2	BM determination	25
6.2.3	HPLC-RI	26
6.2.4	Metabolite profiling	27
6.3	Data Analysis	31
6.3.1	HPLC-RI	31
6.3.2	Determination of physiological parameters (μ , Y , q)	31
6.3.3	LC-MS	36
7	Results	38
7.1	Physiological characterization of <i>C. tenuis</i> , IBB10B05 and <i>S. stipitis</i>	38
7.1.1	BM determination	38
7.1.2	Growth behaviour	39
7.1.3	Substrate consumption and product formation	39
7.2	Analysis of intracellular metabolites.....	45
7.2.1	Global analysis of LC-MS data.....	46
7.2.2	Comparison of intracellular metabolite time profiles of investigated yeasts.....	47
8	Discussion	71
8.1	Macroscopic analysis of investigated yeasts	71
8.1.1	Growth behaviour	71
8.1.2	Substrate consumption and product formation	72
8.2	Intracellular metabolite pattern of xylose metabolization	73
8.2.1	PPP	73
8.2.2	Glycolysis	74
8.2.3	TCA	74
8.2.4	Amino acids.....	75
8.2.5	Redox cofactors	75
8.2.6	Energy charges	76
8.2.7	Mevalonic acid	76
9	Abbreviations.....	78
10	References	81

1 SUMMARY

1.1 Background

Growing global concerns over climate change increase the demand for industrial biotechnology processes that use lignocellulosic raw materials as sustainable alternatives to petrochemical feedstocks. As xylose is the most abundant pentose sugar in most lignocellulosic feedstocks, its utilization is crucial for efficient conversion of lignocellulose to bioethanol and other value-added fermentation products. For this purpose, recently a *Saccharomyces cerevisiae* strain was developed that displays not only excellent xylose fermentation capabilities, but is, unlike native xylose-fermenting yeasts, also capable of anaerobic growth on xylose. However, it forms more by-products and thus less ethanol than its native counterparts, although expressing a similar xylose assimilation pathway. Reasons for these phenotype differentiations are still not fully understood and further investigation is needed. To this end, metabolite profiling is ideally suited, as it provides a clear description of the cellular phenotype with a high level of functional information. This potential was used to determine the dynamic response of intracellular metabolites on changing oxygen concentrations from oxic to anoxic conditions in native xylose-utilizing yeasts *Candida tenuis* and *Scheffersomyces stipitis* and in recombinant yeast *S. cerevisiae* IBB10B05 during batch fermentation of xylose.

1.2 Results

Using LC-MS the dynamics in the concentrations of 54 intracellular metabolites in central carbon, energy and redox metabolism as well as in amino acids were determined either qualitatively or quantitatively. The transition from aerobic to anaerobic conditions went along with an about three-fold increase of xylose uptake in *S. cerevisiae* IBB10B05 and a three-fold decrease of the same in native xylose-fermenting yeasts. This was also reflected on the metabolite level by a transient decline in adenylate and guanylate energy charges and decreased concentrations of most glycolysis-, PPP- as well as TCA-intermediates. In addition, several distinct responses to oxygen deprivation between investigated yeasts were observed: Accumulation of DHAP, FBP, Glyc3P and mevalonic acid in native xylose-utilizing yeasts and increased concentrations of pentose phosphates as well as aromatic amino acids in *S. cerevisiae* IBB10B05. Furthermore, permanent changes in redox cofactors were detected in native xylose-fermenting yeasts, while alterations thereof were only temporary in *S. cerevisiae* IBB10B05.

1.3 Conclusion

By applying a targeted metabolomics approach, fundamental differences in phenotypes of investigated yeasts could be identified. Further development of efficient xylose-utilizing yeast strains can certainly benefit from results presented in this work.

2 ZUSAMMENFASSUNG

2.1 Hintergrund

Wachsende weltweite Sorgen über den Klimawandel erhöhen die Nachfrage nach industriellen biotechnologischen Prozessen, die Lignocellulose als nachhaltige Alternative zu petrochemischen Rohstoffen verwenden. Da Xylose der häufigste Pentose-Zucker in den meisten lignocellulosehaltigen Rohmaterialien ist, ist dessen Nutzung entscheidend für die effiziente Umsetzung von Lignocellulose zu Bioethanol und anderen wertvollen Fermentationsprodukten. Zu diesem Zweck wurde kürzlich ein *Saccharomyces cerevisiae* Stamm entwickelt, der nicht nur exzellente Fermentationseigenschaften zeigt, sondern auch, im Gegensatz zu nativen Xylose-fermentierenden Hefen, fähig zum anaeroben Wachstum auf Xylose ist. Jedoch produziert dieser Stamm wesentlich mehr Nebenprodukte und daher weniger Ethanol als seine natürlichen Opponenten, obwohl er einen ähnlichen Xylose-Assimilierungsweg exprimiert. Die Gründe für diese phänotypischen Unterschiede sind noch immer nicht vollständig geklärt und benötigen weitere Untersuchungen. Metabolitenprofiling ist ideal dafür geeignet, da diese Methode eine klare Beschreibung des zellulären Phänotyps mit einem hohen Level an funktioneller Information liefert. Dieses Potential wurde verwendet, um die dynamische Antwort intrazellulärer Metabolite auf veränderte Sauerstoffkonzentrationen von aeroben zu anaeroben Bedingungen in natürlichen Xylose-verwertenden Hefen *Candida tenuis* und *Scheffersomyces stipitis* und der rekombinanten Hefe *S. cerevisiae* IBB10B05 während der Batch-Fermentation von Xylose zu bestimmen.

2.2 Ergebnisse

Mittels LC-MS konnten die Dynamiken in den Konzentrationen von 54 intrazellulären Metaboliten des zentralen Kohlenstoff-, Energie- und Redox-Metabolismus sowie von Aminosäuren entweder qualitativ oder quantitativ bestimmt werden. Der Übergang von aeroben zu anaeroben Bedingungen wurde von einem ungefähr dreifachen Anstieg in der Xylose-Aufnahmerate in *S. cerevisiae* IBB10B05 und einer dreifachen Abnahme derselben in natürlichen Xylose-fermentierenden Hefen begleitet. Dies spiegelte sich auch auf Metabolitebene durch eine vorübergehende Abnahme in der Adenylat- und Guanylat-Energieladung und sinkenden Konzentrationen der meisten Glykolyse-, PPP- und TCA-Intermediate wider. Zusätzlich konnten mehrere unterschiedliche Antworten auf Sauerstoffmangel zwischen den untersuchten Hefen beobachtet werden: Anhäufung von DHAP, FBP, Glyc3P und Mevalonsäure in natürlichen Xylose-fermentierenden Hefen sowie steigende Konzentrationen von Pentosephosphaten und aromatischen Aminosäuren in *S. cerevisiae* IBB10B05. Weiters wurden dauerhafte Veränderungen in Redox-Kofaktoren von

natürlichen Xylose-verwertenden Hefen festgestellt, wohingegen Veränderungen dieser in *S. cerevisiae* IBB10B05 nur temporär waren.

2.3 Schlussfolgerung

Mittels der Anwendung eines gezielten Metabolomics-Ansatzes, konnten fundamentale Unterschiede in den Phänotypen untersuchter Hefen identifiziert werden. Zukünftige Entwicklungen effizienter Xylose-verwertender Hefestämme können sicherlich von den in dieser Arbeit präsentierten Resultaten profitieren.

3 INTRODUCTION

3.1 Xylose fermentation

Growing global concerns over climate change caused by rising greenhouse gas emissions and depletion of oil reserves increase the demand for industrial biotechnology processes that use sustainable, cost-effective and environmentally favourable raw materials as alternatives to petrochemical feedstocks [1], [2], [3]. These sustainable resources have one thing in common: They are composed of a complex lignocellulosic matrix that consists of lignin (~25%), cellulose (~25-60%) and hemicellulose (~10-35%) [4].

3.1.1 Composition of lignocellulose

Lignin is a complex aromatic and hydrophobic polymer that is made up of phenylpropanoids [5], [6]. It is found in secondary cell walls of plants and some algae [6]. Cellulose is an unbranched homopolysaccharide consisting of several hundred to many thousands of $\beta(1\rightarrow4)$ linked D-glucose units [5], [6], [7]. It is the main component of the primary cell wall of plants and thus the most abundant organic polymer on earth [6]. In contrast to cellulose, hemicelluloses are branched heteropolysaccharides that vary widely within their structure and composition [4], [5]. Frequently occurring hemicelluloses are xylans, arabino-xylan, gluco-mannan and galacto-glucomannan [4]. These polysaccharides are composed of many different sugar monomers, such as D-xylose, L-arabinose, D-mannose, D-glucose, D-galactose and L-rhamnose [6]. Among these, D-xylose is usually the most abundant sugar in hemicelluloses, although in softwoods D-mannose accounts for the largest amount [6].

The overall monomeric sugar composition of lignocellulosic raw materials depends strongly on the biomass source [4]. Usually, the hexose fraction is made up primarily of glucose, while the pentose fraction is made up of 5-20% xylose and 1-5% arabinose [4]. Hence, xylose is the second most abundant monosaccharide after glucose in nature and the most abundant pentose sugar in hardwoods and crop residues [3]. Consequently, the utilization of both xylose and glucose is essential for efficient and thus profitable conversion of lignocellulosic materials to valueable fermentation products [8], [9].

3.1.2 Potential products from xylose

A variety of products like 2,3-butanediol, biohydrogen, butanol, chitosan, ferulic acid, furfural, isopropanol, lactic acid, vanillin, xylitol and xylo-oligosaccharides can be produced by fermentation using xylose as starting material [8], [10]. In the last years, research on the development of these products has increased substantially [8], [10]. However, still most research focused on the production of 2nd-generation bioethanol. In contrast to 1st-generation

bioethanol, which is produced almost exclusively from the starch and sucrose portions of a few edible crops, such as corn, grain, sugar beet and sugar cane, 2nd-generation bioethanol is produced from sustainable lignocellulosic feedstocks, such as bagasse, corn stover, non-recyclable paper, switchgrass or wheat straw [11]. The advantages of 2nd-generation bioethanol over 1st-generation bioethanol are numerous. It does for instance not compete with the food sector and generates also lower greenhouse gas emissions than 1st-generation bioethanol [1], [2], [12]. However, many technical problems need to be overcome for efficient and cost-effective conversion of lignocellulosic materials to biofuels [1], [2]. These are the reduction of process steps and the accordingly high energy demand as well as the reduction of the high costs arising from enzymes required for biomass hydrolysis [2]. But most importantly, robust microbial strains that are more tolerant to inhibitors and also ferment all sugars of the cellulose and hemicellulose portions at sufficiently high yields need to be developed [2], [13], [14].

3.1.3 *Saccharomyces cerevisiae* as organism of choice for xylose fermentation

The Crabtree-positive baker's yeast *Saccharomyces cerevisiae* is the preferred organism for industrial bioethanol production and other value-added chemicals [11], [15]. This is because of its enormous robustness regarding high ethanol concentrations and low pH as well as its great resistance to contaminations and inhibitors [13], [15], [16]. In addition, it displays excellent fermentation and growth properties under anoxic conditions [15], however, only in the presence of essential lipids [17]. This is because molecular oxygen is required for synthesis of membrane sterols [18]. *S. cerevisiae* owes its anaerobic growth ability to numerous factors, among which, many are still not fully understood [19]. One well-known factor is that *S. cerevisiae* possesses, in contrast to various other yeasts, a unique form of dihydroorotate dehydrogenase (EC 1.3.3.1, encoded by *ScURA1*) that catalyzes the conversion of dihydroorotate to orotate with fumarate as alternative terminal electron acceptor to oxygen [18], [20].

However, despite of all previously mentioned advantages, wildtype *S. cerevisiae* can not utilize the pentose D-xylose, although it can efficiently ferment hexose sugars, such as fructose, glucose, galactose and mannose [11]. This is a major drawback for the production of biofuels and other value-added fermentation products from lignocellulosic feedstocks and the reason why huge efforts have been made in the last 20 years to genetically engineer *S. cerevisiae* strains for efficient xylose fermentation [5], [11], [13], [16], [21]. These efforts involved the introduction of xylose assimilation pathways in *S. cerevisiae*.

3.2 Xylose assimilation pathways

Three xylose assimilation pathways exist in nature: the oxido-reductive pathway, the isomerization pathway and the recently discovered oxidative pathway [22], [23].

3.2.1 Oxido-reductive pathway

The oxido-reductive pathway originates from yeasts and fungi that have mainly been isolated from wood-related environments [11], [15]. It includes two steps: Reduction of xylose to xylitol by a NAD(P)H- dependent xylose reductase (XR) (EC 1.1.1.21) and oxidation of xylitol to xylulose by a strictly NAD⁺-dependent xylitol dehydrogenase (XDH) (EC 1.1.1.9) (see Figure 3-1) [15]. Some XR enzymes have a dual cofactor specificity, however, always with a preference for NADPH [15]. Several reviews ([5], [9], [16], [24], [25]) described that the different cofactor usage of XR and XDH enzymes creates a redox imbalance, since yeasts lack a transhydrogenase that can convert NADPH to NADH and vice versa [26]. This redox imbalance results in ethanol yields (Y_{ethanol}) far below the theoretical maximum of 0.51 g g⁻¹ and in high xylitol by-product formation [14], [27].

3.2.2 Isomerization pathway

The isomerization pathway originates from bacteria and consists only of a cofactor-independent xylose isomerase (XI) that converts xylose to xylulose (see Figure 3-1) [15]. Therefore, a redox imbalance does not exist in the isomerization pathway [15]. Nevertheless, identification of suitable XI genes and expression in *S. cerevisiae* proved difficult [14], [28], [29]. Only the XI genes isolated from the thermophilic bacterium *Thermus thermophilus* and from the anaerobic fungus *Piromyces sp.* could be expressed successfully in *S. cerevisiae* [27], [28], [30].

3.2.3 Oxidative pathway

Recently, a third pathway was found in the bacterium *Caulobacter crescentus* and in the halophilic archaeon *Haloferax volcanii* [23]. This pathway involves the oxidation of D-xylose to the citric acid cycle (TCA)-intermediate α -ketoglutarate with D-xylose dehydrogenase, xylonate dehydratase, 2-keto-3-deoxyxylonate dehydratase and α -ketoglutarate semialdehyde dehydrogenase [23].

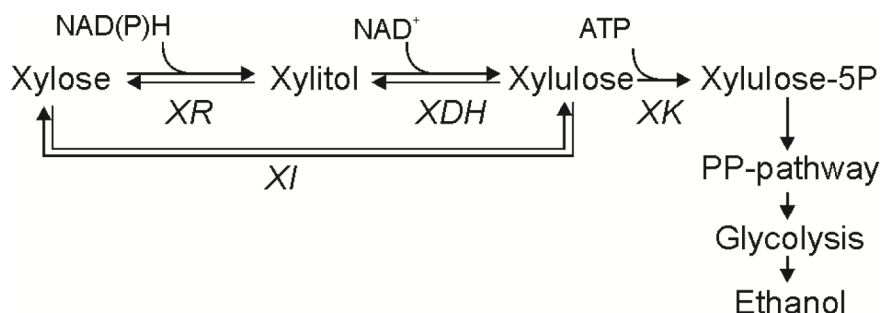


Figure 3-1: Xylose assimilation via the oxido-reductive or the isomerization pathway. The oxido-reductive pathway consists of a xylose reductase (XR) and a xylitol dehydrogenase (XDH), whereas the isomerization pathway consists only of a xylose isomerase (XI) [22]. Both pathways end up in the production of xylulose, which is further phosphorylated to xylulose 5-phosphate (X5P) by an ATP-dependent xylulose kinase (XK) and then channelled through the pentose phosphate pathway (PPP) and glycolysis for ethanol formation [22]. Figure obtained from *Trausinger* ([22]).

3.2.4 Comparison of the oxido-reductive pathway with the isomerization pathway

A comparison of recombinant *S. cerevisiae* strains carrying the *S. stipitis* XR-XDH pathway with those carrying the *Piromyces sp.* XI pathway from *Karhumaa et al.* ([31]) revealed that introduction of the XR-XDH pathway leads to a 2.6-fold faster ethanol formation rate (q_{ethanol}), though the Y_{ethanol} (0.33 g g^{-1}) was, due to the redox imbalance, lower than in the XI-strain (0.43 g g^{-1}) [14]. The key to xylose-utilizing strains that combine high yields and productivity was thus the development of a XR-XDH pathway with balanced coenzyme utilization [14].

3.3 History of the recombinant *S. cerevisiae* strain IBB10B05

The development of the recombinant yeast strain *S. cerevisiae* IBB10B05, involved two steps. In the first step, a xylose-fermenting *S. cerevisiae* strain was engineered for balanced coenzyme utilization by *Petschacher et al.* ([14], [32]) through structure-guided site-directed mutagenesis. To this end, coenzyme specificity of the *Candida tenuis* XR (CtXR) was altered around 170-fold from NADPH in the wild-type to NADH in a mutant that carried two substitutions at Lys274→Arg and Asn276→Asp (K274R-N276D) [14], [32]. Chromosomal integration of the XR double mutant K274R-N276D, XDH from *Galactocandida mastotermitis* and the endogenous XK in *S. cerevisiae* CEN.PK 113-5D resulted in a strain (BP10001) that produced 42% more ethanol ($Y_{\text{ethanol}} = 0.34 \text{ g g}^{-1}$) and less by-products than the wildtype (BP000) [14]. Nevertheless q_{ethanol} ($= 0.05 \text{ g g}_{\text{BM}}^{-1} \text{ h}^{-1}$) was too slow to render it competitive [13]. The slow q_{ethanol} , which fell far below the one of glucose cultivation ($\sim 1.2 \text{ g g}_{\text{BM}}^{-1} \text{ h}^{-1}$) [13], correlates with a low xylose conversion rate in BP10001 [33]. Low xylose conversion leads to limited supply of ATP, which results in growth inability [22], [33]. For recombinant *S. cerevisiae* strains a threshold value required for anaerobic growth on xylose of 1.8-2.0 $\text{mmol}_{\text{ATP}} \text{ g}_{\text{BM}}^{-1} \text{ h}^{-1}$ has been proposed by *Sonderegger et al.* ([34]) and by *Wahlbom* and

Hahn-Hägerdahl ([35]). However, growth is an essential characteristic, as it indicates cells stability and viability and leads to enhanced ethanol productivity [22], [33].

Hence, in the second step evolutionary engineering was applied by *Klimacek et al.* ([13]) to enable anaerobic growth of BP10001 on xylose. This was recently done by two-stage metabolic adaption of BP10001 to anaerobic conditions and resulted in a clon, which was termed *S. cerevisiae* IBB10B05 [13]. In just 61 generations, it displayed ~530% improved strain fitness in terms of anaerobic growth on xylose (specific growth rate (μ) = 0.056 ± 0.003 h⁻¹) and q_{ethanol} (= 0.28 ± 0.04 g g_{BM}⁻¹ h⁻¹) [13]. As a result of its fast q_{ethanol} that surpasses other engineered yeast strains by 3-fold or more, IBB10B05 can be considered as one of the best xylose-utilizing recombinant *S. cerevisiae* strains that carry the XR-XDH pathway [13], [36]. Its robustness under industrial conditions and its excellent xylose fermentation capabilities rendered it competitive [13], [36].

3.4 Native xylose-utilizing yeasts

Contrary to *S. cerevisiae* IBB10B05, all hitherto known natural xylose-utilizing yeast strains are not capable of anaerobic growth on xylose [18], [34]. This is because they rely on a respirofermentative metabolism, where molecular oxygen serves as terminal electron acceptor [18], [37]. Due to their dependance on oxygen and their additional sensitivity to high ethanol concentrations and inhibitors present in lignocellulose hydrolysates, naturally xylose-utilizing yeasts are not suitable for industrial bioethanol production [5], [38], [39], [40]. Nevertheless, the xylose pathways of some of these yeasts served as basis for the construction of numerous xylose-utilizing *S. cerevisiae* strains [14]. Among these, the xylose pathways of the Crabtree-negative yeasts *Scheffersomyces stipitis* and *Candida tenuis*, which belong like *S. cerevisiae* to the phylum of ascomycota [41], were used frequently as these strains show very high Y_{ethanol} accompanied by low by-product formation [22], [42], [43].

3.4.1 *Scheffersomyces stipitis* and *Candida tenuis*

S. stipitis is a homothallic yeast that occurs primarily in haploid form and has become well known for its capacity to rapidly ferment pentose sugars to ethanol [2], [43], [44]. With Y_{ethanol} between 0.35-0.44 g g⁻¹ ([45]) at low oxygen levels [11], it is one of the best xylose-fermenting organisms [44]. Furthermore, its XR enzyme displays a dual cofactor specificity, which provides advantages in terms of Y_{ethanol} and by-product formation compared to XR enzymes that utilize exclusively NADPH [27].

C. tenuis exists in either a yeast (unicellular) or pseudohyphae (multicellular) form [42], [46]. *C. tenuis* (CBS 4435) is also one of the better xylose-fermenting yeast strains and displays like *S. stipitis* a beneficial dual XR cofactor specificity, with an equal *in vivo* usage of NADH

and NADPH [32], [42], [47], [48]. As a result, its xylose assimilating genes have been used for construction of some recombinant *S. cerevisiae* strains, such as BP000, BP10001 [14].

Both *S. stipitis* and *C. tenuis* grow on xylose without production of ethanol under aerobic conditions, while they ferment glucose or xylose rapidly under oxygen-limited conditions [18], [24], [42]. Under fully anaerobic conditions, *S. stipitis* stops to grow within only one generation [18], [44] and *C. tenuis* stops to grow almost entirely [42]. Nevertheless both strains are, because of their dual cofactor specificity, still capable of relatively slow anaerobic xylose fermentation [18], [24], [42]. The inability to grow under anaerobic conditions indicates that the regulation of fermentation is oxygen-dependent [44]. This behavior is mainly different from *S. cerevisiae* that produces ethanol under glucose excess conditions (Crabtree effect), independent of the oxygen availability [44]. The dependence of *S. stipitis* and *C. tenuis* on oxygen for growth and the respiration of xylose under aerobic conditions are expected to decrease Y_{ethanol} [18], [42]. Furthermore, the requirement for controlled low-level aeration increases process costs [18], [42].

As a result, *Shi and Jeffries* ([18]) tried to eliminate the oxygen dependence of *S. stipitis* for growth through introduction of ScURA1. Although this enabled anaerobic growth on glucose (in the presence of essential lipids), anaerobic growth on xylose could not be achieved. As the sugar consumption rate is identical for both xylose [40] and glucose [49] ($0.1 \text{ g g}^{-1}_{\text{BM}} \text{ h}^{-1}$), other factors rather than the rate of ATP generation must inhibit anaerobic growth on xylose [5]. These factors are, however, not known yet [18], [50].

So native xylose-fermenting yeasts and recombinant *S. cerevisiae* strain IBB10B05 differ in their ability to grow anaerobically on xylose. However, that is not the only difference. Recombinant *S. cerevisiae* strains often also display much lower Y_{ethanol} and higher xylitol by-product formation than their native counterparts, although expressing a similar xylose assimilation pathway [22], [42], [43]. This indicates an efficient oxygen-independent ability of coenzyme regeneration in native xylose-fermenting yeasts [22], [42], [43]. Furthermore, recently ([51]) two new targets (phosphofructokinase (PFK) and glycerol 3-phosphatase (GPP)) were presented that play, aside from XR, also important roles in phenotype differentiation. Nevertheless, reasons for phenotypical differences between recombinant and native xylose-fermenting yeasts are still not completely understood and further investigation is required.

To analyze phenotype differentiations between recombinant and native xylose-fermenting yeast strains and to increase our understanding of the cellular processes that lead to a certain phenotype, so-called “omics” technologies are ideally suited [15]. The field of “omics” includes genomics, transcriptomics, proteomics and metabolomics [52]. Among which, metabolomics is the tool of choice for this purpose, as it provides, according to *Ramautar et*

al. ([53]), “a direct functional read-out of the physiological status of an organism”. In the following chapter metabolomics will be explained in more detail.

3.5 Metabolite Profiling

Metabolomics refers to the study of the complete set of metabolites within an organism, tissue or cell, the so-called “metabolome” [54], [55]. It is among genomics, transcriptomics and proteomics the latest of the “omics” technologies and has become increasingly important during the last decade [22], [52]. This is because metabolites, the small intermediates and products of metabolic reactions, directly affect enzyme activities by acting as substrates, products or allosteric effectors [15]. Furthermore they respond very rapidly to changing environmental conditions [22], [55]. Alterations in gene expression due to environmental changes are thus finally reflected in the metabolome [15]. Metabolite profiling provides therefore not only a clear description of the cellular phenotype, it gives also a higher level of functional information than snapshots of the transcriptome or proteome [15].

Metabolite profiling involves two major technical steps: Sample work-up and measurement of intracellular metabolites [22].

3.5.1 Sample-workup

The sample-workup, which includes sampling, quenching and extraction is crucial, since all this steps affect the quantification output significantly [22], [56]. The sample-workup described in the following paragraphs refers explicitly only to *S. cerevisiae* and closely related yeasts.

Quenching means stopping of all enzymatic cell activity by rapidly transferring a defined volume of cell suspension into a precooled quenching solution (QS) [22], [57]. In the past, many different quenching solvents, such as perchloric acid, glycerol saline and methanol were tested for their suitability [58], [59]. Over the last years, pure methanol has become widely accepted in the scientific community as QS for *S. cerevisiae* [22], [59]. An important criterion was that extracellular compounds are separable from the cells without losing any intracellular metabolites [57]. The ratio of sample volume (SV) to QS volume is also important as it strongly affects the quenching quality [57]. A ratio of at least 1 to 5 is recommended [59]. The steps of sampling and quenching should be carried out very rapidly to not alter the metabolomic state [57]. The reason for this is that some metabolites, in particular from catabolic reactions and reactions involved in energy metabolism, display very high turnover rates [57]. ATP and NADH, for instance, have turnover rates in the range of seconds [58]. Fast sampling is especially important under aerobic conditions, where an oxygen limitation would lead to changes in the cell metabolism [57]. In addition, avoidance of contaminations and exact pipetting of a defined volume is obligatory [22]. To obtain

reproducible results with regard to volume and sampling time, sampling devices have been developed in the last years [58]. However, most devices are not commercially available and as a result not accessible to the scientific community [57].

After separation of cells from the medium via centrifugation at sufficiently low temperatures to inhibit enzymatic activity, intracellular metabolites must be extracted from cells. This is typically done by applying a preheated extraction solution (ES) [22], [57]. Among the ES that achieved most acceptance within the yeast research community are boiling ethanol (BE) and chloroform-methanol [22], [57]. Extraction of intracellular metabolites without reactivating enzymatic activity and minimizing metabolite degradation is crucial [22], [57]. Enzymatic activity can be controlled by temperature, while metabolite degradation is strongly dependent on the metabolite species, the ES and the extraction parameters, such as temperature and pH applied [22], [57]. As metabolites are strongly heterogenous within their chemical and structural properties the ideal extraction method may not exist [22].

3.5.2 LC-MS analysis

About 600 metabolites are present in *S. cerevisiae* [57], [60]. Hence, several distinct methods are required to cover as many metabolites as possible [22]. These include enzyme assays, nuclear magnetic resonance (NMR) and mass spectrometry (MS) coupled to capillary electrophoresis (CE), gas chromatography (GC) or liquid chromatography (LC) [57]. Over the last years a clear trend towards MS-based systems became apparent [57]. Especially LC-MS is excellently suited, because of the broad metabolite coverage, high sensitivity and robustness of this method [57], [61]. Almost all metabolites from the central carbon metabolism including metabolites involved in glycolysis, pentose phosphate pathway (PPP) and TCA as well as amino acids (AA) can be addressed with LC-MS [57].

When talking about LC-MS analysis, it is essential to explain the so-called “matrix effects”. Matrix effects are caused by residual substrates, products and ionic compounds, such as phosphates and sulfates, and can significantly change the elution and ionization properties of components analyzed during LC-MS [57], [61], [62]. Moreover co-elution of matrix compounds together with the analyte of interest often causes ion suppression, which affects detection capability, precision and accuracy of results negatively [22], [63]. Matrix effects typically lead to base line signal increases, high signal-to-noise ratios and shifts in retention times [57]. Consequently, very time-consuming manual peak integration is necessary, which is, however, dependent on the operator and as a result not reproducible [22], [56]. To reduce matrix effects, concentrations of disturbing media compounds should be reduced to the lowest levels applicable for the cell system under investigation [57]. In addition, to compensate for metabolite degradation internal metabolite-specific standardization is strongly recommended [64], [65], [66], [67]. In this context, addition of defined amounts of

^{13}C -labeled compounds right before extraction is the preferred approach [57]. The availability of these stable isotope-labeled standards is, however, very limited and they are very expensive [68]. Alternatively, isotope-labeled metabolite extracts can be prepared from yeasts grown on $\text{U-}^{13}\text{C}$ -labeled substrate in standard mineral medium (MM) by applying appropriate quenching and extraction methods [57]. Harvesting of cells should thereby occur in the late exponential growth phase, because it was demonstrated lately that this improves the quality of the internal standard (ISTD) [22]. For the production of ^{13}C -labeled metabolite extracts, *S. stipitis* is ideally suited as it shows very high metabolite coverage and concentration [68].

Although matrix effects and also the sample-workup have a huge impact on the quantification output, the biggest impact arises from biological variabilities, such as differences in cell viabilities and physiological states [22], [56]. These exceed by far the variabilities introduced through modern MS analysis [22], [56].

The potential of metabolite profiling was used to analyze the dynamic response of 64 targeted metabolites on changing oxygen concentrations from fully aerobic to completely anaerobic conditions in recombinant and native xylose-utilizing yeast strains during batch fermentation of xylose. For sample-workup and intracellular metabolite analysis recently at the Institute of Biotechnology and Biochemical Engineering at Graz University of Technology (I.B.B.) established methods ([22]) were used.

3.6 Yeast strains investigated in this work

In this work the xylose-fermenting yeasts *S. cerevisiae* IBB10B05, *C. tenuis* CBS 4435 and *S. stipitis* CBS 6054 were investigated. These strains differ in their ability to grow anaerobically on xylose, though expressing a similar xylose assimilation pathway. Corresponding physiological parameters obtained from literature ([13], [43], [51], [69], [70]) are summarized in Table 3-1.

Table 3-1: Summarized physiological parameters of yeast strains investigated in this work during aerobic and anaerobic xylose fermentation in shake flasks.

Parameter	<i>C. tenuis</i> ^a	IBB10B05 ^b	<i>S. stipitis</i> ^c	<i>C. tenuis</i> ^d	IBB10B05 ^b		<i>S. stipitis</i> ^e
	<i>aerobic</i>			<i>anaerobic</i>			
				Phase I		Phase II	
μ [h ⁻¹]	0.28	0.16 ^h	0.44 ^g	n.a. ^f	0.056 ^g		0.012 ^h
q_{xylose} [g g ⁻¹ _{BM} h ⁻¹]	0.38	n.a. ^f	0.78 ^h	0.10 ^h	0.80 ^g		0.27 ⁱ
Y_{XS} [g g ⁻¹]	0.72	n.a. ^f	0.57 ^g	n.a. ^f	0.07 ^j		n.a. ^f
$Y_{ethanol}$ [g g ⁻¹]	n.a. ^f	n.a. ^f	0	0.44 ^g	0.35 ^g		0.42 ^g
$Y_{xylitol}$ [g g ⁻¹]	n.a. ^f	n.a. ^f	0	0.09 ⁱ	0.03 ^k	0.20 ^g	0.078 ^g
$Y_{glycerol}$ [g g ⁻¹]	n.a. ^f	n.a. ^f	n.a. ^f	0.04 ^l	0.11 ⁱ	0.018 ^g	0.006 ⁱ
$Y_{acetate}$ [g g ⁻¹]	n.a. ^f	n.a. ^f	n.a. ^f	n.d. ^f	0.04 ^j	0.03 ^k	0.020 ^g
Y_{CO_2} [g g ⁻¹]	n.a. ^f	n.a. ^f	n.a. ^f	0.42 ^h	0.37	0.36	n.a. ^f

^a Aerobic data for *C. tenuis* (CBS 4435) was obtained from Kern *et al.* ([69]), growth on complex medium containing 20 g L⁻¹ xylose, no rel. standard deviation (S.D.) available.

^b Data for IBB10B05 was obtained from Klimacek *et al.* ([13]), growth on 50 g L⁻¹ xylose.

^c Aerobic data for *S. stipitis* (CBS 6054) was obtained from Wahlbom *et al.* ([70]), growth on 20 g L⁻¹ xylose.

^d Anaerobic data for *C. tenuis* (CBS 4435) was obtained from Trausinger *et al.* ([51]), growth on 18 g L⁻¹ xylose.

^e Anaerobic data for *S. stipitis* (CBS 6054) was obtained from Krahulec *et al.* ([43]), growth on 22 g L⁻¹ xylose.

^f n.d.: not determinable, n.a.: not available in the data set.

^g Rel. S.D. was < 6%.

^h Rel. S.D. was ≤ 10%.

ⁱ Rel. S.D. was < 20%.

^j Rel. S.D. was < 30%.

^k Rel. S.D. was < 40%.

^l Rel. S.D. was = 50%.

4 AIM OF WORK

The overall goal of this work was to record time-resolved metabolic responses to oxygen depletion in two native xylose-utilizing yeasts *C. tenuis* CBS 4435 and *S. stipitis* CBS 6054 and one recombinant *S. cerevisiae* strain, IBB10B05.

To achieve this, several aims were defined:

1. Development of a working routine, with which aerobic and anaerobic cultivation of all three strains can be reproduced in both bioreactor and shake flasks with xylose as the sole carbon source.
2. Time-resolved sampling according to the workflow established by aim 1 and preparation of samples for LC-MS analysis by methods established at I.B.B.
3. Determination of physiological parameters based on external metabolite analysis and concepts of material balance.
4. Qualitative and quantitative analysis of intracellular metabolites at 31 predefined time points covering aerobic exponential growth as well as short- and long-term responses to oxygen deprivation and preparation of metabolite time profiles.

5 MATERIALS

5.1 Chemicals

Chemicals used in this work as well as compounds for intracellular metabolite quantification are listed in Table 5-1 and Table 5-2, respectively.

Table 5-1: List of chemicals used.

Agar-Agar	Carl Roth GmbH + Co. KG (Karlsruhe, Germany)
Ammonium acetate \geq 98%	Carl Roth GmbH + Co. KG (Karlsruhe, Germany)
Ammonium chloride \geq 99,8%	Carl Roth GmbH + Co. KG (Karlsruhe, Germany)
Ammonium sulfate \geq 99,5%	Carl Roth GmbH + Co. KG (Karlsruhe, Germany)
Antifoam 204	Sigma-Aldrich (St. Louis, USA)
D-[UL- ¹³ C]-Glucose	Omicron Biochemicals, Inc. (South Bend, USA)
D-Xylose \geq 98,5%	Carl Roth GmbH + Co. KG (Karlsruhe, Germany)
Dry ice	Linde Gas GmbH (Graz, Austria)
Ethanol 99.9% (v/v)	VWR (West Chester, USA)
Glucose monohydrate	Carl Roth GmbH + Co. KG (Karlsruhe, Germany)
Glycerol \geq 98%	Carl Roth GmbH + Co. KG (Karlsruhe, Germany)
Hydrochloric acid 37% (v/v)	Carl Roth GmbH + Co. KG (Karlsruhe, Germany)
LC-MS Chromasolv Water	Sigma-Aldrich (St. Louis, USA)
Liquid N ₂	Air Liquide Austria GmbH (Graz, Austria)
Gaseous N ₂ 99,999% (v/v) (5.0)	Air Liquide Austria GmbH (Graz, Austria)
Magnesium sulfate heptahydrate	Carl Roth GmbH + Co. KG (Karlsruhe, Germany)
Methanol, LC-MS grade	Sigma-Aldrich (St. Louis, USA)
Peptone ex casein	Carl Roth GmbH + Co. KG (Karlsruhe, Germany)
Phosphoric acid	Carl Roth GmbH + Co. KG (Karlsruhe, Germany)
Potassium chloride	Carl Roth GmbH + Co. KG (Karlsruhe, Germany)
Potassium dihydrogen phosphate	Carl Roth GmbH + Co. KG (Karlsruhe, Germany)
Potassium hydroxide	E. Merck KG (Darmstadt, Germany)
Sodium chloride	Carl Roth GmbH + Co. KG (Karlsruhe, Germany)
Sodium hydroxide	Carl Roth GmbH + Co. KG (Karlsruhe, Germany)
Sulfuric acid 1N	Carl Roth GmbH + Co. KG (Karlsruhe, Germany)
Trace element solution 1000x	provided by I.B.B.
Vitamin solution 1000x	provided by I.B.B.
Xylitol \geq 99%	Sigma-Aldrich (St. Louis, USA)
Yeast extract	Carl Roth GmbH + Co. KG (Karlsruhe, Germany)

Table 5-2: Compounds used for intracellular metabolite quantification. Concentrated solutions (C-stocks) were provided by the HEALTH department of Joanneum Research GmbH.

compound	concentration [μM]
2,3-Bisphosphoglyceric acid	92,10
3-Methyl-2-oxovaleric acid	84,60
3-Phosphoglyceric acid	92,88
6-Phosphoglyceric acid	72,69
Acetyl-CoA	91,80
Adenosine 5-diphosphate	91,56
Adenosine 5-monophosphate	93,54
Adenosine 5-triphosphate	92,08
Citric acid	95,08
Dihydroxyacetone phosphate	91,94
Erythrose 4-phosphate	91,74
Fructose 1-phosphate	98,70
Fructose 1,6-bisphosphate	94,36
Fructose 6-phosphate	90,66
Fumaric acid	92,10
Glucose 1-phosphate	91,71
Glucose 6-phosphate	93,25
Glyceraldehyde 3-phosphate	107,90
Glycerol 3-phosphate	97,76
Guanosine 5-diphosphate	94,39
Guanosine 5-monophosphate	91,41
Guanosine 5-triphosphate	91,77
L-Alanine	103,03
L-Arginine	94,85
L-Asparagine	96,09
L-Aspartic acid	92,26
L-Citrulline	94,26
L-Cysteine	106,13
L-Glutamic acid	89,02
L-Glutamine	89,82
L-Glycine	97,82
L-Histidine	82,83
L-Isoleucine	97,98
L-Leucine	97,98
L-Lysine	87,91
L-Ornithine	97,24
L-Phenylalanin	88,86
L-Proline	111,63

L-Serine	87,34
L-Threonine	107,88
L-Tryptophan	89,91
L-Tyrosine	91,20
L-Valine	109,70
Lactic acid	122,22
Malic acid	92,86
NAD ⁺	91,67
NADH	93,48
NADP ⁺	93,28
NADPH	81,40
Oxaloacetic acid	89,93
Oxoglutaric acid	71,30
Oxoisovaleric acid	94,81
Phosphoenolpyruvic acid	77,04
Pyruvic acid	96,82
Ribose 5-phosphate	91,74
Ribulose 5-phosphate	99,08
Seduheptulose 7-phosphate	91,74
Succinic acid	94,06
Trehalose	93,92
Trehalose 6-phosphate	91,73
Uridine 5-diphosphoglucose	95,14

5.2 Instruments

Centrifugation

Centrifuge "Eppifuge" 5415R	Eppendorf AG (Hamburg, Germany)
Centrifuge 5804R	Eppendorf AG (Hamburg, Germany)
Centrifuge 5810R	Eppendorf AG (Hamburg, Germany)
Centrifuge tube: 50 mL, 15 mL, 1.5 mL	SARSTEDT AG & Co. (Nümbrecht, Germany)

Cultivation

Erlenmeyer flask, baffled, 1000 mL, 300 mL	Schott DURAN Produktions GmbH & Co. KG (Mainz, Germany)
Penicilline flask, 100 mL	provided by I.B.B.
Screw-cap	provided by I.B.B.
Sealing shim	provided by I.B.B.
Fermentation system	Infors HT (Bottmingen-Basel, Switzerland)
Fermenter Labfors 1	
1 L working volume	
Three baffled element	
Six bladed Rushton disk impeller	
Software Iris NT	
Air inlet filter Midisart 2000 (17805-G), 0.2 µm	Sartorius AG (Goettingen, Germany)
Air outlet filter Acro 50 (PN4251), 0.2 µm	Pall Corporation (Port Washington, USA)
pH electrode	Hamilton Messtechnik GmbH (Höchst im Odenwald, Germany)
pO ₂ electrode	Hamilton Messtechnik GmbH (Höchst im Odenwald, Germany)
Shaking incubator GFL 3033	GFL Gesellschaft für Labortechnik GmbH (Burgwedel, Germany)
Shaking incubator CERTOMAT BS-1	Sartorius AG (Goettingen, Germany)

Filters

Syringe filter Minisart ^R , 0.2 µm and 0.45 µm	Sartorius AG (Goettingen, Germany)
Polyamide filter Sartolon, 0.2 µm	Sartorius AG (Goettingen, Germany)
Membrane filter Millipore, 0.45 µm	Millipore (Billerica, USA)

HPLC-UV/RI system

Pump L-7100	
RI detector L-7490	
UV detector L-7400	
Autosampler L-7250	
HPLC system manager software D-7000	Merck-Hitachi LaChrom (Darmstadt, Germany-San Jose, USA)
Degasys DG-2410	UniFlows (Tokyo, Japan)

Cation H-Cartridge Micro-Guard 125-0129
Column Aminex HPX-87H
HPLC vials 200 µL, caps, microinserts

Biorad (Hercules, USA)
Biorad (Hercules, USA)
Markus Bruckner Analysetechnik
(Linz, Austria)

LC-MS system

HPLC Dionex Ultimate3000
Autosampler WPS-3000
Solvent rack SRD-3600
Pump LGP-3600 (LPG-3000)
Flow manager FLM-3300

Thermo Fisher Scientific (Waltham, USA)

Pre-column Atlantis T3 C18, 3 µM, 100 A, 10 x 2.1 mm

Waters Corporation (Milford, USA)

Column Atlantis T3 C18, 3 µm, 100 A, 150 x 2.1 mm

Waters Corporation (Milford, USA)

HPLC vials, 200 µL, TopSert TPX-Short Thread Vial, 32x11.6

VWR (West Chester, USA)

Heated electrospray ionization source (HESI)

Thermo Fisher Scientific (Waltham, USA)

Mass spectrometer Exactive™

Thermo Fisher Scientific (Waltham, USA)

Spectrophotometry

Spectrophotometer DU800

Beckman Coulter Inc. (Fullerton, USA)

Peltier temperature controller

System and applications software version 2.0

pH measurement

pH meter 691

Metrohm AG (Herisau, Switzerland)

pH meter inoLab 720

WTW Wissenschaftlich-Technische
Werkstätten GmbH (Weilheim, Germany)

Pipettes

PeqPETTE, 5 mL

PEQLAB Biotechnologie GmbH

Pipette tips, 5 mL

PEQLAB Biotechnologie GmbH

Pipette Pipetman, 10 µL, 100 µL, 1000 µL

Gilson, Inc. (Middleton, USA)

Pipette tips, 10 µL, 100 µL, 1000 µL

Greiner Bio-One GmbH (Frickenhausen,
Germany)

Miscellaneous

8-channel Multi-Input Thermometer PCE-T800

PCE Instruments (Meschede, Germany)

Needle Sterican, Ø 0.8 mm x 120 mm

B. Braun Medical AG (Emmenbrücke,
Switzerland)

Needle Sterican, Ø 0.9 mm x 40 mm

B. Braun Medical AG (Emmenbrücke,
Switzerland)

Vortex shaker REAX top

Heidolph Instruments GmbH & Co. KG
(Schwabach, Germany)

Waterbath type 1083, $\leq 99^{\circ}\text{C}$	GFL Gesellschaft für Labortechnik GmbH (Burgwedel, Germany)
Evaporator®	Gebr. Liebisch GmbH & Co. KG (Bielefeld, Germany)
Rotavapor	Heidolph Instruments GmbH & Co. KG (Schwabach, Germany)
Drying cabinet	Memmert GmbH + Co. KG (Schwabach, Germany)
Desiccator	Kartell Labware (Noviglio, Italy)

5.3 Yeast strains

Candida tenuis CBS 4435, Centraalbureau voor Schimmelcultures (Baarn, The Netherlands)

Saccharomyces cerevisiae IBB10B05 [13], evolved out of BP10001 (CEN.PK 113-5D *ura3::*(GPDp-XKS1-CYC1t, GPDp-CtXRDm-CYC1t, GPDp-GmXDH-CYC1t), I.B.B.

Scheffersomyces stipitis CBS 6054, Dr. Marko Kuijper (BIRD Engineering, HG Schiedam, The Netherlands)

5.4 Media

5.4.1 Yeast peptone dextrose medium

Composition of Yeast Peptone Dextrose (YPD) medium is shown in Table 5-3. Solution B was prepared separately and adjusted to a pH of 5.7 with 1 M HCl and 1 M NaOH. Both solutions were autoclaved for 20 min at 121°C and 1 bar and then combined to the concentrations shown in the table below.

Table 5-3: Composition of YPD medium.

Solution	Component	[g L ⁻¹] ^a
A ^b	Glucose	20.0
	Agar-Agar	16.0
B	Peptone	20.0
	Yeast extract	10.0

^a Values indicate final medium concentrations.

^b A 10-fold stock was prepared for solution A.

5.4.2 Mineral medium

Compositions of the used MM are shown in Table 5-4. Concentrated solutions of A₁ and A₂ were autoclaved for 20 min at 121°C and 1 bar. Solution B was adjusted to a predefined pH value (see Section 6.1 Table 6-1, Table 6-2 and Table 6-3) with 1 M HCl and 1 M NaOH before sterilization (20 min, 121°C, 1 bar). Vitamins (C) and trace elements (D) were sterilized by filtration (0.2 µm) and autoclavation (20 min, 121°C, 1 bar), respectively. Prior to inoculation all four MM solutions were combined to the final concentrations.

Table 5-4: Composition of mineral media MM1-MM4.

Solution	Component	MM1	MM2	MM3	MM4
[g L ⁻¹] ^a					
A ₁ ^b	Glucose	20.0	-	-	-
A ₂ ^b	Xylose	-	50	50	50
B	KH ₂ PO ₄	14.1	14.1	14.1	0.25
	KCl	-	-	1.5	1.5
	(NH ₄) ₂ SO ₄	5.0	5.0	-	-
	NH ₄ Cl	-	-	4.05	4.05
	MgSO ₄ x 7H ₂ O	0.5	0.5	0.5	0.5
	Antifoam 204	-	-	0.015% (v/v)	0.015% (v/v)
	C ^c	D-Biotin	0.00005		
Ca-Pantothenate		0.001			
Thiamin-HCl		0.001			
Pyridoxin-HCl		0.001			
Nicotinic acid		0.001			
<i>p</i> -Aminobenzoic acid		0.002			
<i>m</i> -Inositol		0.025			
D ^c	FeSO ₄ x 7H ₂ O	0.003			
	ZnSO ₄ x 7H ₂ O	0.0045			
	CaCl ₂ x 6H ₂ O	0.0045			
	MnCl ₂ x 2H ₂ O	0.00084			
	CoCl ₂ x 6H ₂ O	0.0003			
	CuSO ₄ x 5H ₂ O	0.0003			
	Na ₂ MoO ₄ x 2H ₂ O	0.0004			
	H ₃ BO ₃	0.001			
	KI	0.0001			
Na ₂ EDTA	0.015				

^a Values indicate final medium concentrations.

^b Stock solutions were prepared for A₁ (10-fold) and A₂ (4-fold).

^c Solutions of C (vitamins) and D (trace elements) were provided in concentrated form (each 1000-fold) by I.B.B.

6 METHODS

6.1 Fermentation

Cultivations on YPD agar plates were carried out at 25°C and pH 5.7 for *C. tenuis* and 30°C and pH 5.7 for IBB10B05 and *S. stipitis*. Fermentations in shake flasks and stirred bioreactor were performed at 25°C and pH 5.5 for *C. tenuis*, at 30°C and pH 6.5 for IBB10B05 and at 30°C and pH 5.7 for *S. stipitis*.

6.1.1 Preculture

For each yeast strain the preculture (PC) was performed in two-steps with PC1 on glucose and PC2 on xylose. 50 µL of a glycerol stock cell suspension were plated on YPD agar and incubated for 2 days. After incubation, a loop full of cells was used for inoculation of a 300 mL baffled Erlenmeyer flask (BEF) filled with 30 mL MM1. PC1 was incubated aerobically overnight.

Cells obtained from PC1 served for inoculation of PC2 to initial optical densities at 600 nm (OD_{600}) of 0.05 (*C. tenuis*), 0.1 (*S. stipitis*) and 0.3 (IBB10B05). PC2 was performed in a 300 mL BEF containing 60 mL MM2. Cultivation conditions for PC are shown in Table 6-1.

Table 6-1: Cultivation conditions for PC.

Parameter	PC1			PC2		
	<i>C. tenuis</i>	IBB10B05	<i>S. stipitis</i>	<i>C. tenuis</i>	IBB10B05	<i>S. stipitis</i>
		aerobic			aerobic	
T [°C]	25	30	30	25	30	30
pH	5.5	6.5	5.7	5.5	6.5	5.7
Stirrer [rpm]		125			125	
MM		MM1			MM2	

After incubation, aliquots of PC2 with volumes to reach an initial OD_{600} of 0.3 in the mainculture (MC) were harvested via centrifugation for 10 min, 5000 rpm and 4°C. Subsequently, the cells were washed with sterile 0.9% NaCl solution to avoid contamination of MC with remaining PC compounds. After the washing step, the cells were centrifuged and resuspended in sterile 0.9% NaCl solution again. *C. tenuis* was always harvested at OD_{600} of 3.5-4.5, IBB10B05 at OD_{600} of 1.5-2.0 and *S. stipitis* at OD_{600} 15-23.

6.1.2 Mainculture in shake flasks

Fermentations for *C. tenuis* and *S. stipitis* were performed once, while fermentations for IBB10B05 were performed twice. Cells were cultivated aerobically at 125 rpm in a 1 L BEF containing 100 mL MM3 until an OD₆₀₀ of approximately 2 was reached. Then 80 mL of each cell suspension were transferred to 100 mL flasks. After transfer the flasks were sealed and purged with filtered (0.2 µm) nitrogen for 30 min to guarantee anaerobic conditions. The agitation rate was changed to 180 rpm. Cultivation conditions for MC in shake flask are shown in Table 6-2.

Table 6-2: Cultivation conditions for MC in shake flask.

Parameter	<i>C. tenuis</i>	IBB10B05	<i>S. stipitis</i>	<i>C. tenuis</i>	IBB10B05	<i>S. stipitis</i>
		<i>aerobic</i>			<i>anaerobic</i>	
T [°C]	25	30	30	25	30	30
pH	5.5	6.5	5.7	5.5	6.5	5.7
Stirrer [rpm]		125			180	
MM		MM3			MM3	

6.1.3 Mainculture in bioreactor

Fermentations for each strain were performed twice in a Labfors 1 bioreactor with a working volume of 1 L. The bioreactor is equipped with a three baffled element and two six bladed Rushton disk impellers. Cultivations were carried out in MM4. Stirrer speed was adjusted to 400 rpm. Gasflow (GF) in the aerobic phase was regulated by a PID-controller to reach a pO₂ saturation of 40%. PID-controlled addition of 0.5 M (w/v) H₃PO₄ and 0.5 M (w/v) KOH was used to keep pH values constant. At OD₆₀₀ of about 2, aeration was switched to N₂ (sterile-filtered) and the cultivation broth was sparged at a constant flow of 0.16 L min⁻¹. Simultaneously, the stirrer speed was decreased to 200 rpm. Settings for bioreactor fermentations are listed in Table 6-3.

Table 6-3: Cultivation conditions for MC in bioreactor.

Parameter	<i>C. tenuis</i>	IBB10B05	<i>S. stipitis</i>	<i>C. tenuis</i>	IBB10B05	<i>S. stipitis</i>
		<i>aerobic</i>			<i>anaerobic</i>	
T [°C]	25	30	30	25	30	30
pH	5.5	6.5	5.7	5.5	6.5	5.7
Stirrer [rpm]		400			200	
GF [L min ⁻¹]		PID, pO ₂ = 40%			0.16	
MM		MM4			MM4	

6.1.4 Sampling

Samples were withdrawn over the whole fermentation period at predefined time intervals to observe cell growth as well as substrate consumption and product formation. OD₆₀₀ were measured spectrophotometrically according to Section 6.2.1. Afterwards samples were centrifuged for 10 min at 13000 rpm and 4°C. Supernatants were stored at -20°C prior to analysis of extracellular metabolites with high-performance liquid chromatography (HPLC).

For intracellular metabolite analysis¹, 1 mL samples of cell suspension were taken and quenched at predefined time points in replicates (see Figure 6-1 and Table 6-5 in Section 6.2.4.1).

6.2 Analytics

6.2.1 Determination of cell density (OD₆₀₀)

Cell density was determined at 600 nm (OD₆₀₀) with a Beckmann coulter spectrophotometer DU800. NaCl 0.9% (w/v) was used as reference. Samples were diluted with 0.9% NaCl solution to reach an OD₆₀₀ of 0.05-0.5.

Experimentally determined biomass (BM)-OD₆₀₀ ratios (see Section 6.2.2) were used to convert OD₆₀₀ to BM [g L⁻¹]. Applied OD₆₀₀-specific BM values are shown in Section 7.1.1 Table 7-1.

6.2.2 BM determination

For BM (= cell dry weight (CDW)) determination, first of all HPLC vials were dried at 105°C overnight in a drying cabinet and afterwards 2 h in a desiccator. Subsequently, the weight of the empty HPLC vials (weight A) was measured. PC and MC were carried out as described in Section 6.1.1 and Section 6.1.3, respectively. During bioreactor fermentations, volumes of 40 OD₆₀₀ units² were taken at 4 time points in replicates: before switch (pO₂ = 40%) at OD₆₀₀ ~2 (4x) and 120 min (4x), 24 h (3x) and 48 h (3x) after oxygen was replaced by nitrogen. The cell suspensions were centrifuged for 20 min at 4000 rpm and 4°C. The cell density was determined at each time point as explained in Section 6.2.1. After centrifugation the supernatants were discarded and the cell pellets resuspended in the same volume of distilled water as drawn from the bioreactor. In the following step, the samples were centrifuged for 20 min at 4000 rpm and 4°C again. After decantation of supernatants, the pellets were resuspended in 0.5 mL distilled water and transferred to the dried HPLC vials. The Sarstedt tubes and pipette tips were washed with 0.5 mL distilled water, which was then also

¹ Only for fermentations in bioreactor.

² At OD₆₀₀ of 1 = 40 mL, at OD₆₀₀ of 2 = 20 mL etc.

transferred to the HPLC vials. HPLC vials containing washed cell suspensions were dried at 105°C overnight in a drying cabinet. Afterwards the weight of the HPLC vials containing the dried cell suspension (weight *B*) was measured. OD₆₀₀-specific BM values [g L⁻¹ OD₆₀₀⁻¹] were calculated by Equation 6-1. *V* stands thereby for the volume taken [L].

$$BM = \frac{B - A}{V \cdot OD_{600}} \quad \text{(Equation 6-1)}$$

6.2.3 HPLC-RI

Extracellular metabolites were analyzed by HPLC-RI. HPLC was performed with a HPX-87H ion exchange column at a temperature of 65°C. Degassed and filtered 5 mM H₂SO₄ served as mobile phase at a flow rate of 0.6 mL min⁻¹. The injection volume was 20 µL and the run time per sample was 30 min. Samples were measured undiluted or 1:3 diluted with 5 mM H₂SO₄. 6 standards comprised of 5 components at different concentrations (see Table 6-4) were used to establish calibration. The standards were measured at the beginning and the end of the HPLC analysis.

Table 6-4: Composition of HPLC standards used for calibration.

Standard	Xylose	Xylitol	Glycerol	Acetate	Ethanol
[g L ⁻¹]					
1	20.20	10.00	0.95	2.00	14.48
2	15.15	7.50	0.71	1.50	10.86
3	10.10	5.00	0.48	1.00	7.24
4	5.05	2.50	0.24	0.50	3.62
5	2.53	1.25	0.12	0.25	1.81
6	1.25	0.62	0.06	0.12	0.90

6.2.4 Metabolite profiling

6.2.4.1 Quenching

First of all 50 mL tubes were filled with 10 mL methanol (QS) and precooled for 15 min on dry ice. The centrifuge and rotor inserts were cooled to -9°C . At predefined time points (see Figure 6-1 and Table 6-5) 1 mL of fermentation broth was quickly pipetted into the precooled (-76°C) QS tubes. As pipetting occurred in between 4-6 sec (average = 4.2 sec), an oxygen limitation and therefore alteration of the metabolic state could be ruled out (see Figure 6-2). Directly after sample transfer the suspension was vortexed and placed on dry ice. After quenching of 3-4 samples, the tubes were centrifuged at 5000 rpm and -9°C for 3 min. The supernatants were discarded and the pellets shock frozen in liquid nitrogen before storage at -80°C .

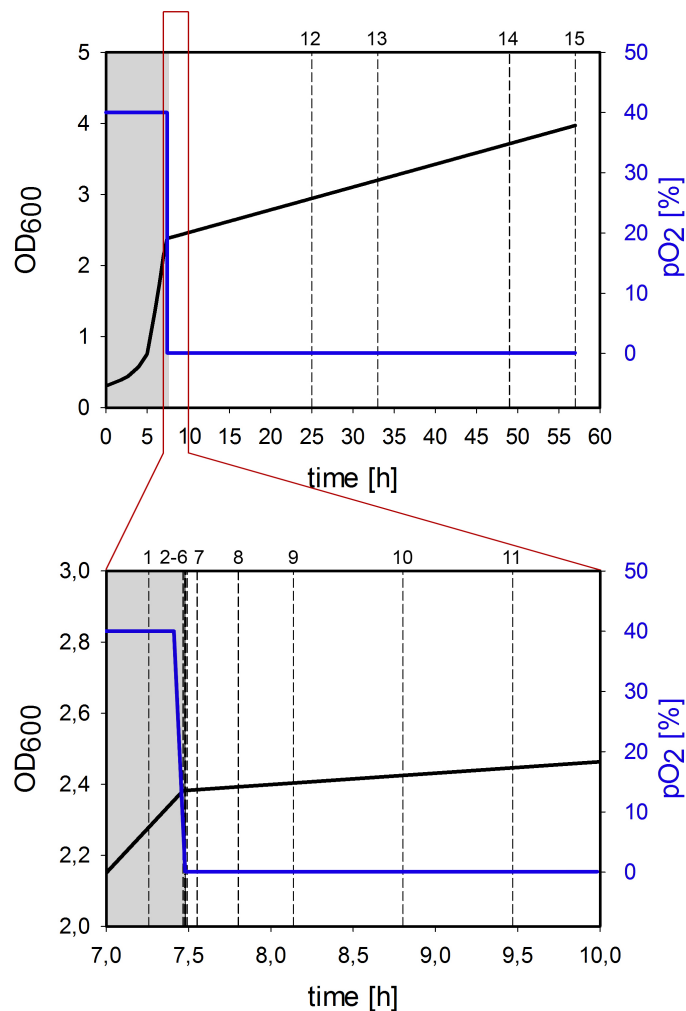


Figure 6-1: Quenching time points in a typical OD_{600} and pO_2 vs. time plot. Quenching time points are indicated by dotted lines and small numbers above (see also Table 6-5). The aerobic phase is highlighted in grey. The small segment between 7-10 h of fermentation is enlarged in the picture below for a better demonstration of the crucial switching time phase and the first quenching time points. Data shown were obtained from *S. stipitis* batch 1.

Table 6-5: Quenching time points and number of replicates.

Quenching time points	Replicates	Dotted lines in Figure 6-1
before switch at OD ₆₀₀ ~2	3x	1
pO ₂ = 0	1x	2
0.5 min ^a	1x	3
1 min ^a	1x	4
1.5 min ^a	1x	5
5 min ^a	2x	6
10 min ^a	2x	7
20 min ^a	2x	8
40 min ^a	2x	9
80 min ^a	2x	10
120 min ^a	2x	11
16-19 h ^a	3x	12
24-27 h ^a	3x	13
40-43 h ^a	3x	14
48-57 h ^a	3x	15

^a Passed time since pO₂ = 0.

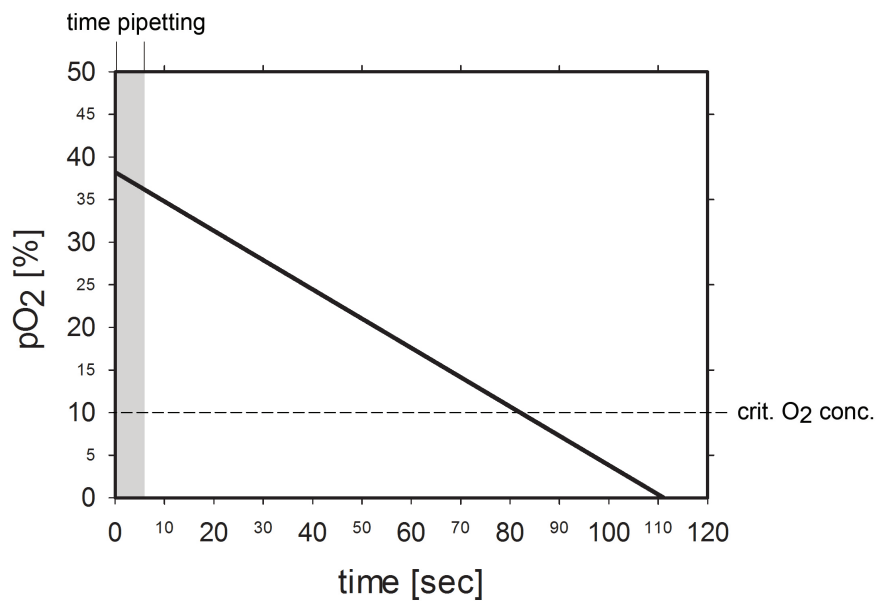


Figure 6-2: Sampling time vs. oxygen consumption. The grey shaded section represents the time needed for pipetting, which lies beneath 6 sec. The dotted line indicates the critical oxygen concentration, which lies beneath 10% pO₂ [71]. Data shown were obtained from *C. tenuis* batch 2 at an OD₆₀₀ of 2.

6.2.4.2 Extraction

15 mM ammonium acetate ethanol buffer 80% (v/v) pH 7.5 was used as ES. 1.5 mL ES were filled in 15 mL tubes. Afterwards the tubes were heated in a water bath ($> 90^{\circ}\text{C}$) for about 5 min. 50 mL tubes containing the frozen (-80°C) cell pellets were placed on dry ice and added with 100 μL of an on ice precooled ^{13}C -labeled ISTD (^{13}C -ISTD) (see Section 6.2.4.4). The cell pellet tubes were placed into the hot water bath right before addition of the ES. The tubes were then immediately vortexed and incubated in the water bath for the next 3 min. During this time, the tubes were vortexed every 60 sec. Subsequently, samples were centrifuged at 5000 rpm and 0°C for 3 min and the supernatants stored at -80°C .

6.2.4.3 Concentration of samples

The supernatants containing the intracellular metabolites were treated with nitrogen gas to remove the aqueous phase. Afterwards the dried metabolite extracts were dissolved in 100 μL LC-MS grade water and stored at -80°C until analysis with LC-MS.

6.2.4.4 Preparation of ^{13}C -labeled metabolite extract

A ^{13}C -labeled metabolite extract was used for internal standardization. ^{13}C -ISTD was produced with *S. stipitis*. The PC was performed as explained in Section 6.1.1 with some alterations: The glycerol stock was plated on MM1 containing 16 g L^{-1} agar-agar and 5 g L^{-1} ^{13}C -labeled glucose, which was sterilized by filtration ($0.2\text{ }\mu\text{m}$). The PC contained MM1 with 5 g L^{-1} ^{13}C -labeled glucose. PC2 was skipped completely. With the exceptions working volume (0.5 L) and initial OD_{600} (0.05), the MC was carried out in a bioreactor under aerobic conditions as described in Section 6.1.3. Cells were cultivated aerobically and quenched at the end of the exponential growth phase at an OD_{600} value of about 5. 50 mM ice-cold ammonium acetate solution pH 7.0 was used as QS. 80 mL cell suspension were transferred to 320 mL of QS (see Section 6.2.4.1). Resultant cells were extracted through the addition of 200 mL 15 mM ammonium acetate ethanol buffer 80% (v/v) pH 7.5 (ES) as described in Section 6.2.4.2. Centrifugation settings were changed for quenching to 6000 rpm, 4°C , 5 min and extraction to 6000 rpm, 4°C , 10 min. Supernatants were pooled and concentrated by evaporation in a rotavapor at 30°C . Prior to concentration, the rotavapor was cleaned carefully with ethanol absolute. 160 mL "ready to use" ^{13}C -ISTD were obtained and stored in aliquots at -80°C .

6.2.4.5 Quantification

For quantification of intracellular metabolites external standards were prepared. Therefore 61 identical compounds of the central carbon metabolism¹ were dissolved in LC-MS grade water to reach a concentration of 10 mM (A-stocks). Subsequently, the A-stocks were combined to 5 B-stocks. Each of the B-stocks contained 500 μ M of all corresponding compounds. Combination of all B-stocks and spiking of acetyl-CoA, erythrose 4-phosphate and sedoheptulose 7-phosphate resulted in a C-stock containing 61 metabolites with a concentration of 100 μ M. Concentrations are summarized in Section 5.1 Table 5-2. Based on the C-stock, eight calibration standards (CS) were prepared. Therefore the C-stock was diluted in a ratio of 1:2. The 1:2 dilution was then taken as basis for preparation of a dilution series containing six 1:3 dilutions. LC-MS grade water was used for diluting. 50 μ L of ¹³C-ISTD were added to each CS during extraction. In parallel, biological samples were extracted and added with the same ¹³C-labeled metabolite extract. Prior to LC-MS analysis the CS were dried and dissolved in 50 μ L LC-MS grade water as described in Section 6.2.4.3.

6.2.4.6 LC-MS

A LC-MS system from Thermo Fisher ScientificTM was used for metabolite analysis. The system consists of a Dionex Ultimate 3000 HPLC equipped with an Atlantis T3 C18 analytical column for chromatographic separation and an ExactiveTM Orbitrap system for MS detection. Metabolites were separated with a reversed-phase ion-pairing HPLC method (adapted from *Büscher et al.* [61]) at a temperature of 45°C. The mobile phase was composed of 2-propanol (eluent 1) and a solution containing 5% (v/v) methanol, 10 mM tributylamine and 15 mM acetic acid (eluent 2). Tributylamin acts as ion-pairing agent. The running time per sample was 40 min and the injection volume 10 μ L. The metabolites were ionized via negative mode heated electrospray ionization (HESI). A quality control (QC) sample was prepared by unifying equal aliquots from each sample measured in one batch. LC-MS grade water was used as blank (BL). In accordance with sampling schedule shown in Section 6.2.4.1 Table 6-5, 31 biological samples were obtained per batch. Samples for each batch were divided into two measuring series á three blocks. Thus, six blocks were measured in total, whereas each block started with a BL followed by a QC sample. The first measuring series consisted of 15 randomized biological samples plus 8 CS, while the second one consisted of 16 randomized biological samples plus 8 CS. Untreated ¹³C-ISTD samples were measured three times during the whole LC-MS measurement.

¹ Metabolites of glycolysis, PPP and TCA as well as AA, energy metabolites and redox cofactors.

6.3 Data Analysis

6.3.1 HPLC-RI

Merck-Hitachi software was used for compound identification and peak integration. The baseline was corrected manually. Raw data was processed in Microsoft Excel 2008 for Mac.

Calibration curves were established by plotting of known concentrations [g L^{-1}] against the corresponding peak areas for selected compounds. Resulting linear regression equations were used for calculation of extracellular metabolite concentrations in biological samples.

6.3.2 Determination of physiological parameters (μ , Y , q)

Following physiological parameters were determined: specific growth rate (μ), biomass yield (Y_{XS}), product yields (Y_{PS}), specific xylose uptake rate (q_{xylose}), specific oxygen uptake rate (q_{O_2}) and oxygen demand (a).

Prior to determination of these parameters, BM values as well as substrate and product concentrations needed to be corrected in case of bioreactor experiments. This was done because a significant reduction of fermentation volume due to evaporation was observed in the anaerobic phase. To avoid biased representation of data, the following correction procedure was applied: The volume at the end of fermentations and all volumes taken during fermentations were measured. Base addition during fermentation was recorded by Iris NT software. Recorded base volume values were corrected to mL by a factor of 1.43. This factor was determined by multiple testing of the base pump, which showed that the actual volume of base added was 1.43 times higher than the value recorded by the software. Addition of acid was so low as to be negligible. By knowing the starting volume (V_s), which was always 1 L, as well as the end-volume (V_e), which was measured with a measuring cylinder at the end of fermentation, the volume taken (V_t) and the added base volumes (V_b), the evaporation volume (V_{ev}) could be calculated (see Equation 6-2). Assuming a constant evaporation over the anaerobic time phase (t_{AN}) [min], the evaporation rate ($rate_{ev}$) [mL min^{-1}] could be determined (see Equation 6-3). It was assumed that evaporation was only affecting the anaerobic phase, because only here a constant massflow was applied. In addition, the aerobic phase was too short to make a significant contribution to evaporation. Subsequently, actual working volumes at each time point during fermentation (see Equation 6-4 and Equation 6-5) and hypothetical volumes without evaporation and base addition (see Equation 6-6) were calculated. Afterwards, OD_{600} values were multiplied by actual volumes and divided by corresponding volumes without evaporation and addition of base (see Equation 6-7). V_{aAE1} (Equation 6-4) and V_{aAN1} (Equation 6-5) stand thereby for the actual working volume at time point 1 [mL] in the aerobic and anaerobic phase, respectively. V_{ti} (Equation 6-4 and Equation 6-6) and V_{bi} (Equation 6-4) indicate the volume taken [mL] and the added

base volume [mL] up to and including time point 1, respectively. In Equation 6-5, V_0 stands for the volume [mL] at time point 0 and t_1 and t_0 for the time [min] at time point 1 and 0, respectively. In addition, V_{t1} indicates the volume taken [mL] at time point 1 and V_{b1} and V_{b0} the added base volumes [mL] at time point 1 and 0, respectively. In Equation 6-6, V_{h1} refers to the hypothetical volume without evaporation and addition of base at time point 1 [mL]. In Equation 6-7, OD_{c1} indicates the corrected OD_{600} value at time point 1, OD_{m1} the measured OD_{600} value at time point 1 and V_{a1} the actual working volume [mL].

$$V_{ev} = V_s + 1.43 \cdot V_b - (V_e + V_t) \quad \text{(Equation 6-2)}$$

$$rate_{ev} = \frac{V_{ev}}{t_{AN}} \quad \text{(Equation 6-3)}$$

$$V_{aAEA1} = V_s - V_{ti} + 1.43 \cdot V_{bi} \quad \text{(Equation 6-4)}$$

$$V_{aAN1} = V_0 - \left\{ (t_1 - t_0) \cdot rate_{ev} \right\} + V_{t1} + 1.43 \cdot (V_{b1} - V_{b0}) \quad \text{(Equation 6-5)}$$

$$V_{h1} = V_s - V_{ti} \quad \text{(Equation 6-6)}$$

$$OD_{c1} = \frac{OD_{m1} \cdot V_{a1}}{V_{h1}} \quad \text{(Equation 6-7)}$$

6.3.2.1 Specific growth rate (μ)

The μ [h^{-1}] was expressed by the slope of the linear part of a time versus $\ln OD_{600}$ plot.

6.3.2.2 Biomass yield (Y_{XS})

1. Method¹:

The biomass yield Y_{XS} was determined by plotting the substrate concentration against the BM. The slope of the linear part represents thereby Y_{XS} .

2. Method²:

As the aerobic time phase was too short to observe significant xylose consumption in aerobic bioreactor fermentations, a different approach was used to calculate Y_{XS} . This approach involved the determination of the slope of a glycerol versus BM plot [Y_{XG} in $g_{BM} g_{glycerol}^{-1}$]. Resulting values were converted into $mol_{BM} mol_{glycerol}^{-1}$ (c/f [71]) and $g_{BM} mol_{glycerol}^{-1}$. Latter values were used for calculation of $q_{glycerol}$ [$mmol_{glycerol} g_{BM}^{-1} h^{-1}$] (see Equation 6-8). Substitution of the experimentally determined q_{O_2} [$mmol_{O_2} g_{BM}^{-1} h^{-1}$] in Equation 6-9, results in the ratio of a/f [71]. Based on this ratio, f [$mol_{glycerol} mol_{xylose}^{-1}$] and $Y_{glycerol}$ could be calculated by applying electron balances (see Equation 6-10). The γ indicate thereby degrees of reduction. Stoichiometric coefficients arise from the general stoichiometric equation for aerobic growth and product synthesis: $C_wH_xO_yN_z + a O_2 + b H_gO_hN_i \rightarrow c CH_aO_bN_d + d CO_2 + e H_2O + f C_jH_kO_lN_m$. For biomass composition the average elemental formula $CH_{1.79}O_{0.5}N_{0.2}$ (molecular weight (MW) = $25.88 g mol^{-1} + 5\%$ ash) for yeasts was applied [71]. Finally, multiplication of f by c/f led to c [$mol_{BM} mol_{xylose}^{-1}$] and as a result to Y_{XS} .

$$q_{glycerol} \left[\frac{mmol}{g_{BM} \cdot h} \right] = \frac{1000 \cdot \mu \left[\frac{1}{h} \right]}{Y_{XG} \left[\frac{g_{BM}}{g_{glycerol}} \right] \cdot MW_{glycerol} \left[\frac{g}{mol} \right]} \quad \text{(Equation 6-8)}$$

$$\frac{a}{f} = \frac{q_{O_2}}{q_{glycerol}} \quad \text{(Equation 6-9)}$$

$$f = \frac{W \cdot \gamma_{xylose}}{\gamma_{BM} \cdot \frac{c}{f} + j \cdot \gamma_{glycerol} + \gamma_{xylose} \cdot \frac{a}{f}} \quad \text{(Equation 6-10)}$$

¹ Carried out for all shake flask experiments, anaerobic bioreactor fermentations and the 2nd aerobic bioreactor fermentation with *C. tenuis*.

² Carried out for all aerobic bioreactor fermentations except for 2nd fermentation with *C. tenuis*.

6.3.2.3 Product yields (Y_{PS})

1. Method¹:

Product yields (Y_{PS}) were determined by plotting substrate [g L^{-1}] against product concentrations [g L^{-1}]. The slope of the linear part represents thereby the product yield [g g^{-1}].

2. Method:

Y_{glycerol} in all aerobic bioreactor fermentations were determined as explained in Section 6.3.2.2 method 2. The only exception was the 2nd fermentation with *C. tenuis*, where the Y_{glycerol} was calculated as described in Section 6.3.2.3 method 1.

3. Method:

As ethanol evaporated during anaerobic bioreactor fermentations, estimates for Y_{ethanol} were calculated by applying electron balances and assuming complete carbon balance [71].

4. Method:

For fermentations under anaerobic conditions the amount of produced CO_2 per gram substrate (Y_{CO_2}) was calculated based on Y_{ethanol} and Y_{acetate} . It was assumed that with the production of 1 mol ethanol or acetate also 1 mol CO_2 was produced [68].

5. Method:

In case of lacking ethanol or acetate production, which was the case in aerobic fermentations, the Y_{CO_2} was calculated by the relation $\text{C}_w\text{H}_x\text{O}_y\text{N}_z + a \text{O}_2 + b \text{H}_g\text{O}_h\text{N}_i \rightarrow c \text{CH}_a\text{O}_b\text{N}_d + d \text{CO}_2 + e \text{H}_2\text{O} + f \text{C}_j\text{H}_k\text{O}_l\text{N}_m$ [71]. For biomass composition the average elemental formula $\text{CH}_{1.79}\text{O}_{0.5}\text{N}_{0.2}$ for yeasts was applied [71]. Hence, the MW was 25.88 g mol^{-1} (+5% ash).

6.3.2.4 C-recovery

The C-recovery was calculated by dividing all outgoing by all incoming C-atoms.

6.3.2.5 Specific xylose uptake rate (q_{xylose})

1. Method²:

The ratio of μ -to- Y_{XS} was used to calculate q_{xylose} [$\text{g}_{\text{xylose}} \text{g}_{\text{BM}}^{-1} \text{h}^{-1}$] [72]. Both parameters were determined in the same time range of fermentation.

¹ Carried out for all fermentations except for determination of Y_{glycerol} in aerobic bioreactor fermentations, for determination of Y_{ethanol} in anaerobic bioreactor fermentations and all determinations of Y_{CO_2} .

² Carried out for all fermentations except for anaerobic bioreactor fermentations of *C. tenuis*.

2. Method¹:

As *C. tenuis* did not grow under anaerobic conditions in bioreactor cultivations, q_{xylose} was calculated from the xylose decrease over time divided by the corresponding BM.

6.3.2.6 Specific oxygen uptake rate (q_{O_2}) and oxygen demand (a)

1. Method²:

For determination of q_{O_2meas} [$mmol_{O_2} g_{BM}^{-1} h^{-1}$] the oxygen supply during fermentation was switched off and the decrease of pO_2 was recorded until a pO_2 of only 20% was reached. The slope of pO_2 decrease over time was determined and used to calculate q_{O_2meas} with Equation 6-11. L stands for solubility of oxygen in water, which is $8.1 mg kg_{H_2O}^{-1}$ at $25^\circ C$ and $7.4 mg kg_{H_2O}^{-1}$ at $30^\circ C$ at an atmospheric pressure of 745 mmHg [73] and k stands for the pO_2 decrease over time [$\% h^{-1}$].

2. Method³:

For shake flask cultivations, q_{O_2calc} was calculated as indicated by Equation 6-12. The value of a_{calc} [$mol_{O_2} mol_{xylose}^{-1}$] was thereby previously determined by applying electron balances and assuming complete carbon balance [71]. These calculations were also done for bioreactor fermentations to verify values obtained from method 1.

3. Method:

Calculation of a_{meas} [$mol_{O_2} mol_{xylose}^{-1}$] was done by inserting q_{O_2meas} (determination explained in method 1) and the corresponding q_{xylose} [$g_{xylose} g_{BM}^{-1} h^{-1}$] into Equation 6-13.

$$q_{O_2meas} \left[\frac{mmol_{O_2}}{g_{BM} \cdot h} \right] = \frac{k \left[\frac{\%}{h} \right] \cdot L \left[\frac{mg}{L} \right]}{BM [g_{BM}] \cdot 100 \cdot MW_{O_2} \left[\frac{mg}{mmol} \right]} \quad \text{(Equation 6-11)}$$

$$q_{O_2calc} \left[\frac{mmol_{O_2}}{g_{BM} \cdot h} \right] = a_{calc} \cdot \left[\frac{mmol_{O_2}}{mmol_{xylose}} \right] \cdot \frac{q_{xylose} \left[\frac{mmol_{xylose}}{g_{BM} \cdot h} \right]}{MW_{xylose} \left[\frac{g}{mmol} \right]} \quad \text{(Equation 6-12)}$$

¹ Carried out for anaerobic bioreactor fermentations of *C. tenuis*.

² Carried out for all bioreactor fermentations.

³ Carried out for all fermentations.

$$a_{meas} = \frac{q_{O_2_{meas}} \left[\frac{mmol_{O_2}}{g_{BM} \cdot h} \right] \cdot MW_{xylose} \left[\frac{g}{mmol} \right]}{q_{xylose} \left[\frac{mmol_{xylose}}{g_{BM} \cdot h} \right]} \quad \text{(Equation 6-13)}$$

6.3.3 LC-MS

The data generated by LC-MS were analyzed with Thermo Scientific™ Xcalibur™ software (version 2.2 SP1). Automated as well as manual peak integration was performed by Dipl.-Ing. Gert Trausinger, Bakk.techn. (GT) from Joanneum Research GmbH and me with TraceFinder™ (*C. tenuis* and *S. stipitis* batch 1) and PeakScout™ (*S. cerevisiae* batch 1 and *C. tenuis*, *S. cerevisiae* and *S. stipitis* batch 2) software. Data was sorted precisely and signals that should be treated with caution were highlighted. Raw data was processed in Microsoft Excel 2008 for Mac.

For quantitative analysis, calibration curves were established by plotting known metabolite concentrations [μM] of CS against the corresponding $^{12}\text{C}/^{13}\text{C}$ area ratios. As the ^{12}C content of some metabolites of the ^{13}C -ISTD was significant, appropriate corrections were made (see Equation 6-14). Subscript *a* indicates thereby area values from CS or biological samples, while subscript *b* indicates average area values from individual ^{13}C -ISTD measurements.

For intracellular metabolite quantification in biological samples, $^{12}\text{C}/^{13}\text{C}$ area ratios considering the ^{12}C fraction of the ^{13}C -ISTD were calculated (see Equation 6-14) and substituted in corresponding linear equations arising from external calibration. Mean concentrations [μmol] were determined for all time points at which replicates were carried out. Values are based on the BM [g L^{-1}] of all per time point recorded replicates (see Table 6-5 in Section 6.2.4.1) according to Equation 6-15. Concentration of samples and back calculation on actual biomass was thereby also considered. The volume of ISTD added was 0.0001 L (V_1) and of the SV 0.001 L (V_2). Quantified values throughout this thesis are presented as $\mu\text{mol g}_{\text{BM}}^{-1}$ (= $\mu\text{mol g}_{\text{CDW}}^{-1}$ in corresponding figures).

In case of experiments in which no ^{13}C -ISTD was applied, ^{12}C data was calculated. If quantification was not possible, qualified data presented as normalized response $\text{g}_{\text{BM}}^{-1}$ (or $\text{g}_{\text{CDW}}^{-1}$ in corresponding figures) was calculated with Equation 6-14. Subsequently, again mean values of all per time point recorded replicates (see Table 6-5 in Section 6.2.4.1) were formed and based on corresponding BM values.

$$\frac{{}^{12}\text{C}^{corr}}{{}^{13}\text{C}} = \frac{{}^{12}\text{C}_a - {}^{13}\text{C}_a \cdot \left[\frac{{}^{12}\text{C}_b}{{}^{13}\text{C}_b} \right]}{{}^{13}\text{C}_a}$$

(Equation 6-14)

$$C^{met} \left[\frac{\mu\text{mol}}{\text{gBM}} \right] = \frac{C^{met} \left[\frac{\mu\text{mol}}{\text{L}} \right] \cdot V_1 [\text{L}]}{C^{BM} \left[\frac{\text{g}}{\text{L}} \right] \cdot V_2 [\text{L}]}$$

(Equation 6-15)

7 RESULTS

7.1 Physiological characterization of *C. tenuis*, IBB10B05 and *S. stipitis*

Fermentations for *C. tenuis*, IBB10B05 and *S. stipitis* were carried out in both shake flasks and stirred bioreactor using a defined MM and xylose as the sole carbon source. Cells were grown aerobically until switch to anaerobic conditions at OD₆₀₀ of approximately 2. The switching point at OD₆₀₀~2 was chosen, because at this point all three strains were in the exponential growth phase. Results from preliminary fermentations showed that the exponential growth phase lies in the OD₆₀₀-range from 0.5-2.7, 0.3-6 and 0.7-30 for *C. tenuis*, IBB10B05 and *S. stipitis*, respectively. Furthermore at an OD₆₀₀~2, sufficient cell material for LC-MS analysis was available.

7.1.1 BM determination

For detailed characterization of yeast strains, the BM of *C. tenuis*, IBB10B05 and *S. stipitis* was determined. Fermentations were carried out in stirred bioreactor under controlled pH and temperature. Samples were taken before switch (pO₂ = 40%) at OD₆₀₀~2 (4x) and 120 min (4x), 24 h (3x) and 48 h (3x) after pO₂ = 0. Mean OD₆₀₀-specific BM values of all determinations are shown in Table 7-1. IBB10B05 had the highest BM with values ranging from 0.47-0.51, followed by *C. tenuis* with values ranging from 0.45-0.48 and *S. stipitis* with values ranging from 0.38-0.43. While the BM of *C. tenuis* and *S. stipitis* decreased over the fermentation period, the BM of IBB10B05 increased. However, in general the BM does not depend on the oxygen concentration, as differences between single time points were within the experimental error.

Table 7-1: BM determination of *C. tenuis*, IBB10B05 and *S. stipitis*.

	<i>C. tenuis</i>	IBB10B05	<i>S. stipitis</i>
	BM [g L ⁻¹ OD ₆₀₀ ⁻¹]		
aerobic and 120 min (N = 4)	0.48 ± 0.03	0.47 ± 0.02	0.43 ± 0.02
24 h (N = 3)	0.47 ± 0.02	0.47 ± 0.02	0.40 ± 0.02
48 h (N = 3)	0.45 ± 0.03	0.51 ± 0.01	0.38 ± 0.02

7.1.2 Growth behaviour

The growth behaviour of *C. tenuis*, IBB10B05 and *S. stipitis* is shown in Figure 7-1. Values for μ are summarized in Table 7-2 to Table 7-5. Under aerobic conditions *S. stipitis* was the fastest growing strain ($\mu = 0.28-0.48 \text{ h}^{-1}$), followed by *C. tenuis* ($\mu = 0.26-0.32 \text{ h}^{-1}$) and IBB10B05 ($\mu = 0.054-0.102 \text{ h}^{-1}$), whereas under anaerobic conditions only IBB10B05 was capable of growth ($\mu = 0.015-0.021 \text{ h}^{-1}$). *S. stipitis* stopped to grow within only one generation ($\mu = 0.010-0.011 \text{ h}^{-1}$) and *C. tenuis* showed nearly no growth ($\mu = 0.005 \text{ h}^{-1}$). Moreover, growth of IBB10B05 and *S. stipitis* under aerobic conditions was faster in bioreactor cultivations compared to shake flask cultivations.

7.1.3 Substrate consumption and product formation

Representative time courses of substrate utilization and product formation are displayed in Figure 7-2. In this context it is important to mention that the decrease of ethanol during bioreactor fermentations of IBB10B05 (Panel D) and *S. stipitis* (Panel F) was most likely due to evaporation. The physiological parameters of *C. tenuis*, IBB10B05 and *S. stipitis* are summarized in Table 7-2 to Table 7-5. Y_{xs} , Y_{glycerol} for aerobic and Y_{ethanol} for anaerobic bioreactor fermentations were calculated by applying electron balances and Y_{CO_2} for all aerobic fermentations was calculated based on the general stoichiometric equation for aerobic growth and product synthesis [71] and by assuming complete carbon balance (as already described in Section 6.3.2). As a result, the C-recoveries of all aerobic fermentations as well as anaerobic bioreactor fermentations had to equal 100%. The physiological data shows that under aerobic conditions *C. tenuis* and *S. stipitis* produced, besides carbon dioxide and small amounts of glycerol, no by-products, while IBB10B05 formed significant amounts of glycerol ($Y_{\text{glycerol}} = 0.14-0.34 \text{ g g}^{-1}$). *C. tenuis* and *S. stipitis* instead used most xylose for production of biomass ($Y_{\text{xs}} = 0.40-0.64 \text{ g g}^{-1}$ and $0.47-0.63 \text{ g g}^{-1}$, respectively) and carbon dioxide ($Y_{\text{CO}_2} = 0.36-0.79 \text{ g g}^{-1}$ and $0.37-0.66 \text{ g g}^{-1}$, respectively). In contrast to *C. tenuis* and *S. stipitis*, IBB10B05 produced lower amounts of biomass ($Y_{\text{xs}} = 0.29-0.46 \text{ g g}^{-1}$). Furthermore, oxygen and xylose consumption was faster in *C. tenuis* ($q_{\text{O}_2} = 3.23-3.78 \text{ mmol}_{\text{O}_2} \text{ g}_{\text{BM}}^{-1} \text{ h}^{-1}$, $q_{\text{xylose}} = 0.48-0.64 \text{ g g}_{\text{BM}}^{-1} \text{ h}^{-1}$) and *S. stipitis* ($q_{\text{O}_2} = 5.42-8.61 \text{ mmol}_{\text{O}_2} \text{ g}_{\text{BM}}^{-1} \text{ h}^{-1}$, $q_{\text{xylose}} = 0.61-0.75 \text{ g g}_{\text{BM}}^{-1} \text{ h}^{-1}$) compared to IBB10B05 ($q_{\text{O}_2} = 0.83-2.87 \text{ mmol}_{\text{O}_2} \text{ g}_{\text{BM}}^{-1} \text{ h}^{-1}$, $q_{\text{xylose}} = 0.15-0.22 \text{ g g}_{\text{BM}}^{-1} \text{ h}^{-1}$). This was accompanied by a higher μ in those strains. Interestingly, the oxygen demand (a) was quite similar in all three strains, though the one of *C. tenuis* ($0.75-1.17 \text{ mol}_{\text{O}_2} \text{ mol}_{\text{xylose}}^{-1}$) was slightly lower than the ones of IBB10B05 ($0.84-2.00 \text{ mol}_{\text{O}_2} \text{ mol}_{\text{xylose}}^{-1}$) and *S. stipitis* ($1.08-2.12 \text{ mol}_{\text{O}_2} \text{ mol}_{\text{xylose}}^{-1}$). The values of $q_{\text{O}_2\text{calc}}$ and a_{calc} for *C. tenuis* fermentation 2 and of $q_{\text{O}_2\text{meas}}$ and a_{meas} for *S. stipitis* fermentation 1 are expected to be outliers, as these values differ significantly from those of other measurements of q_{O_2} and a performed in this work. Under anaerobic conditions, the physiological behaviour of the yeast

strains changed completely. Here IBB10B05 displayed the fastest conversion of xylose ($q_{\text{xylose}} = 0.36\text{-}0.61 \text{ g g}_{\text{BM}}^{-1} \text{ h}^{-1}$). Xylose consumption in *C. tenuis* ($q_{\text{xylose}} = 0.19 \text{ g g}_{\text{BM}}^{-1} \text{ h}^{-1}$) and *S. stipitis* ($q_{\text{xylose}} = 0.25\text{-}0.62 \text{ g g}_{\text{BM}}^{-1} \text{ h}^{-1}$) was slower. In addition, formation of by-products like xylitol ($Y_{\text{xylitol}} = 0.074\text{-}0.19 \text{ g g}^{-1}$), glycerol ($Y_{\text{glycerol}} = 0.043\text{-}0.08 \text{ g g}^{-1}$) and acetate ($Y_{\text{acetate}} = 0.056\text{-}0.07 \text{ g g}^{-1}$) was higher in IBB10B05. This was also the reason for the lower Y_{ethanol} of IBB10B05 ($Y_{\text{ethanol}} = 0.33\text{-}0.39 \text{ g g}^{-1}$) compared to *C. tenuis* ($Y_{\text{ethanol}} = 0.35\text{-}0.49 \text{ g g}^{-1}$) and *S. stipitis* ($Y_{\text{ethanol}} = 0.41\text{-}0.46 \text{ g g}^{-1}$). *C. tenuis* and *S. stipitis* formed only small amounts of xylitol ($Y_{\text{xylitol}} = 0.02\text{-}0.103 \text{ g g}^{-1}$ and $0.063\text{-}0.10 \text{ g g}^{-1}$, respectively), glycerol ($Y_{\text{glycerol}} = 0.022\text{-}0.052 \text{ g g}^{-1}$ and $0.007\text{-}0.008 \text{ g g}^{-1}$, respectively) and acetate ($Y_{\text{acetate}} = 0.007 \text{ g g}^{-1}$ and $0.015\text{-}0.028 \text{ g g}^{-1}$, respectively). In this context it is important to mention that Y_{ethanol} for *C. tenuis* obtained from anaerobic shake flask cultivations was lower than reported elsewhere ([51]). As a result, the C-recovery of this fermentation was not closed. In general, *C. tenuis*, IBB10B05 and *S. stipitis* consumed 28.43 g, 49.27 g and 18.21 g xylose and produced 6.42 g, 15.71 g and 6.51 g ethanol in 162 h, respectively. These results were obtained from shake flask cultivations.

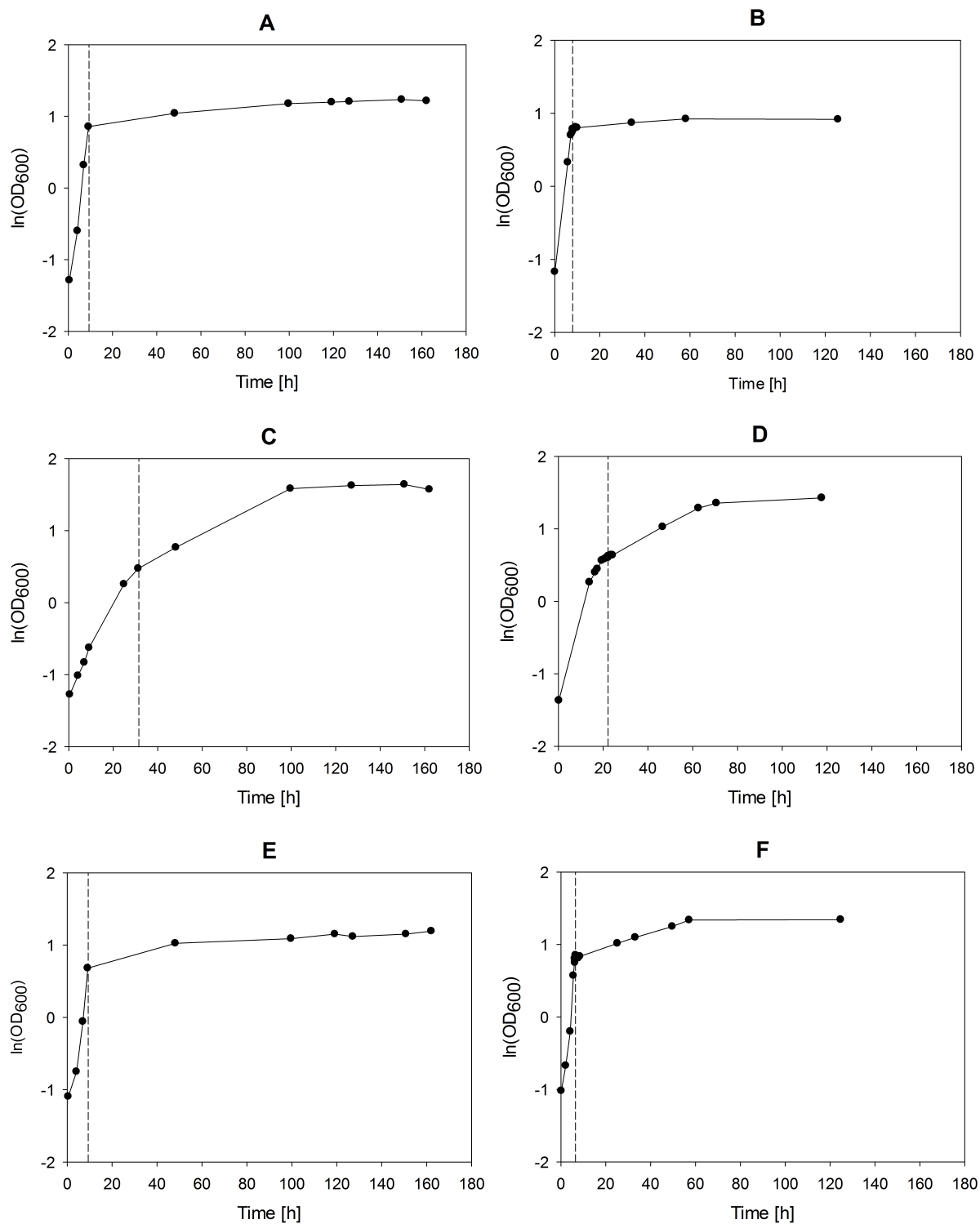


Figure 7-1: Growth characteristic of *C. tenuis*, IBB10B05 and *S. stipitis* on xylose under aerobic and anaerobic conditions. Dotted lines represent time point of switch from aerobic to anaerobic conditions. **Panel A and B** show the growth of *C. tenuis* in shake flask and bioreactor (fermentation 2) cultivations, respectively. **Panel C and D** show the growth of IBB10B05 in shake flask (fermentation 1) and bioreactor (fermentation 1) cultivations, respectively. **Panel E and F** show the growth of *S. stipitis* in shake flask and bioreactor (fermentation 2) cultivations, respectively.

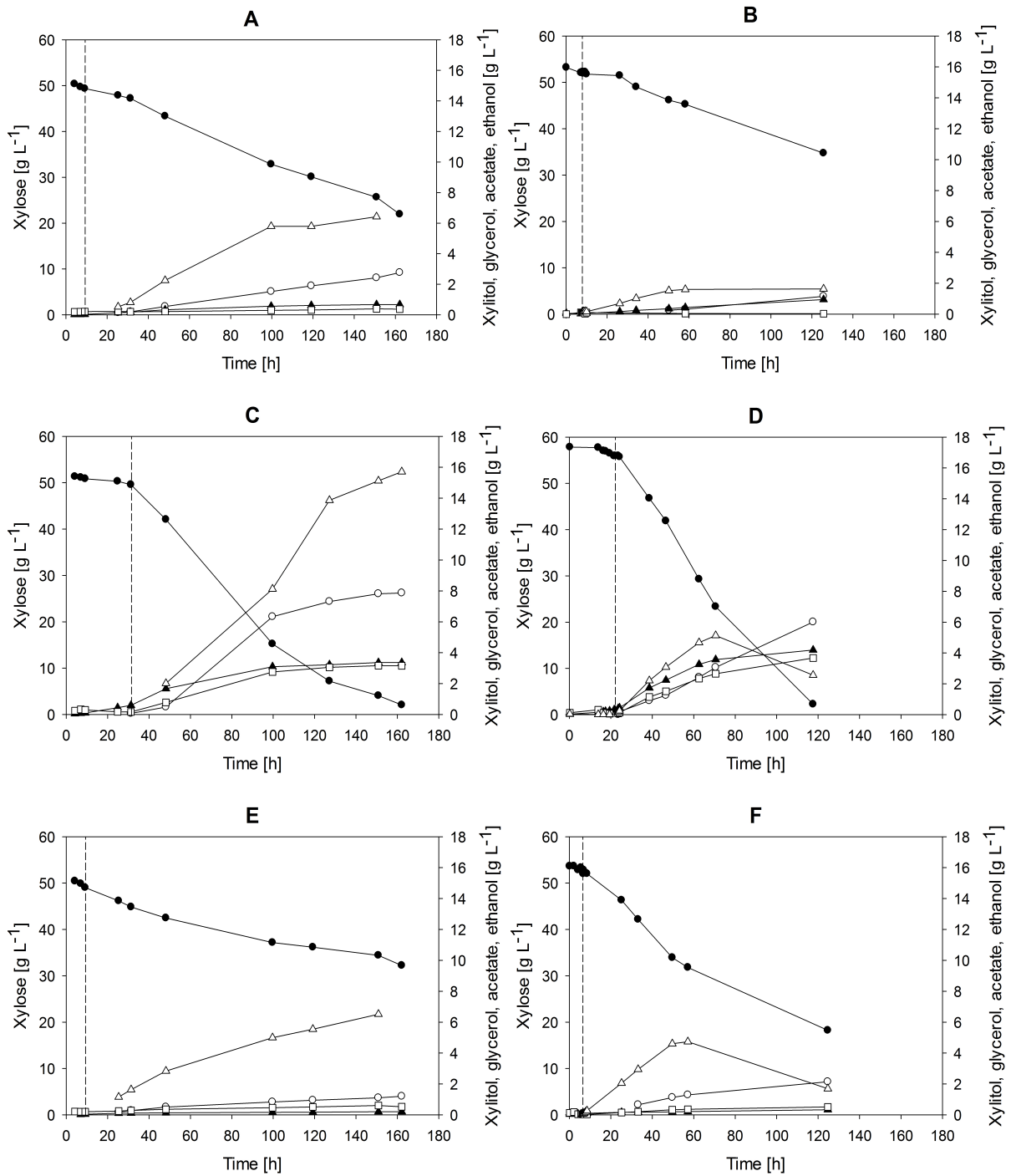


Figure 7-2: Representative time courses of xylose consumption and product formation by *C. tenuis*, IBB10B05 and *S. stipitis*. Full circles, xylose; empty circles, xylitol; full triangles, glycerol; empty squares, acetate; empty triangles, ethanol. Dotted lines represent time point of switch from aerobic to anaerobic conditions. Same panel numbering used as in Figure 7-1.

Table 7-2: Physiological parameters obtained from xylose fermentations of *C. tenuis*, IBB10B05 and *S. stipitis* in aerobic shake flask cultivation.

Parameter ^b	<i>C. tenuis</i>		IBB10B05		<i>S. stipitis</i>
	1 ^a	1 ^a	2 ^a	1 ^a	
μ^c	0.29 ± 0.02	0.054 ± 0.004	0.063 ± 0.003	0.28 ± 0.03	
q_{O2calc}^d	3.78	0.83	2.87	8.61	
a_{calc}^d	1.17	0.84	2.00	2.12	
q_{xylose}^e	0.48	0.15	0.22	0.61	
Y_{XS}^f	0.61 ^j	0.36 ± 0.05	0.29 ± 0.01	0.47 ± 0.05	
$Y_{xylitol}^g$	n.d. ^k	n.d. ^k	n.d. ^k	n.d. ^k	
$Y_{glycerol}^g$	0.01 ^j	0.34 ± 0.05	0.21 ± 0.01	0.01 ^j	
$Y_{acetate}^g$	0.019 ± 0.003	n.d. ^k	n.d. ^k	n.d. ^k	
$Y_{ethanol}^g$	n.d. ^k	n.d. ^k	n.d. ^k	n.d. ^k	
Y_{CO2}^h	0.39	0.36	0.66	0.66	
C-recoveryⁱ	100	100	100	100	

^a Numbering of fermentation.

^b μ , q_{O2} , a , q_{xylose} and $Y_{product}$ are presented as h⁻¹, mmol_{O2} g_{BM}⁻¹ h⁻¹, mol_{O2} mol_{xylose}⁻¹, g_{xylose} g_{BM}⁻¹ h⁻¹ and g_{product} g_{xylose}⁻¹, respectively.

^c μ was determined in the time range from 4.17 h-9.17 h (*C. tenuis*), 7.00 h-31.25 h (IBB10B05 fermentation 1), 3.00 h-30.50 h (IBB10B05 fermentation 2), 4.17 h-9.17 h (*S. stipitis*).

^d q_{O2calc} and a_{calc} were calculated as described in Section 6.3.2.6 method 2.

^e q_{xylose} was calculated as described in Section 6.3.2.5 method 1.

^f Y_{XS} was calculated as described in Section 6.3.2.2 method 1.

^g Y_{PS} were calculated as described in Section 6.3.2.3 method 1.

^h Y_{CO2} was calculated as described in Section 6.3.2.3 method 5.

ⁱ Based on C-moles.

^j Determined from two values, therefore no S.D. given.

^k n.d. not determinable.

Table 7-3: Physiological parameters obtained from xylose fermentations of *C. tenuis*, IBB10B05 and *S. stipitis* in anaerobic shake flask cultivation.

Parameter ^b	<i>C. tenuis</i>		IBB10B05		<i>S. stipitis</i>
	1 ^a	1 ^a	2 ^a	1 ^a	
μ^c	0.005 ^j	0.0161 ± 0.0003	0.0210 ± 0.0002	0.01 ^j	
q_{xylose}^d	0.19	0.40	0.36	0.27	
Y_{XS}^e	0.024 ± 0.004	0.04 ± 0.01	0.06 ⁱ	0.032 ± 0.004	
$Y_{xylitol}^f$	0.103 ± 0.003	0.19 ± 0.02	0.16 ⁱ	0.074 ± 0.002	
$Y_{glycerol}^f$	0.022 ± 0.002	0.043 ± 0.004	0.07 ⁱ	0.007 ± 0.001	
$Y_{acetate}^f$	0.007 ± 0.001	0.06 ± 0.01	0.07 ⁱ	0.028 ± 0.002	
$Y_{ethanol}^f$	0.35 ± 0.01	0.34 ± 0.04	0.33 ⁱ	0.44 ± 0.02	
Y_{CO2}^g	0.34	0.37	0.37	0.44	
C-recovery^h	84	104	105	103	

^a Numbering of fermentation.

^b μ , q_{xylose} and $Y_{product}$ are presented as h⁻¹, g_{xylose} g_{BM}⁻¹ h⁻¹ and g_{product} g_{xylose}⁻¹, respectively.

^c μ was determined in the time range from 9.17 h-48.17 h (*C. tenuis*), 31.25 h-99.67 h (IBB10B05 fermentation 1), 32.38 h-81.05 h (IBB10B05 fermentation 2), 9.17 h-48.17 h (*S. stipitis*).

^d q_{xylose} was calculated as described in Section 6.3.2.5 method 1.

^e Y_{XS} was calculated as described in Section 6.3.2.2 method 1.

^f Y_{PS} were calculated as described in Section 6.3.2.3 method 1.

^g Y_{CO2} was calculated as described in Section 6.3.2.3 method 4.

^h Based on C-moles.

ⁱ Determined from two values, therefore no S.D. given.

Table 7-4: Physiological parameters obtained from xylose fermentations of *C. tenuis*, IBB10B05 and *S. stipitis* in aerobic bioreactor cultivation.

Parameter ^b	<i>C. tenuis</i>		IBB10B05		<i>S. stipitis</i>	
	1 ^a	2 ^a	1 ^a	2 ^a	1 ^a	2 ^a
μ^c	0.32 ± 0.02	0.26 ± 0.01	0.10 ± 0.01	0.102 ± 0.002	0.46 ± 0.04	0.48 ± 0.05
q_{O2meas}^d	3.54	3.23	1.72	2.00	1.71	5.42
q_{O2calc}^e	3.54	11.02	1.71	1.99	5.42	5.42
a_{meas}^f	1.06	0.75	1.23	1.37	0.41	1.08
a_{calc}^e	1.06	2.58	1.23	1.36	1.10	1.08
q_{xylose}^g	0.50	0.64	0.21	0.22	0.74	0.75
Y_{XS}^h	0.64	0.40 ^j	0.46	0.46	0.62	0.63
$Y_{xylitol}^k$	n.d. ⁿ	n.d. ⁿ	n.d. ⁿ	n.d. ⁿ	n.d. ⁿ	n.d. ⁿ
$Y_{glycerol}^i$	0.01	n.d. ^{j,n}	0.17	0.14	0.02	0.01
$Y_{acetate}^k$	n.d. ⁿ	n.d. ⁿ	n.d. ⁿ	n.d. ⁿ	n.d. ⁿ	n.d. ⁿ
$Y_{ethanol}^k$	n.d. ⁿ	n.d. ⁿ	n.d. ⁿ	n.d. ⁿ	n.d. ⁿ	n.d. ⁿ
Y_{CO2}^l	0.36	0.79	0.44	0.47	0.38	0.37
C-recovery^m	100	100	100	100	100	100

^a Numbering of fermentation.

^b μ , q_{O2} , a , q_{xylose} and $Y_{product}$ are presented as h^{-1} , $mmol_{O2} g_{BM}^{-1} h^{-1}$, $mol_{O2} mol_{xylose}^{-1}$, $g_{xylose} g_{BM}^{-1} h^{-1}$ and $g_{product} g_{xylose}^{-1}$, respectively.

^c μ was determined in the time range from 4.00 h-8.25 h (*C. tenuis* fermentation 1), 0.08 h-7.67 h (*C. tenuis* fermentation 2), 0.25 h-21.58 h (IBB10B05 fermentation 1), 0.00 h-17.08 h (IBB10B05 fermentation 2), 4.00 h- 7.00 h (*S. stipitis* fermentation 1), 4.18 h-6.28 h (*S. stipitis* fermentation 2).

^d q_{O2meas} was calculated as described in Section 6.3.2.6 method 1.

^e q_{O2calc} and a_{calc} were calculated as described in Section 6.3.2.6 method 2.

^f a_{meas} was calculated as described in Section 6.3.2.6 method 3.

^g q_{xylose} was calculated as described in Section 6.3.2.5 method 1.

^h Y_{XS} was calculated as described in Section 6.3.2.2 method 2.

ⁱ $Y_{glycerol}$ was calculated as described in Section 6.3.2.3 method 2.

^j Y_{XS} and $Y_{glycerol}$ for 2nd fermentation with *C. tenuis* were calculated as described in Section 6.3.2.2 method 1 and Section 6.3.2.3 method 1, respectively.

^k Y_{PS} were calculated as described in Section 6.3.2.3 method 1.

^l Y_{CO2} was calculated as described in Section 6.3.2.3 method 5.

^m Based on C-moles.

ⁿ n.d. not determinable.

Table 7-5: Physiological parameters obtained from xylose fermentations of *C. tenuis*, IBB10B05 and *S. stipitis* in anaerobic bioreactor cultivation.

Parameter ^b	<i>C. tenuis</i>		IBB10B05		<i>S. stipitis</i>	
	1 ^a	2 ^a	1 ^a	2 ^a	1 ^a	2 ^a
μ ^c	n.d. ^l	n.d. ^l	0.016 ± 0.001	0.015 ± 0.001	0.011 ± 0.001	0.0100 ± 0.0003
q_{xylose} ^d	0.16 ^e	0.14 ^e	0.60	0.61	0.25	0.62
Y_{XS} ^f	n.d. ^l	n.d. ^l	0.027 ± 0.002	0.025 ± 0.002	0.042 ± 0.004	0.016 ± 0.001
$Y_{xylitol}$ ^g	0.02 ^k	0.0791 ± 0.0004	0.11 ± 0.01	0.074 ± 0.003	0.10 ± 0.01	0.063 ± 0.001
$Y_{glycerol}$ ^g	0.022 ± 0.002	0.052 ± 0.002	0.08 ± 0.01	0.07 ± 0.01	0.008 ± 0.001	0.007 ± 0.001
$Y_{acetate}$ ^g	n.d. ^l	n.d. ^l	0.069 ± 0.004	0.056 ± 0.004	0.023 ± 0.005	0.015 ± 0.001
$Y_{ethanol}$ ^h	0.49	0.44	0.36	0.39	0.41	0.46
Y_{CO_2} ⁱ	0.47	0.42	0.39	0.41	0.41	0.45
C-recovery ^j	99	98	102	102	100	100

^a Numbering of fermentation

^b μ , q_{xylose} and $Y_{product}$ are presented as h⁻¹, g_{xylose} g_{BM}⁻¹ h⁻¹ and g_{product} g_{xylose}⁻¹, respectively.

^c μ was determined in the time range from 22.20 h-70.58 h (IBB10B05 fermentation 1), 17.35 h-62.92 h (IBB10B05 fermentation 2), 7.47 h-57.00 h (*S. stipitis* fermentation 1), 6.52 h-57.17 h (*S. stipitis* fermentation 2).

^d q_{xylose} was calculated as described in Section 6.3.2.5 method 1.

^e q_{xylose} for *C. tenuis* was calculated as described in Section 6.3.2.5 method 2.

^f Y_{XS} was calculated as described in Section 6.3.2.2 method 1.

^g Y_{PS} were calculated as described in Section 6.3.2.3 method 1.

^h $Y_{ethanol}$ was calculated as described in Section 6.3.2.3 method 3.

ⁱ Y_{CO_2} was calculated as described in Section 6.3.2.3 method 4.

^j Based on C-moles.

^k Determined from two values, therefore no S.D. given.

^l n.d. not determinable.

7.2 Analysis of intracellular metabolites

64 metabolites of the central carbon metabolism belonging to glycolysis, PPP and TCA as well as AA, energy metabolites and redox cofactors were analyzed for *C. tenuis*, IBB10B05 and *S. stipitis* metabolizing xylose. Metabolite extracts generated from samples withdrawn at 31 predefined time points (see Section 6.2.4.1 Figure 6-1 and Table 6-5) were thereby subjected to quantitative or qualitative metabolite analysis. ¹²C/¹³C ratios were calculated from the automatically integrated peak areas (controlled manually and corrected if miss-integrated) obtained from LC-MS measurements for biological samples and standards. Resultant molar concentrations or normalized response of metabolites were based on the corresponding BM (for calculation of metabolite concentrations see Section 6.3.3). Metabolite time profiles are shown in Figure 7-3 to Figure 7-9 (the first two hours of fermentation) and in Figure 7-10 to Figure 7-16 (the whole fermentation). Abbreviations of metabolites are clarified in Section 9.

7.2.1 Global analysis of LC-MS data

Among the 64 selected metabolites, 54 metabolites could be analyzed either qualitatively or quantitatively. 10 metabolites could not be analyzed at all, because:

- No ^{12}C signals could be detected (ALA and oxaloacetic acid).
- Metabolites showed a very low signal-to-noise ratio (3-methyl 2-oxovaleric acid, citric acid, E4P, fumarate, lactic acid, oxoisovaleric acid, succinate and trehalose). Results were not reliable and affected metabolites therefore not considered in further analysis.

Of the 54 metabolites that could be analyzed either qualitatively or quantitatively, 43 could be quantified individually. 11 metabolites could not be quantified individually, because:

- Metabolites could not be baseline-separated by LC (G1P, G6P, F1P and F6P; R5P and Ru5P; LEU and ILE). They are therefore presented as collective sums HXPs, PXP and XLEU, which were correlated to the integrated area of all corresponding compounds.
- Metabolites were not part of the multi-component standard mixture (MET, mevalonic acid and UTP).

Among the 43 metabolites that could be quantified individually, 39 could be quantified for all three yeast strains. 4 metabolites (6PG, AcCoA, ASN, pyruvic acid) could only be quantified for fermentations with *C. tenuis* and IBB10B05, but not for fermentations with *S. stipitis*. This was because metabolites showed either a low signal-to-noise ratio (6PG and ASN) or because external calibration was not linear (AcCoA and pyruvic acid). For those 4 metabolites only qualitative data presented as normalized response per gram dry cells were determined.

For other metabolites, quantification was feasible, but internal standardization not, as no ^{13}C signals could be detected. This was the case for CYS (*C. tenuis* and IBB10B05), DHAP (IBB10B05 and *S. stipitis*), GLY (*C. tenuis* and IBB10B05) and pyruvic acid (*C. tenuis*). Here ^{12}C data was applied (tagged with an asterisk in the legend of corresponding figures).

For CYS, GLY and PXP only data from *C. tenuis* and IBB10B05, for PEP only data from *C. tenuis* and *S. stipitis* and for SER and T6P only data from IBB10B05 and *S. stipitis* are given, as no ^{12}C signals could be obtained for the remaining yeast strains.

7.2.2 Comparison of intracellular metabolite time profiles of investigated yeasts

Intracellular metabolite time profiles of all three yeasts were compared to analyze the differences in their response on changing oxygen conditions. The whole fermentation period was therefore divided into three major parts: the aerobic phase where oxygen saturation decreased from $pO_2 = 40\%$ to 0% , the first 120 min of the anaerobic phase and the anaerobic phase after the first 120 min until the end of the fermentation.

7.2.2.1 Aerobic phase

Almost all metabolite levels of PPP and glycolysis decreased when switching to anaerobic conditions. Only the pool of Glyc3P and pyruvic acid in *C. tenuis* increased. Metabolite levels of TCA reacted differently. While pools of AcCoA and oxoglutaric acid declined during oxygen decrease, malate rose when shifting to anaerobic conditions. Most AA levels did not change significantly during the switching time phase. Only the pool of ASP dropped notably. AMP, ADP, GMP and GDP levels increased during switch, while the level of ATP and GTP fell. As a consequence, both the adenylate and guanylate energy charges (AEC and GEC, respectively) decreased from about ~ 0.9 to $\sim 0.4-0.5$ in native yeasts and from ~ 0.9 to ~ 0.7 in IBB10B05. NAD^+ and $NADP^+$ pools remained at approximately the same level, whereas the one of NADPH decreased slightly and the one of NADH increased. Furthermore UDP-glucose and UTP levels dropped when shifting to anaerobic conditions.

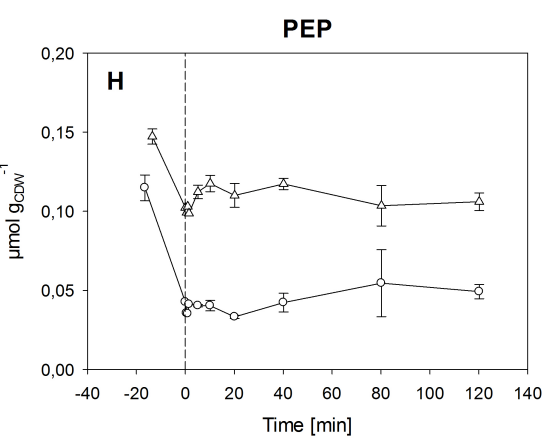
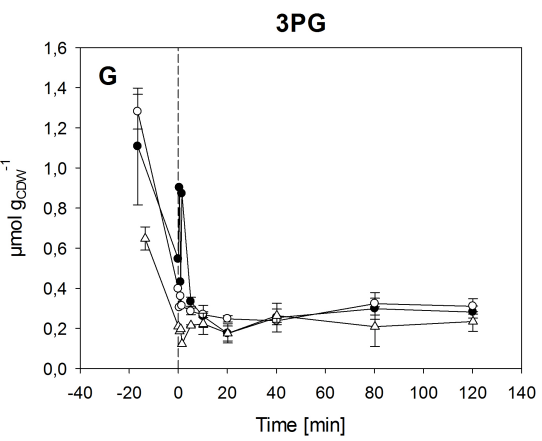
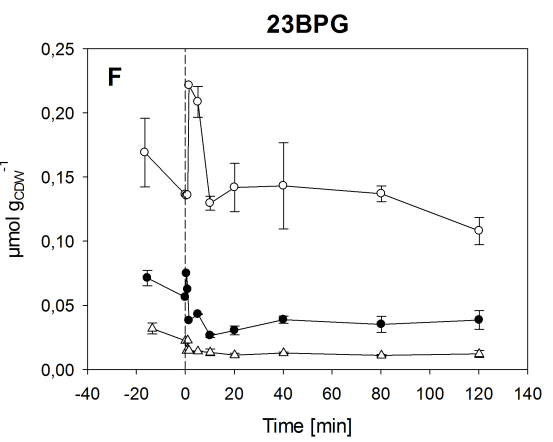
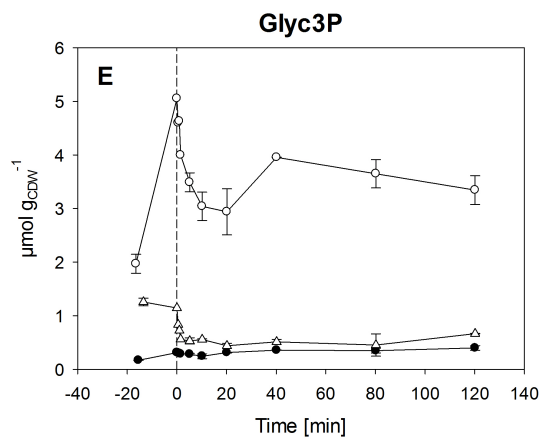
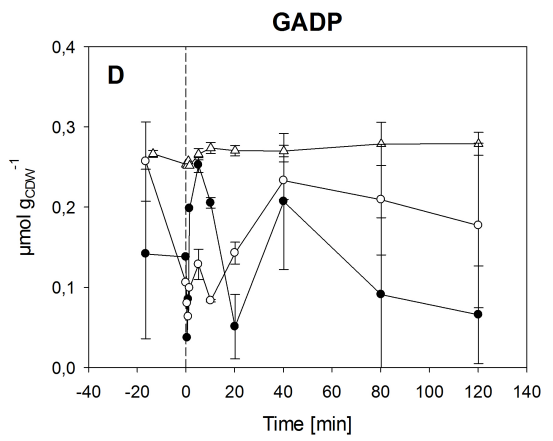
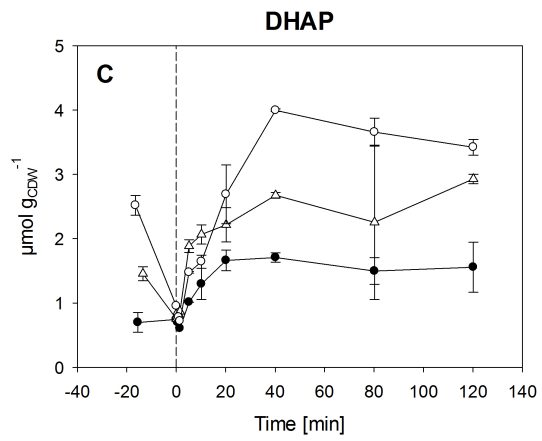
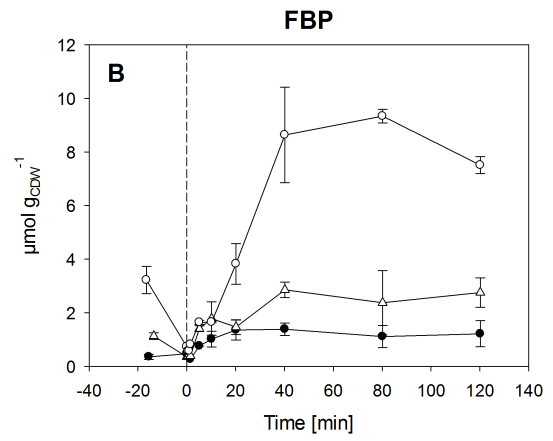
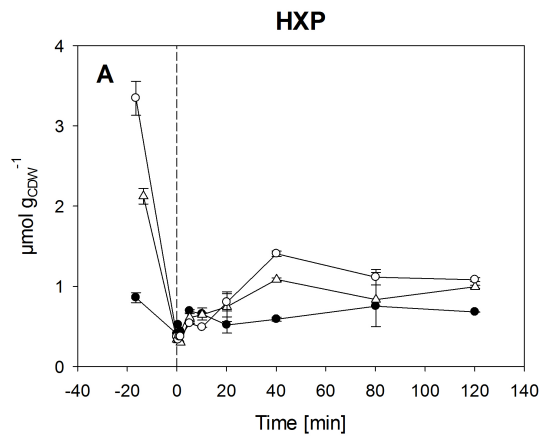
7.2.2.2 Anaerobic phase - first 120 min

After the switch most metabolite levels of glycolysis remained at a constant level. Only pools of DHAP and FBP increased directly after switch, especially for *C. tenuis*. After 20-40 min of anaerobic fermentation, they reached a stable level. The pool of Glyc3P in *C. tenuis* decreased immediately after transition and got to a constant niveau after about 40 min. Metabolite pools of PPP leveled out after switch, apart from the PXP level in IBB10B05, which started to rise after about 10 min until it reached a stable niveau after 20 min. Metabolite pools of TCA reacted again in a different manner. While levels of AcCoA and oxoglutaric acid remained nearly constant after switch, malate dropped. Levels of aromatic AA (PHE, TRP and TYR) started to rise after 20-40 min after switch in IBB10B05, while they did not change over time in native xylose-fermenting yeasts. GLN and GLU levels increased in natural xylose-utilizing yeasts and reached a constant niveau after 20 min. In IBB10B05, concentrations of GLN and GLU dropped until they began to rise after 10 min. ARG, HIS and PRO pools in *C. tenuis* increased and settled down after 40 h of anaerobic fermentation. The level of ASP decreased in native yeasts, while it increased in IBB10B05. After 10 min, it reached a stable niveau. SER and THR levels dropped in *S. stipitis* and increased in *C. tenuis*, whereas they fell in IBB10B05 directly after switch and started to increase after 10

min. The pool of MET rose in native xylose-fermenting yeasts and did not change in IBB10B05. AMP, ADP, GMP and GDP levels declined until they reached a stable niveau after 10 min. ATP and GTP levels rose directly after switch and stayed constant after about 10 min. The AEC and GEC rose to ~0.6-0.7 in native yeasts and to ~0.8 in IBB10B05. After reaching this level, the energy charges (EC) did not change anymore. The level of NAD⁺ in IBB10B05 remained stable, while it increased in *C. tenuis* and *S. stipitis* until it reached its constant niveau after 40 min. The pool of NADH stayed relatively stable in all three yeast strains over the first 120 min after switch. NADP⁺ and NADPH levels rose in IBB10B05 immediately after shift and reached after 40 min their aerobic starting level. In contrast, levels of NADP⁺ and NADPH declined in *C. tenuis* and *S. stipitis* and remained then low over time. Pools of mevalonic acid and UDP-glucose increased in native xylose-fermenting yeasts, while they stayed stable in recombinant IBB10B05.

7.2.2.3 Anaerobic phase - 120 min until fermentation end

Pools of glycolytic metabolites stayed at approximately the same level apart from Glyc3P and HXPs, which rose in *C. tenuis*. Levels of PPP-metabolites remained also at a constant niveau, except for S7P, which fell in IBB10B05. Most TCA-metabolite levels stayed stable. Only the malate level in *C. tenuis* increased. Aromatic AA rose in *C. tenuis* and IBB10B05, while they stayed at a stable level in *S. stipitis*. Pools of GLY, HIS and XLEU increased in IBB10B05 and *C. tenuis*, but remained steady in *S. stipitis*. ARG, ASP, citrulline, GLN, GLU, PRO, THR and VAL levels rose only in IBB10B05, while in natural yeast strains these pools remained constant. The ornithine pool increased only in *S. stipitis*, while the one of ASN rose in *S. stipitis* and IBB10B05. The MET level dropped in native xylose-fermenting yeasts and stayed constant in IBB10B05. AMP and ADP levels in IBB10B05 started to rise after about 20 h of anaerobic fermentation, while they remained constant in native xylose-utilizing yeasts. ATP, GMP, GDP and GTP levels stayed stable in all three yeast strains. Redox cofactors levels remained constant in all three yeasts. The UTP level increased in IBB10B05 and stayed constant in native yeasts. In contrast the pool of UDP-glucose rose in *C. tenuis* and *S. stipitis* and stayed stable in IBB10B05. The level of mevalonic acid declined in native yeasts and remained steady in IBB10B05.



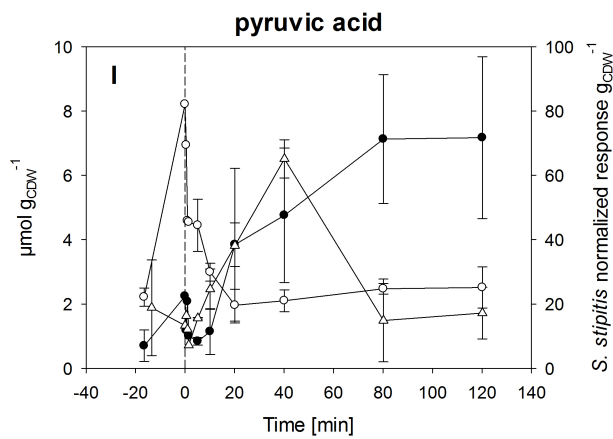


Figure 7-3: Intracellular metabolite time profiles aerobic and 120 min anaerobic - glycolysis. Empty circles, *C. tenuis*; full circles, IBB10B05; empty triangles, *S. stipitis*. Dotted lines represent time point of switch from aerobic to anaerobic conditions. **Panel A and G:** *C. tenuis* 2, IBB10B05 1 and *S. stipitis* 2. **Panel B, C, E and F:** *C. tenuis* 2, IBB10B05 2 and *S. stipitis* 2. **Panel D:** *C. tenuis* 2, IBB10B05 1* and *S. stipitis* 2*. **Panel H:** *C. tenuis* 2 and *S. stipitis* 2. **Panel I:** *C. tenuis* 2*, IBB10B05 1 and *S. stipitis* 2. An asterisk (*) indicates that ^{12}C data was applied. For *S. stipitis* fermentation 2 no physiological data recorded.

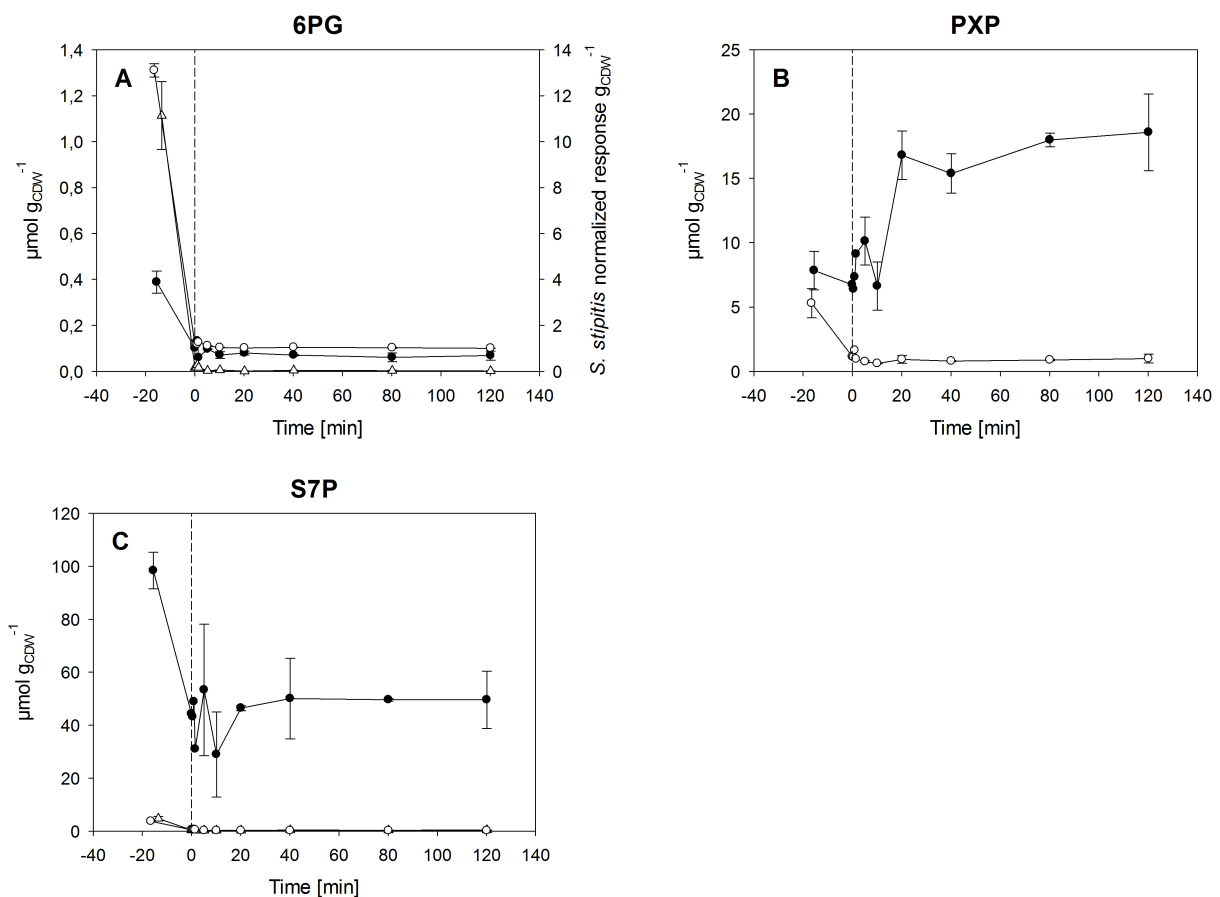


Figure 7-4: Intracellular metabolite time profiles aerobic and 120 min anaerobic - PPP. Empty circles, *C. tenuis*; full circles, IBB10B05; empty triangles, *S. stipitis*. Dotted lines represent time point of switch from aerobic to anaerobic conditions. **Panel A and C:** *C. tenuis* fermentation 2, IBB10B05 2, *S. stipitis* 2. **Panel B:** *C. tenuis* 2 and IBB10B05 2. For *S. stipitis* fermentation 2 no physiological data recorded.

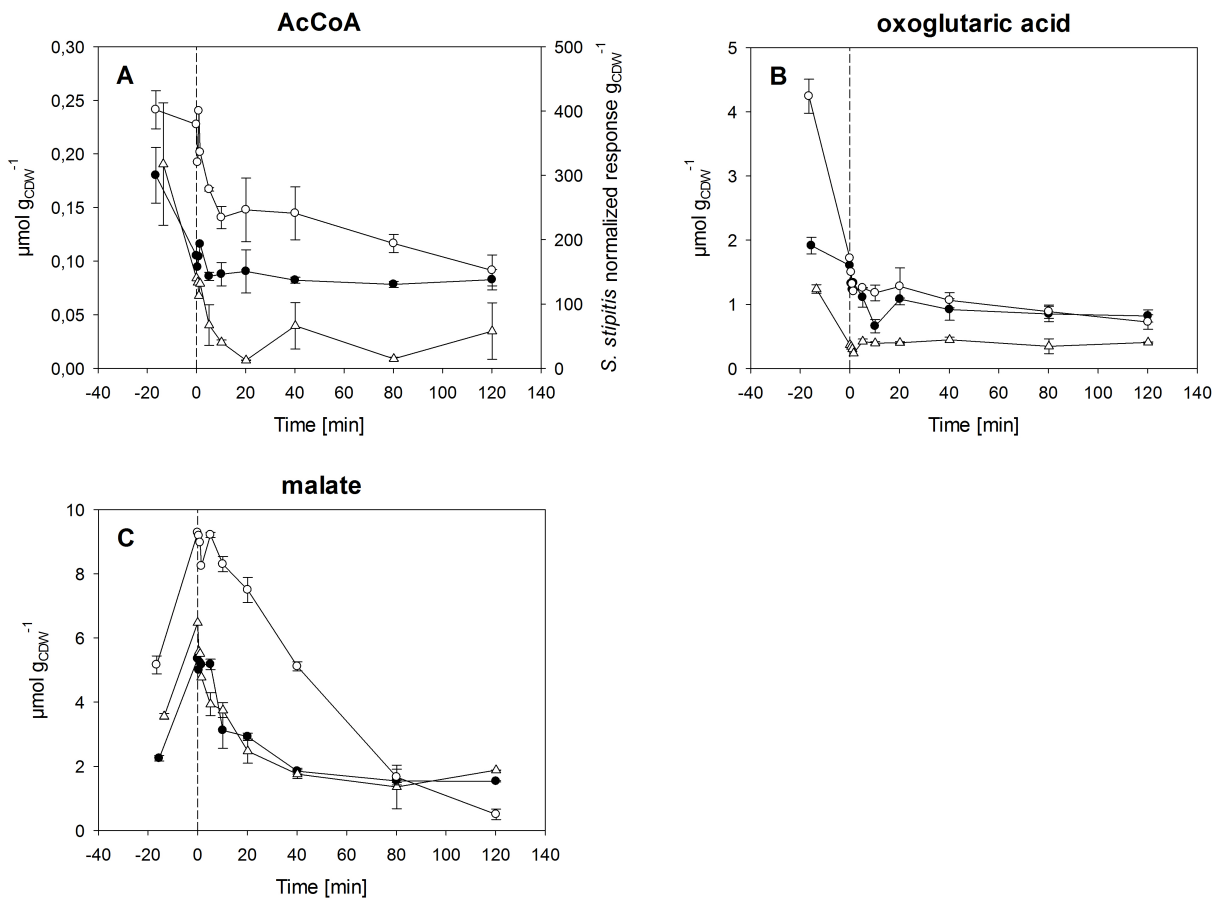
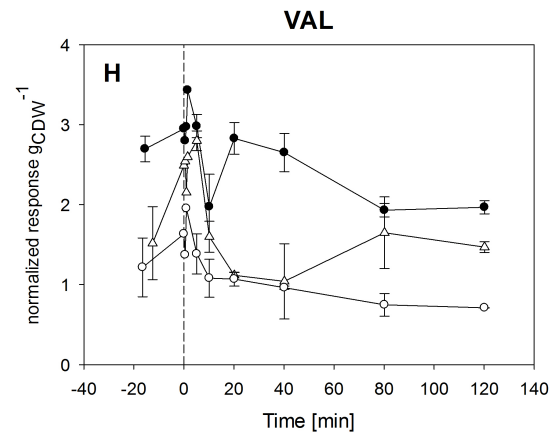
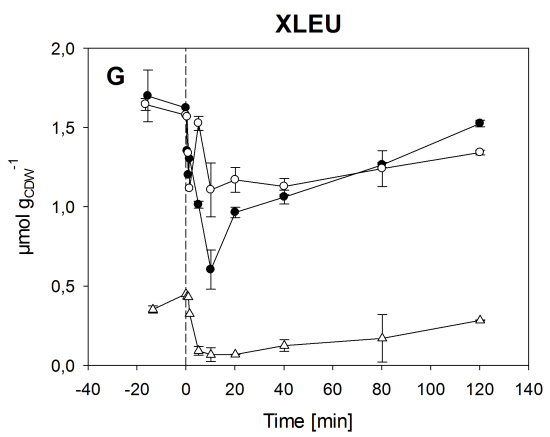
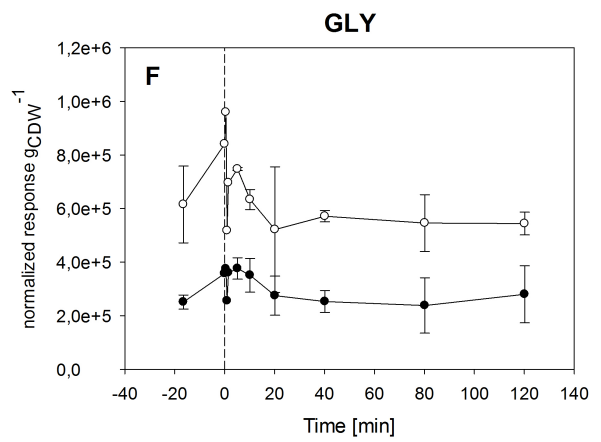
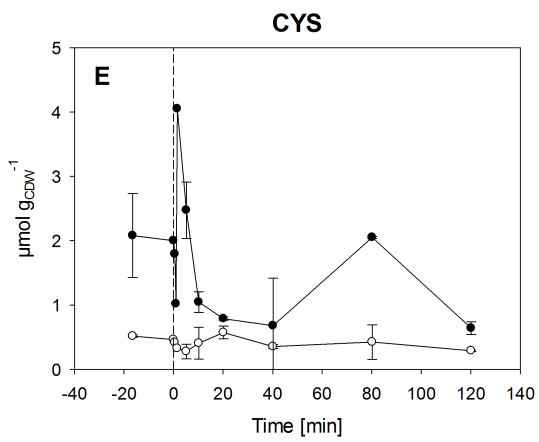
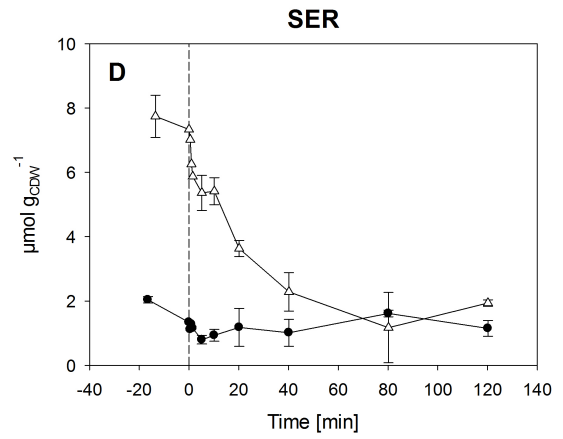
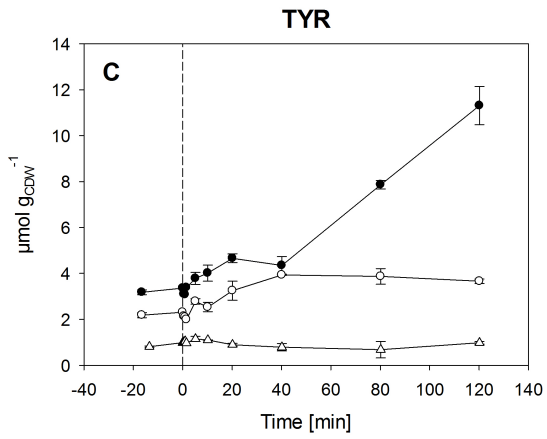
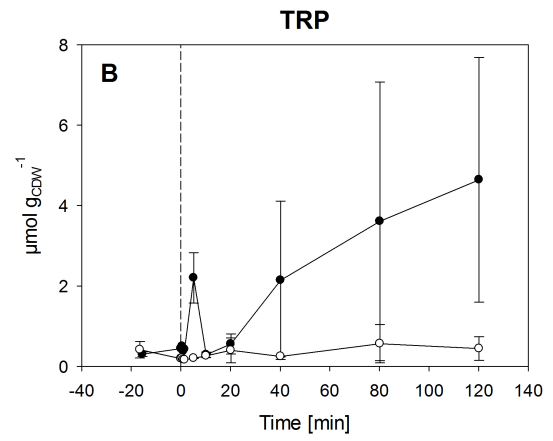
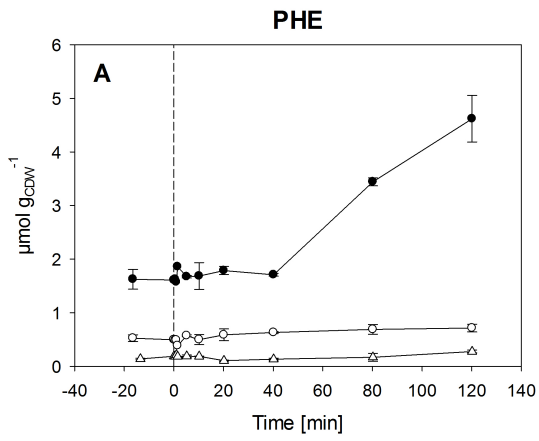
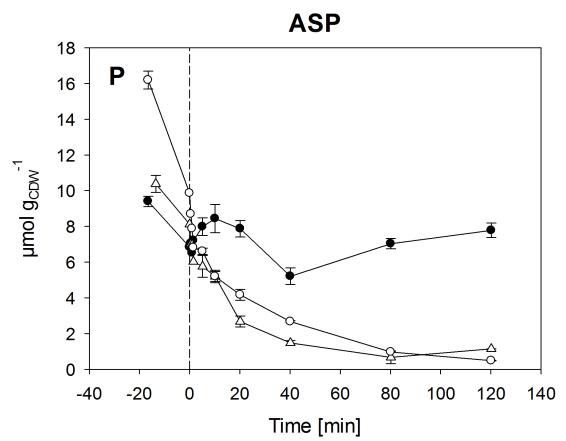
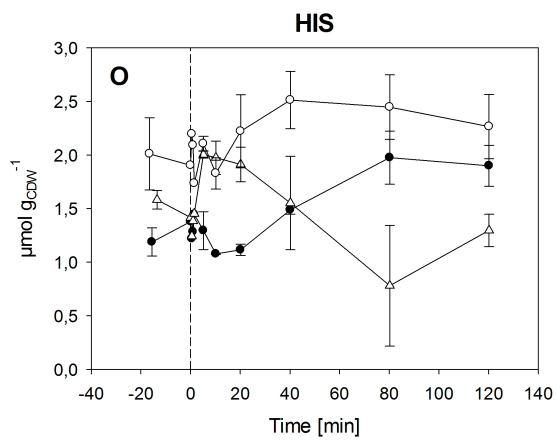
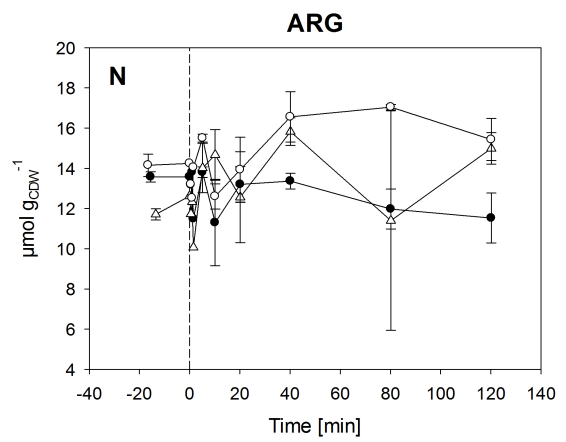
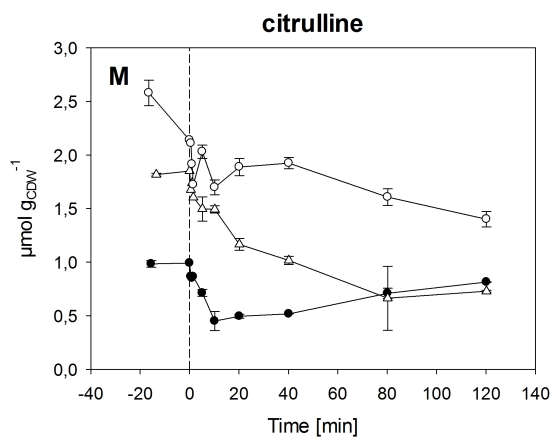
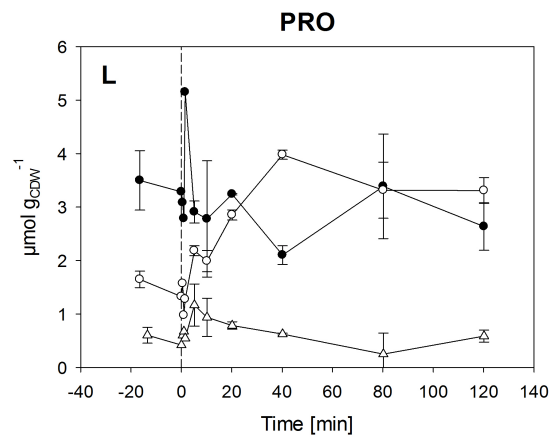
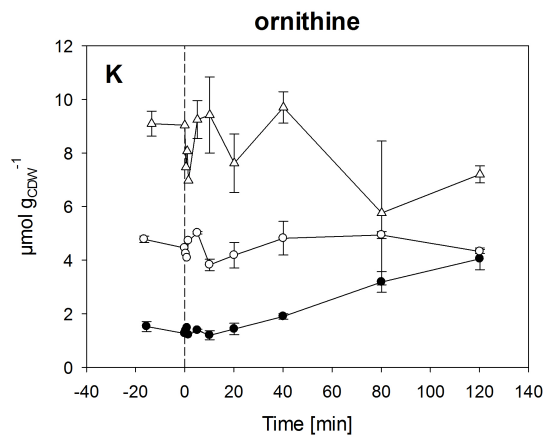
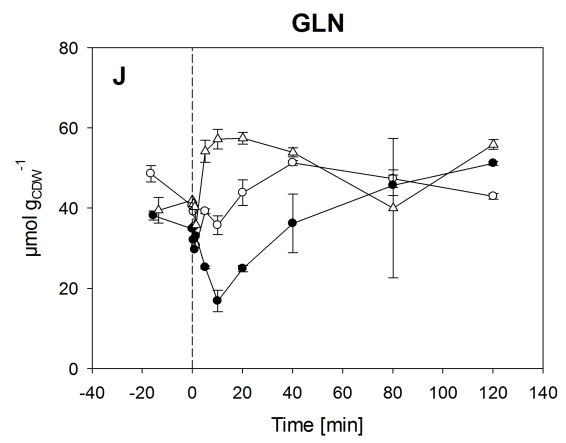
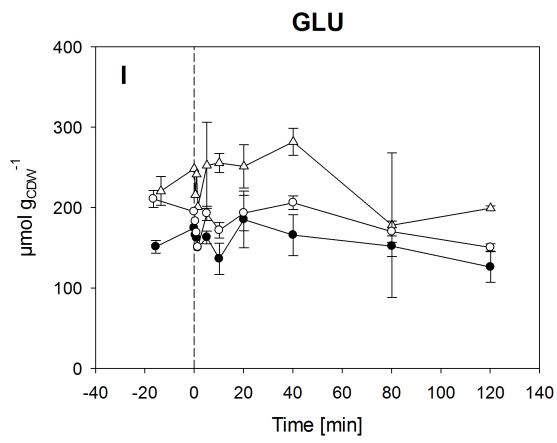


Figure 7-5: Intracellular metabolite time profiles aerobic and 120 min anaerobic - TCA. Empty circles, *C. tenuis*; full circles, IBB10B05; empty triangles, *S. stipitis*. Dotted lines represent time point of switch from aerobic to anaerobic conditions. **Panel A:** *C. tenuis* 2, IBB10B05 1 and *S. stipitis* 2. **Panel B and C:** *C. tenuis* 2, IBB10B05 2 and *S. stipitis* 2. For *S. stipitis* fermentation 2 no physiological data recorded.





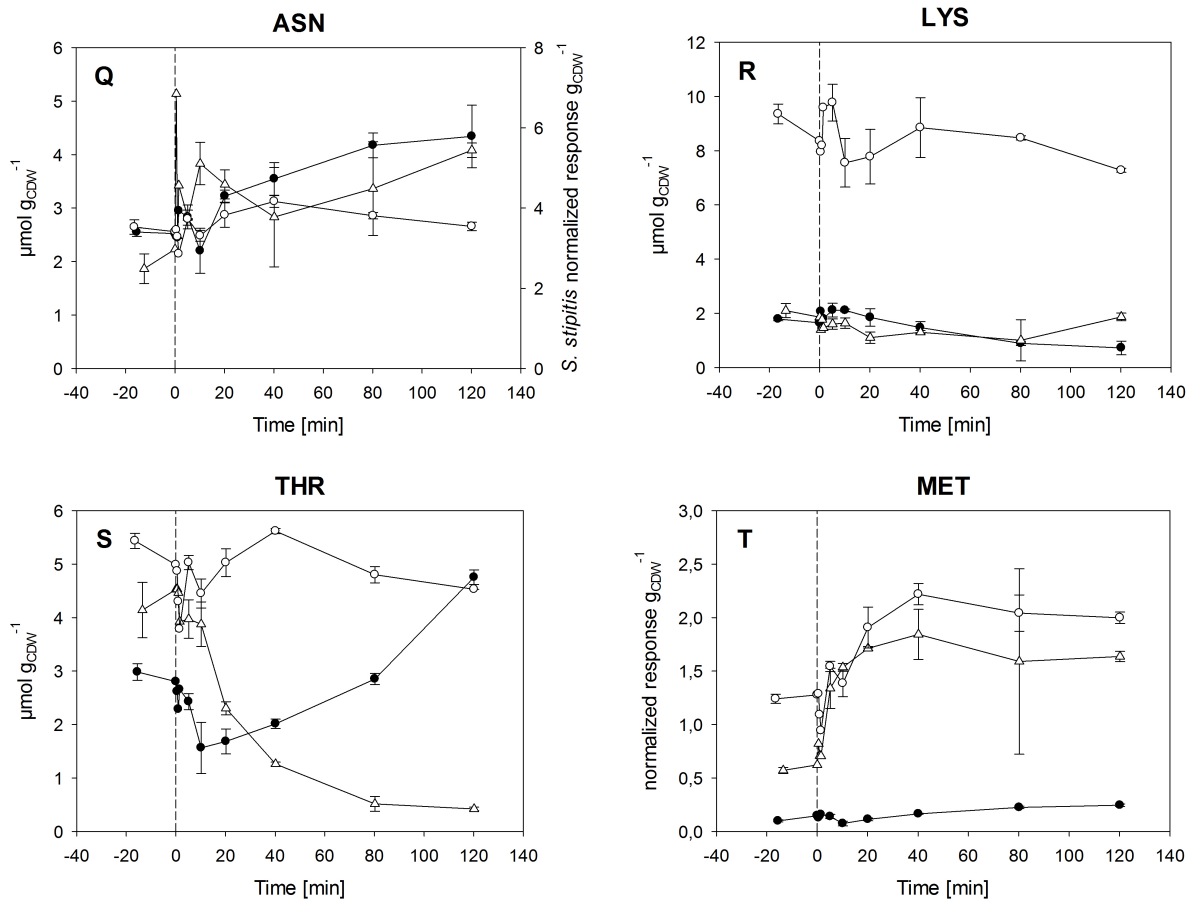
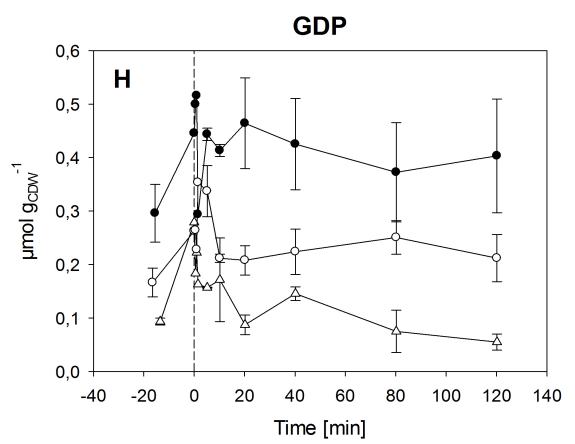
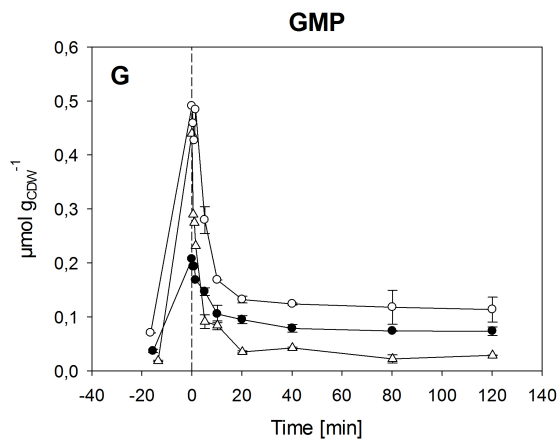
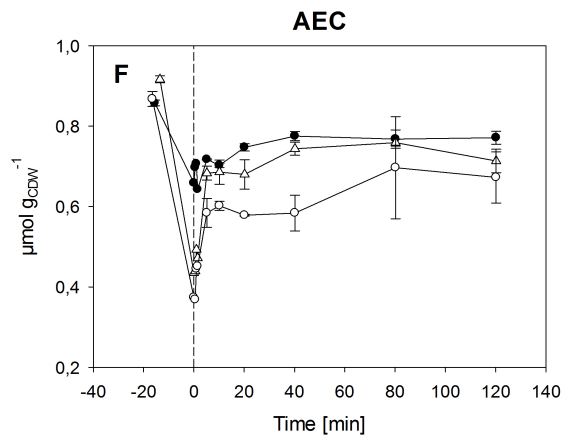
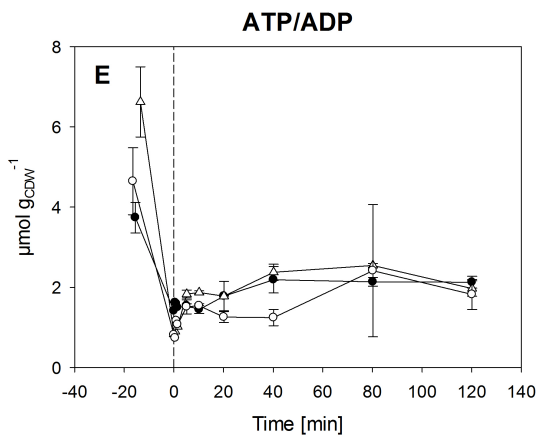
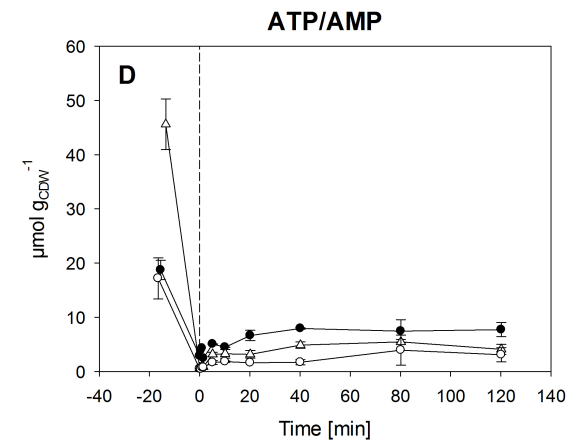
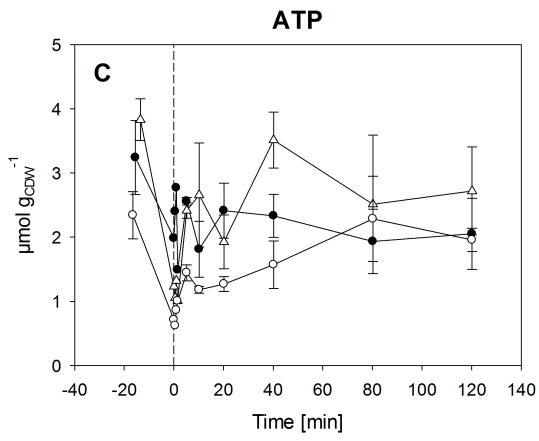
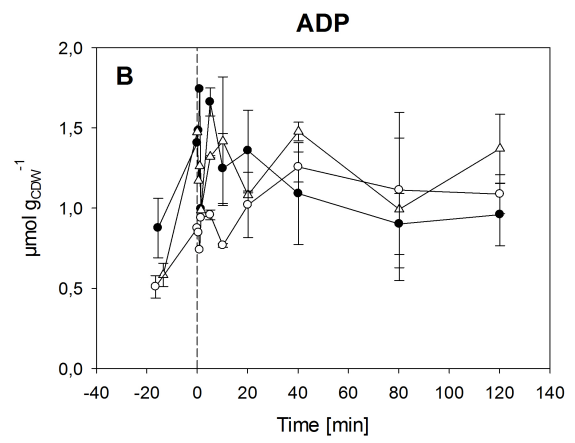
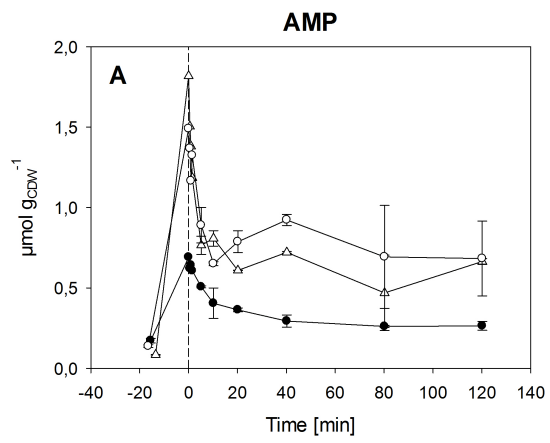


Figure 7-6: Intracellular metabolite time profiles aerobic and 120 min anaerobic - AA. Empty circles, *C. tenuis*; full circles, IBB10B05; empty triangles, *S. stipitis*. Dotted lines represent time point of switch from aerobic to anaerobic conditions. **Panel A, C, L, P and R:** *C. tenuis* 2, IBB10B05 1 and *S. stipitis* 2. **Panel B:** *C. tenuis* 2 and IBB10B05 2. **Panel D:** IBB10B05 1 and *S. stipitis* 2. **Panel E and F:** *C. tenuis* 2* and IBB10B05 1*. **Panel G, I, J, K, M, N, O, S and T:** *C. tenuis* 2, IBB10B05 2 and *S. stipitis* 2. **Panel H:** *C. tenuis* 1, IBB10B05 2 and *S. stipitis* 1. Panel Q: *C. tenuis* 2, IBB10B05 2 and *S. stipitis* 1. An asterisk (*) indicates that ¹²C data was applied. For *S. stipitis* fermentation 2 no physiological data recorded.



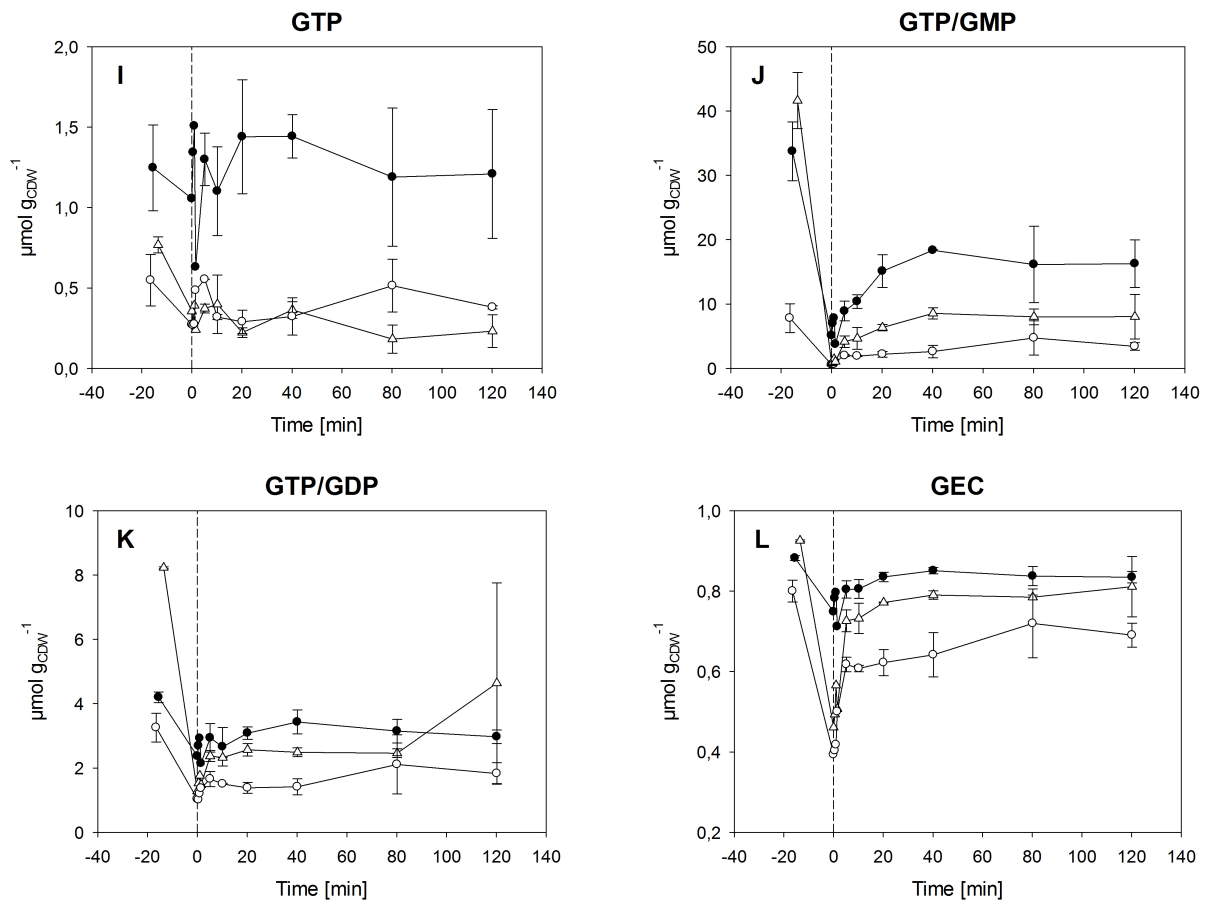


Figure 7-7: Intracellular metabolite time profiles aerobic and 120 min anaerobic - energy metabolites. Empty circles, *C. tenuis*; full circles, IBB10B05; empty triangles, *S. stipitis*. Dotted lines represent time point of switch from aerobic to anaerobic conditions. **All Panels:** *C. tenuis* 2, IBB10B05 2 and *S. stipitis* 2. For *S. stipitis* fermentation 2 no physiological data recorded.

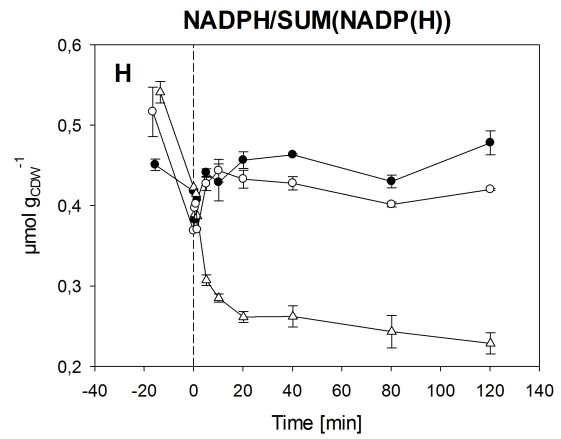
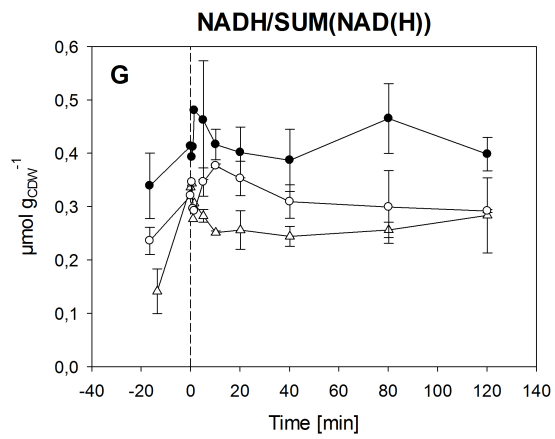
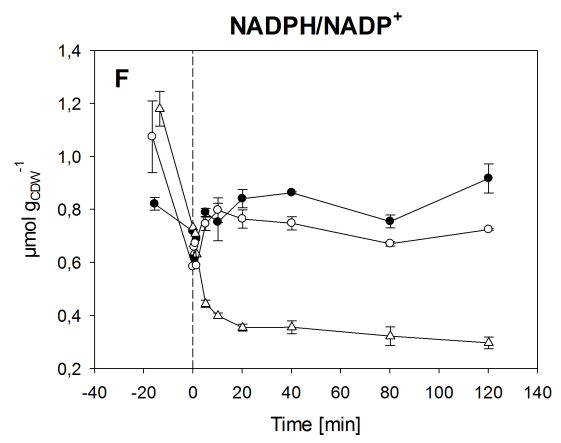
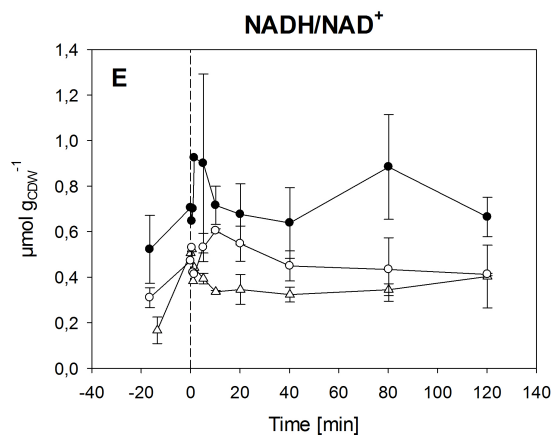
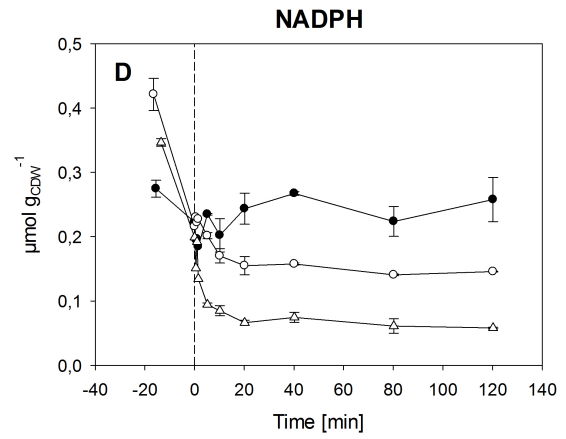
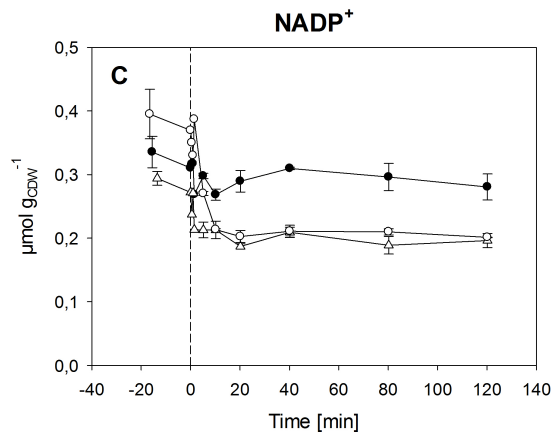
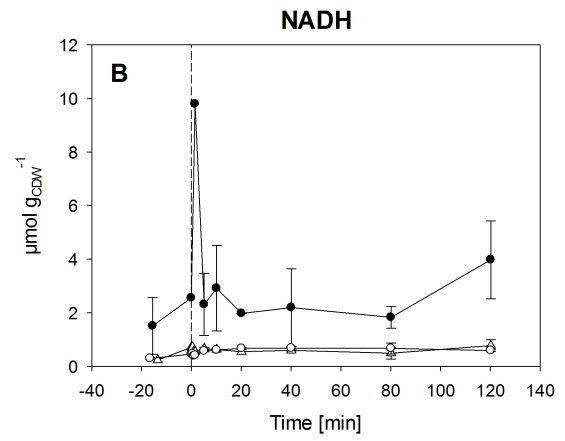
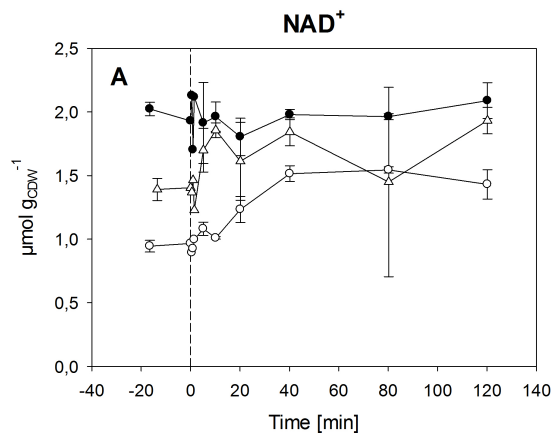


Figure 7-8: Intracellular metabolite time profiles aerobic and 120 min anaerobic - redox cofactors. Empty circles, *C. tenuis*; full circles, IBB10B05; empty triangles, *S. stipitis*. Dotted lines represent time point of switch from aerobic to anaerobic conditions. **Panel A, E and G:** *C. tenuis* 2, IBB10B05 1 and *S. stipitis* 2. **Panel B, C, D, F and H:** *C. tenuis* 2, IBB10B05 2 and *S. stipitis* 2. For *S. stipitis* fermentation 2 no physiological data recorded.

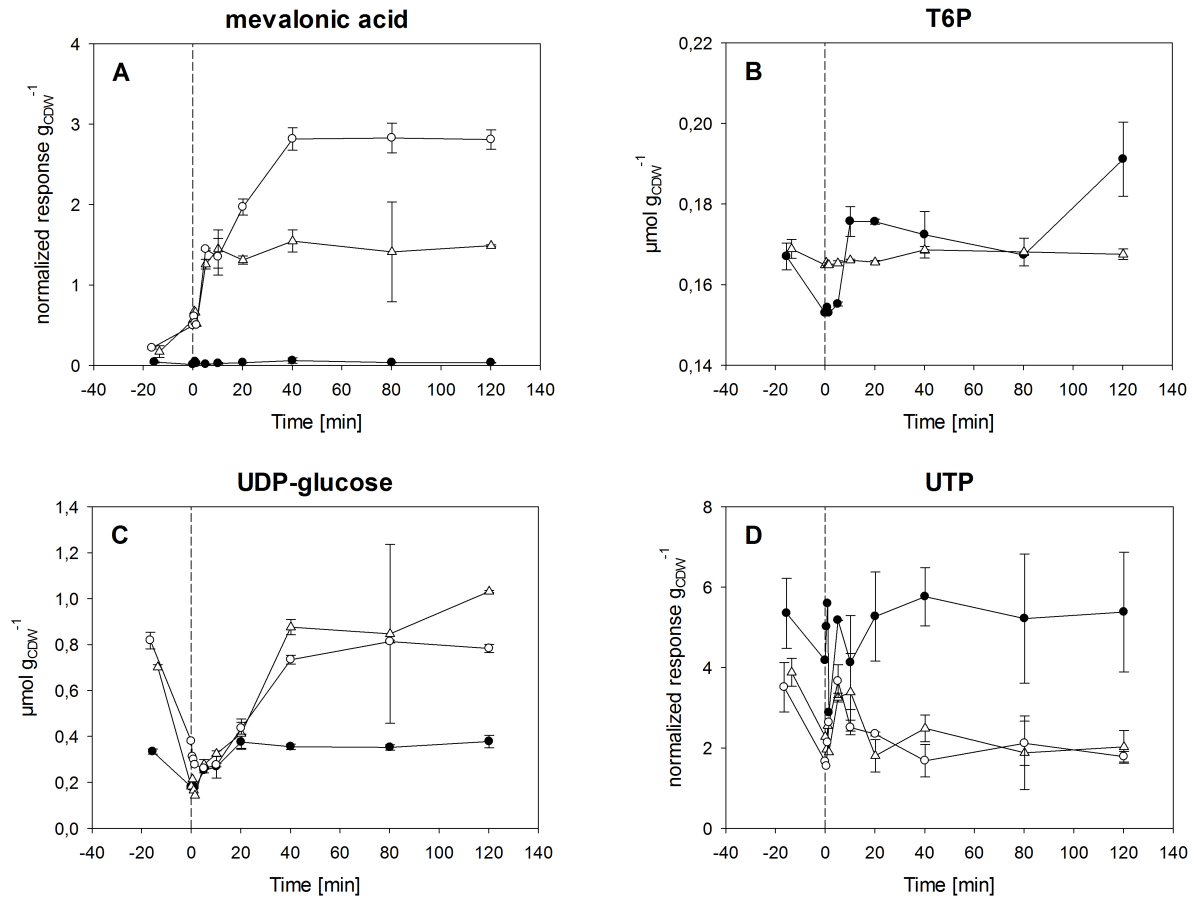
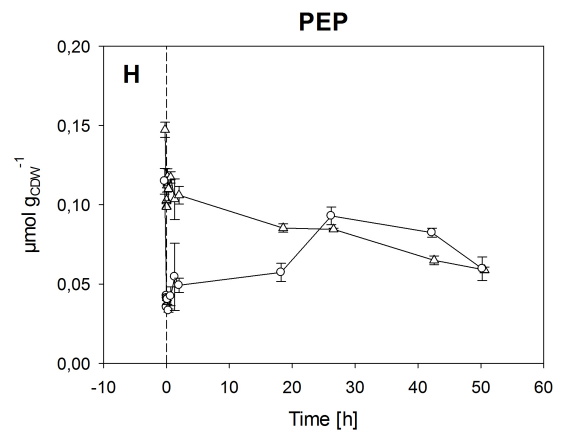
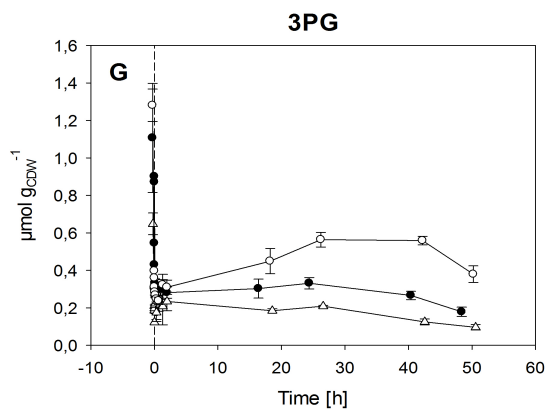
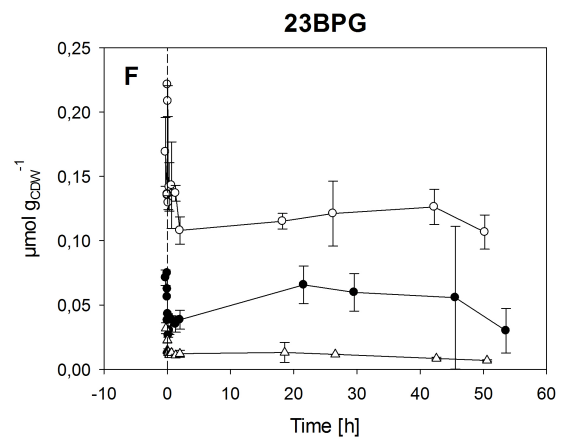
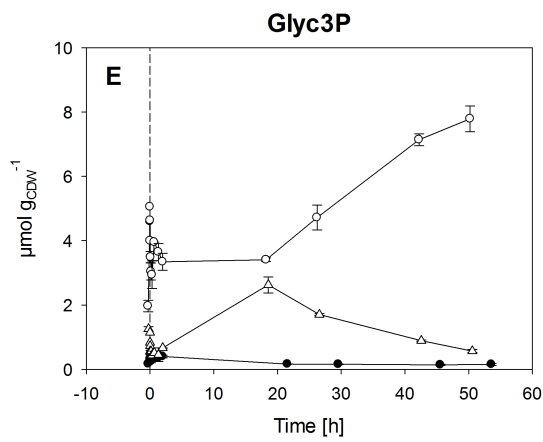
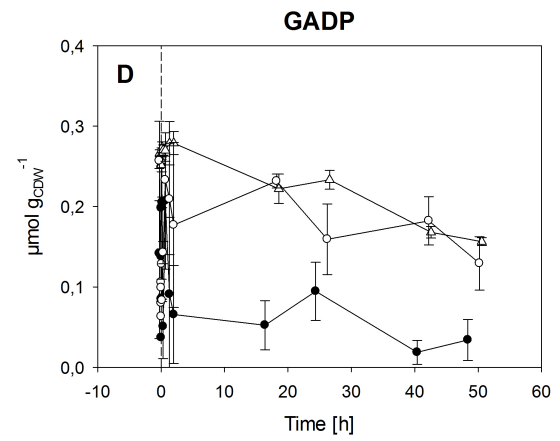
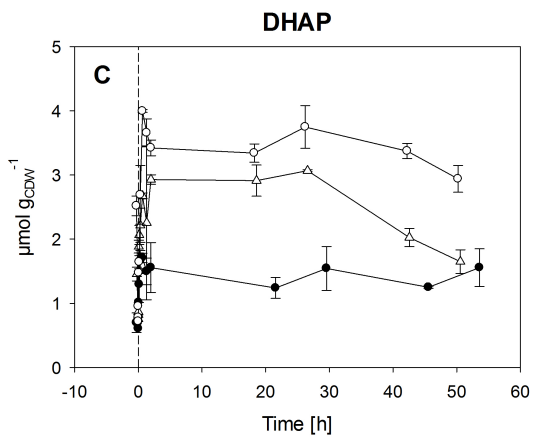
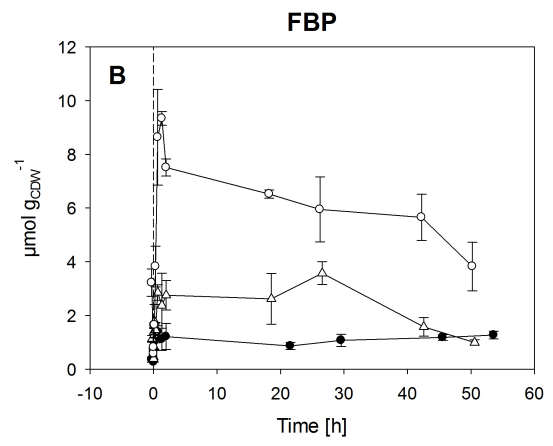
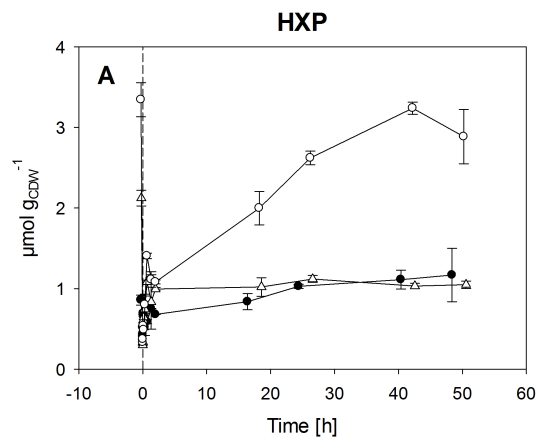


Figure 7-9: Intracellular metabolite time profiles aerobic and 120 min anaerobic - others. Empty circles, *C. tenuis*; full circles, IBB10B05; empty triangles, *S. stipitis*. Dotted lines represent time point of switch from aerobic to anaerobic conditions. **Panel A, C and D:** *C. tenuis* 2, IBB10B05 2 and *S. stipitis* 2. **Panel B:** IBB10B05 2 and *S. stipitis* 2. For *S. stipitis* fermentation 2 no physiological data recorded.



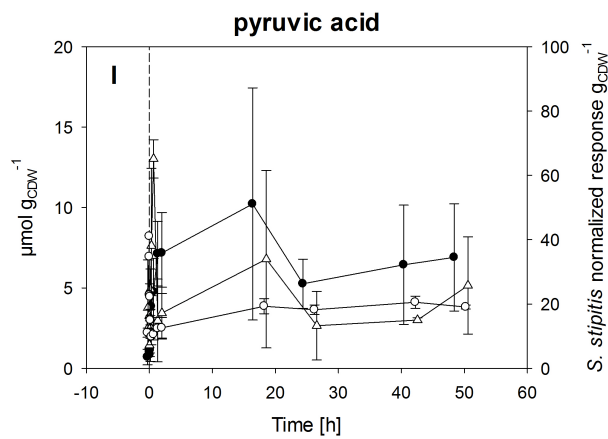


Figure 7-10: Intracellular metabolite time profiles whole fermentation - glycolysis. Empty circles, *C. tenuis*; full circles, IBB10B05; empty triangles, *S. stipitis*. Dotted lines represent time point of switch from aerobic to anaerobic conditions. Same panel numbering used as in Figure 7-3. For *S. stipitis* fermentation 2 no physiological data recorded.

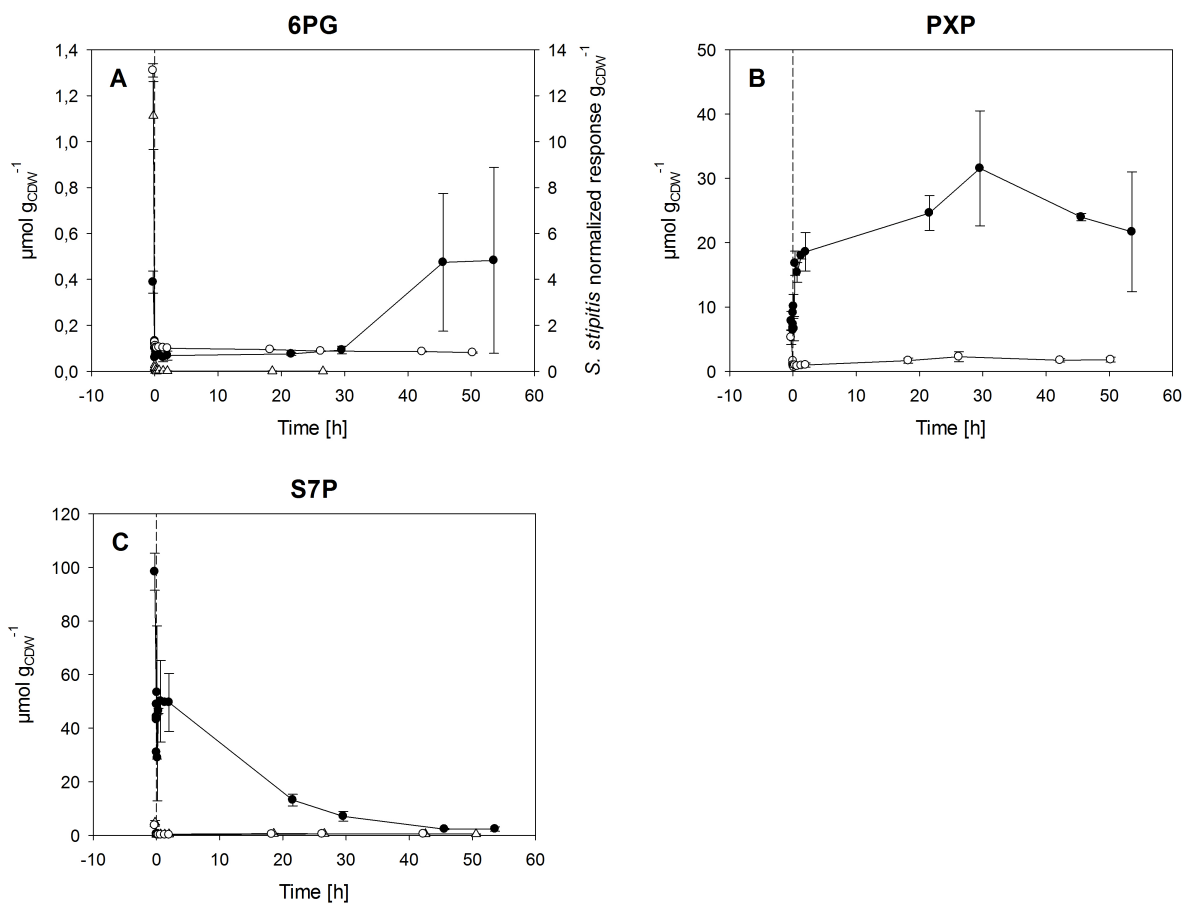


Figure 7-11: Intracellular metabolite time profiles whole fermentation - PPP. Empty circles, *C. tenuis*; full circles, IBB10B05; empty triangles, *S. stipitis*. Dotted lines represent time point of switch from aerobic to anaerobic conditions. Same panel numbering used as in Figure 7-4. For *S. stipitis* fermentation 2 no physiological data recorded.

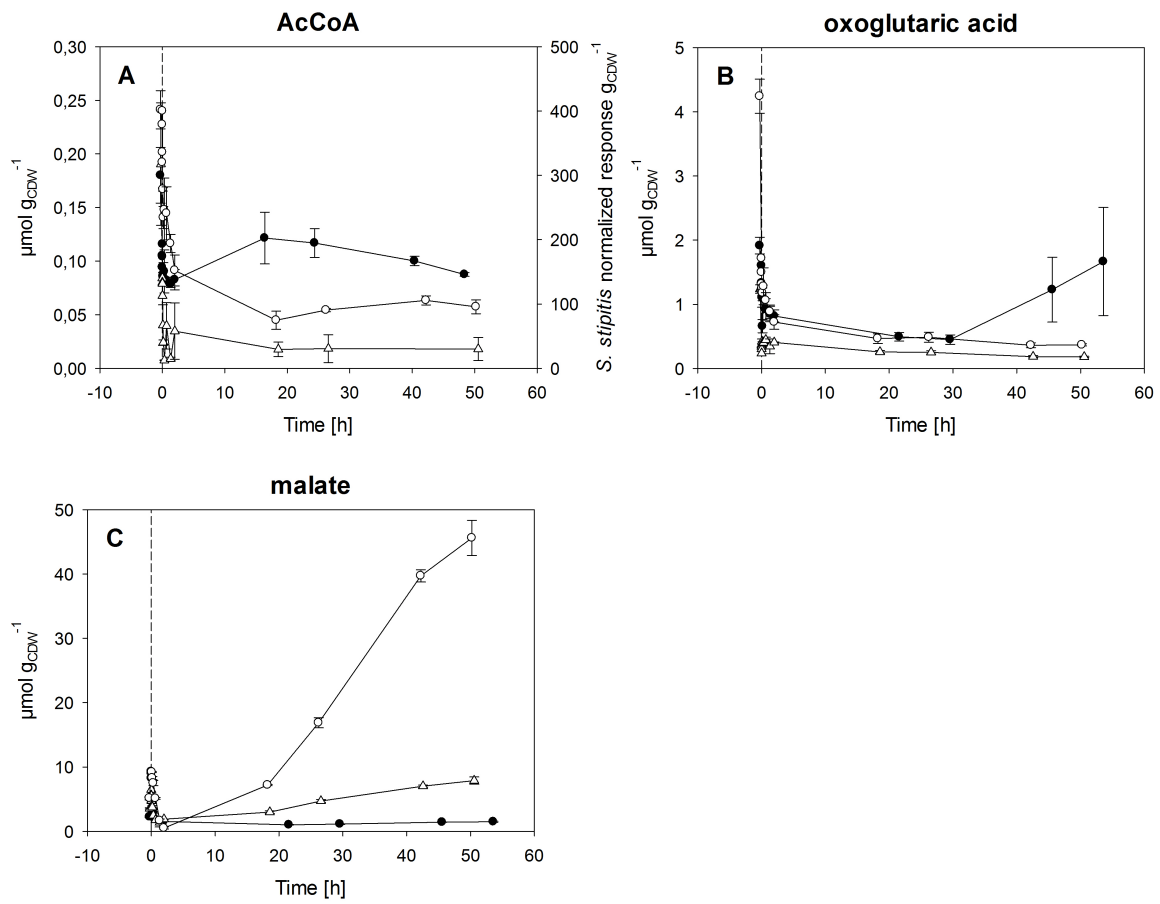
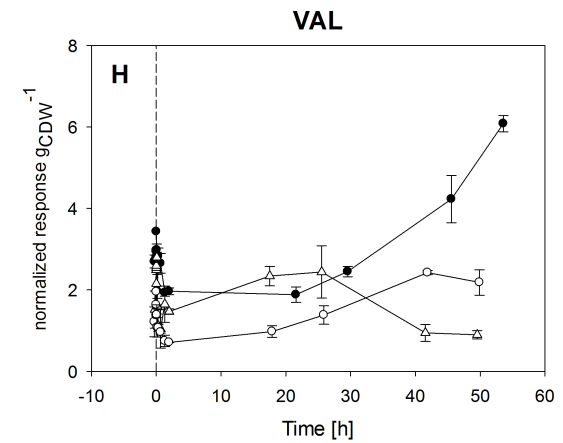
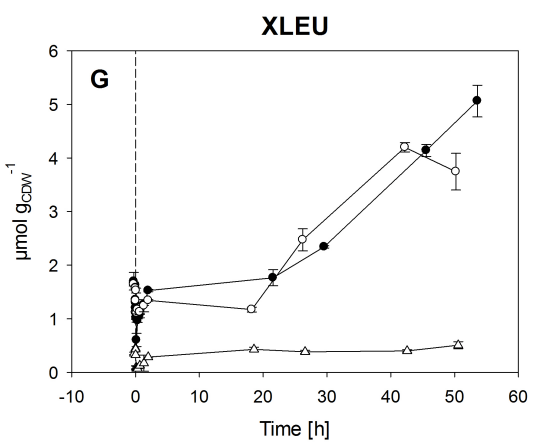
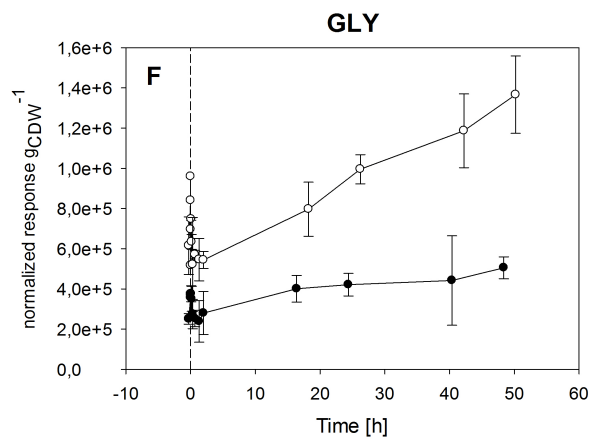
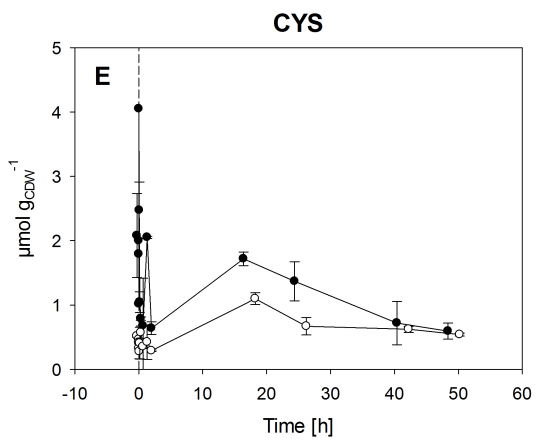
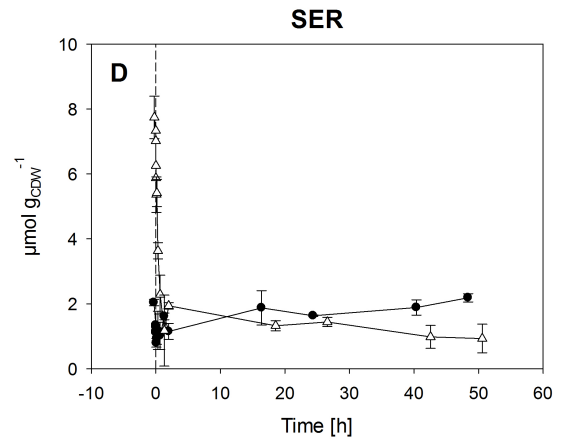
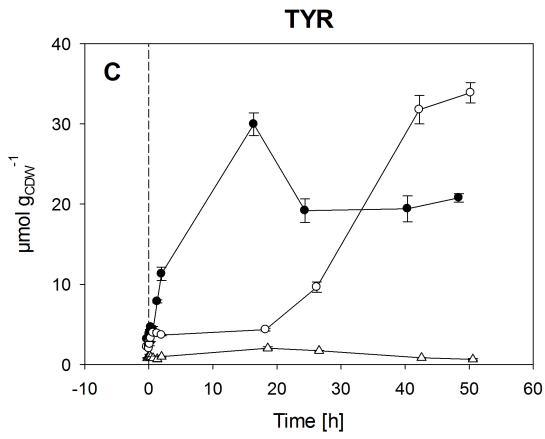
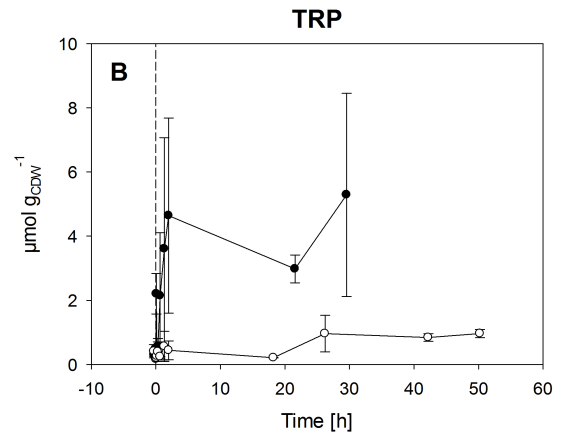
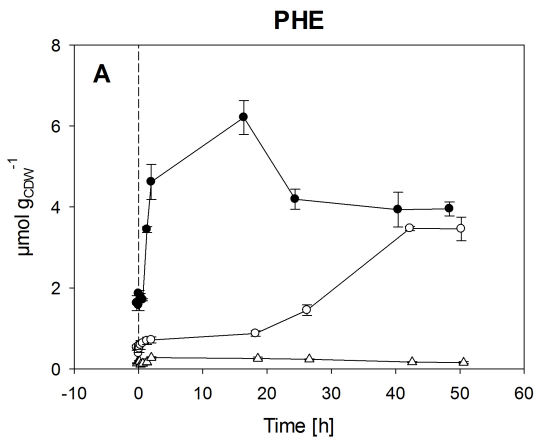
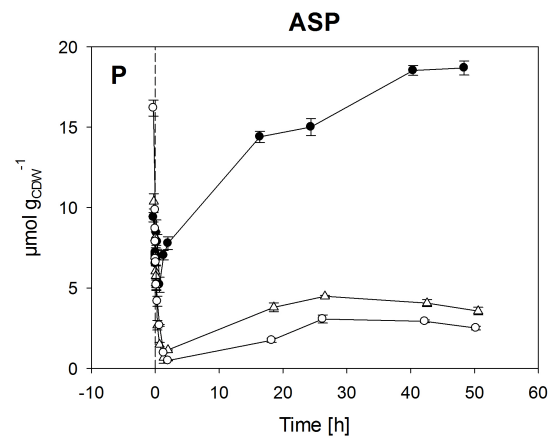
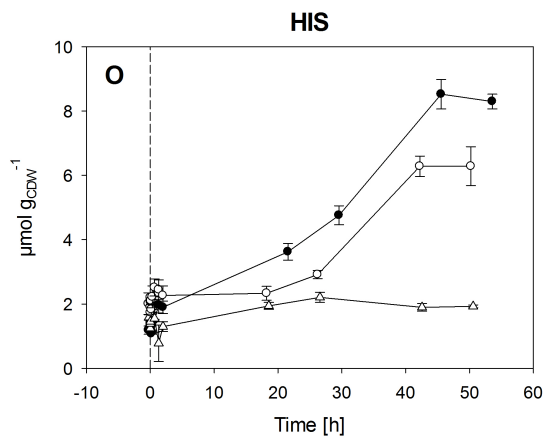
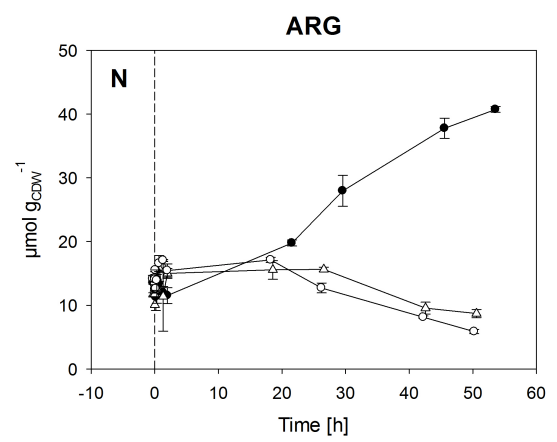
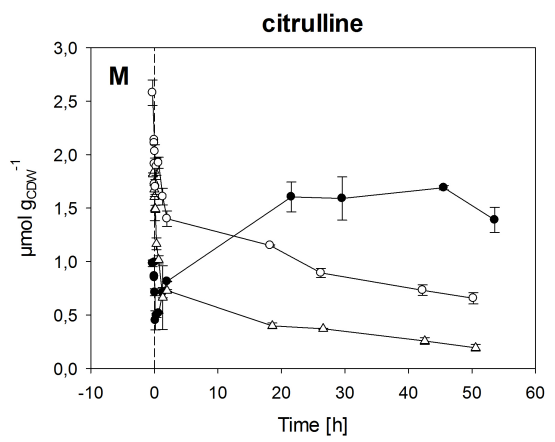
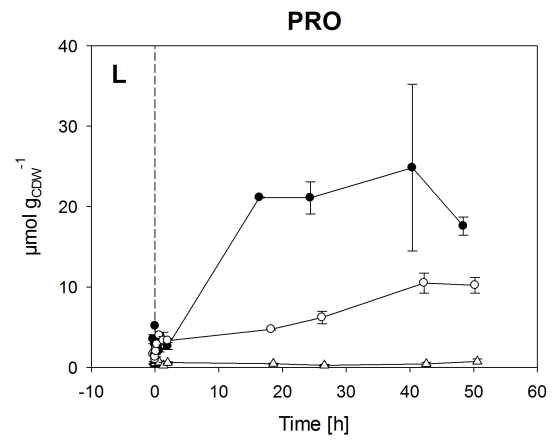
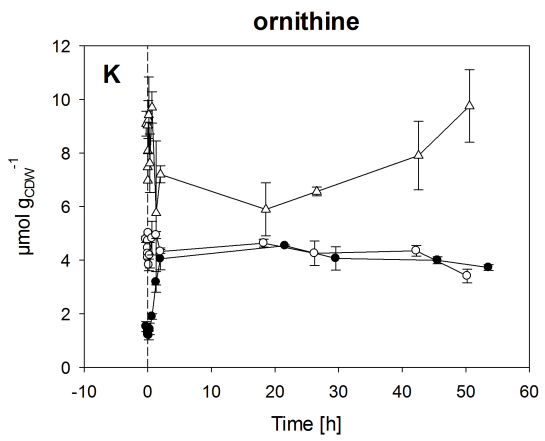
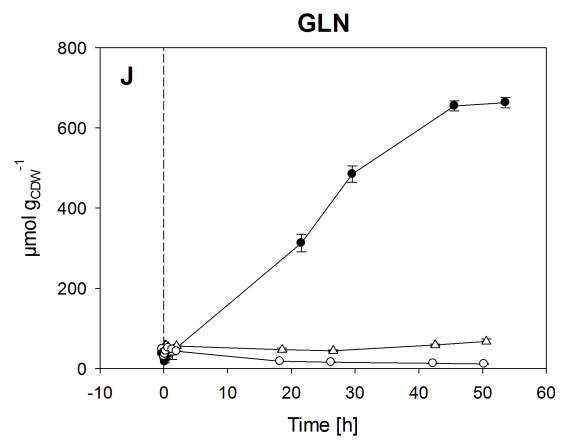
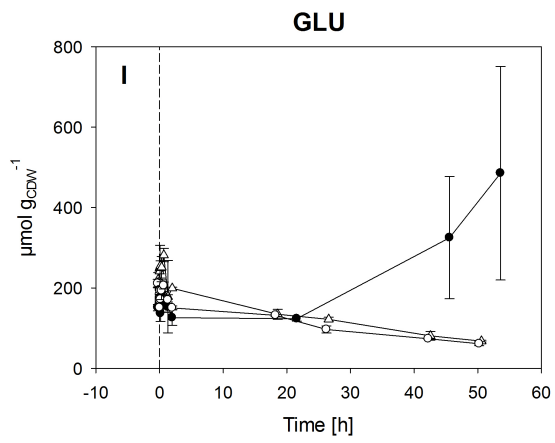


Figure 7-12: Intracellular metabolite time profiles whole fermentation - TCA. Empty circles, *C. tenuis*; full circles, IBB10B05; empty triangles, *S. stipitis*. Dotted lines represent time point of switch from aerobic to anaerobic conditions. Same panel numbering used as in Figure 7-5. For *S. stipitis* fermentation 2 no physiological data recorded.





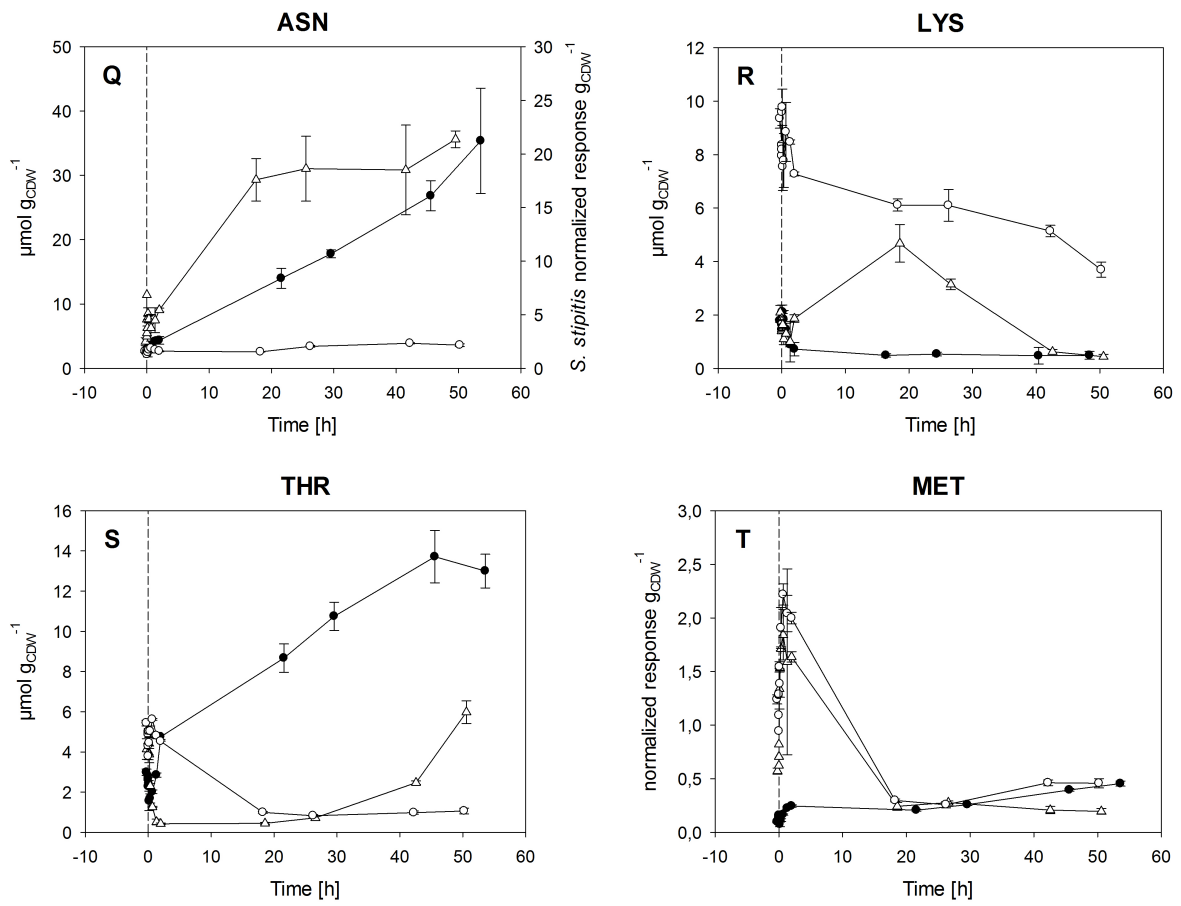
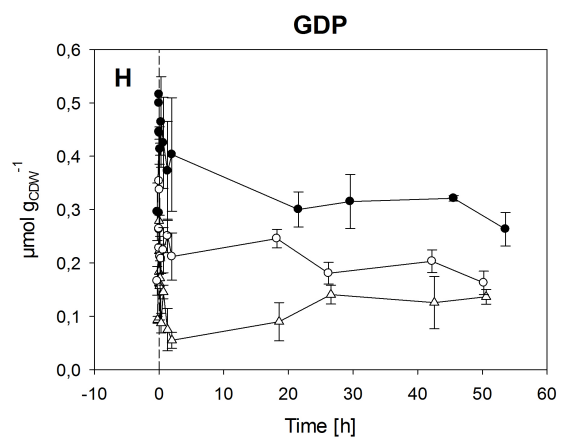
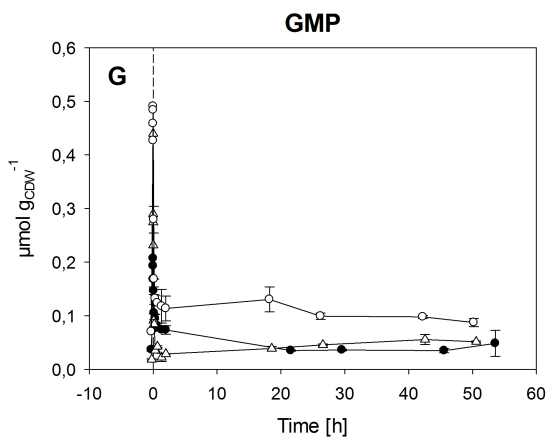
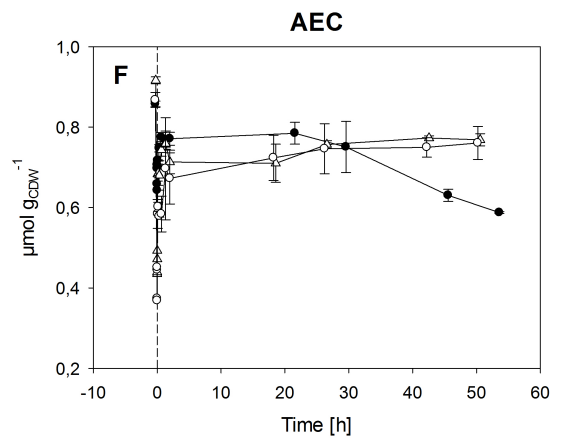
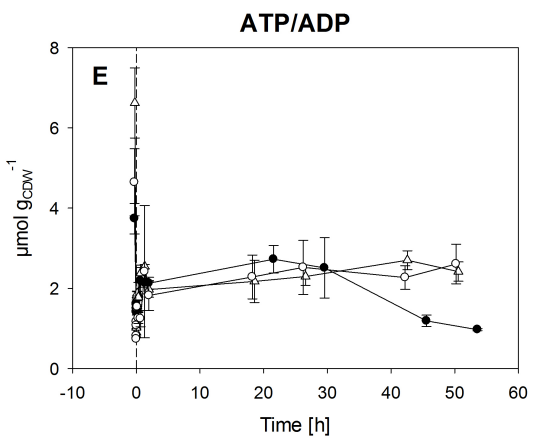
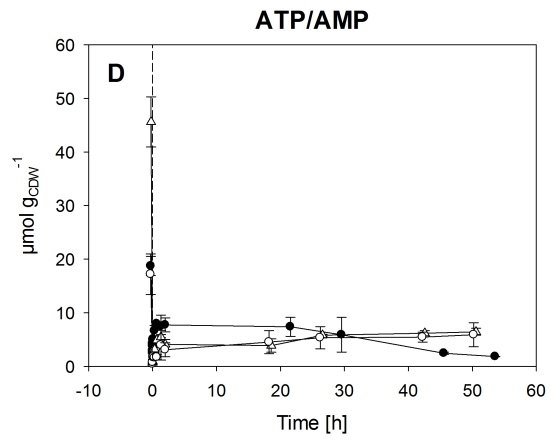
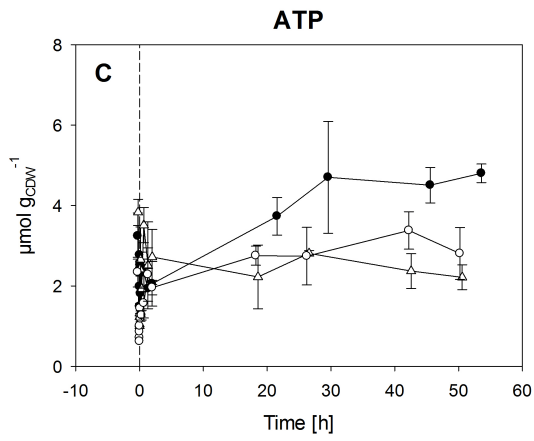
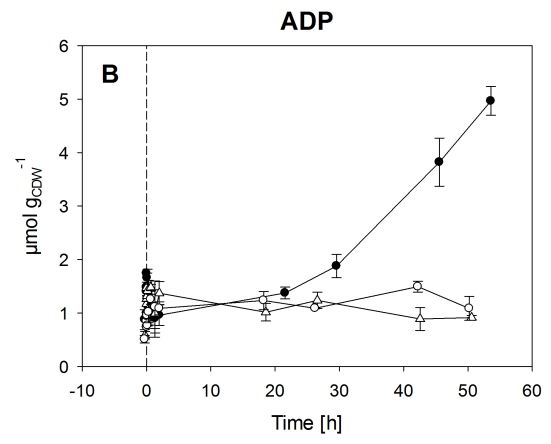
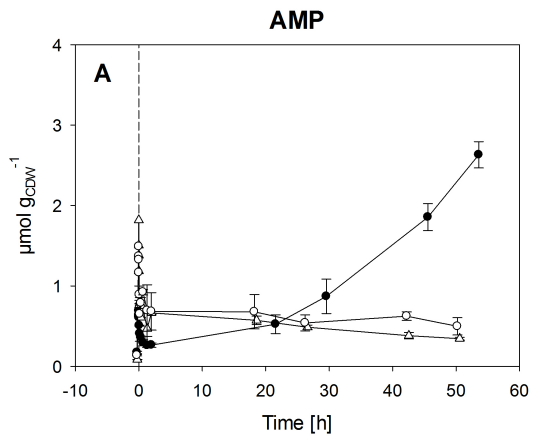


Figure 7-13: Intracellular metabolite time profiles whole fermentation - AA. Empty circles, *C. tenuis*; full circles, IBB10B05; empty triangles, *S. stipitis*. Dotted lines represent time point of switch from aerobic to anaerobic conditions. Same panel numbering used as in Figure 7-6. For *S. stipitis* fermentation 2 no physiological data recorded.



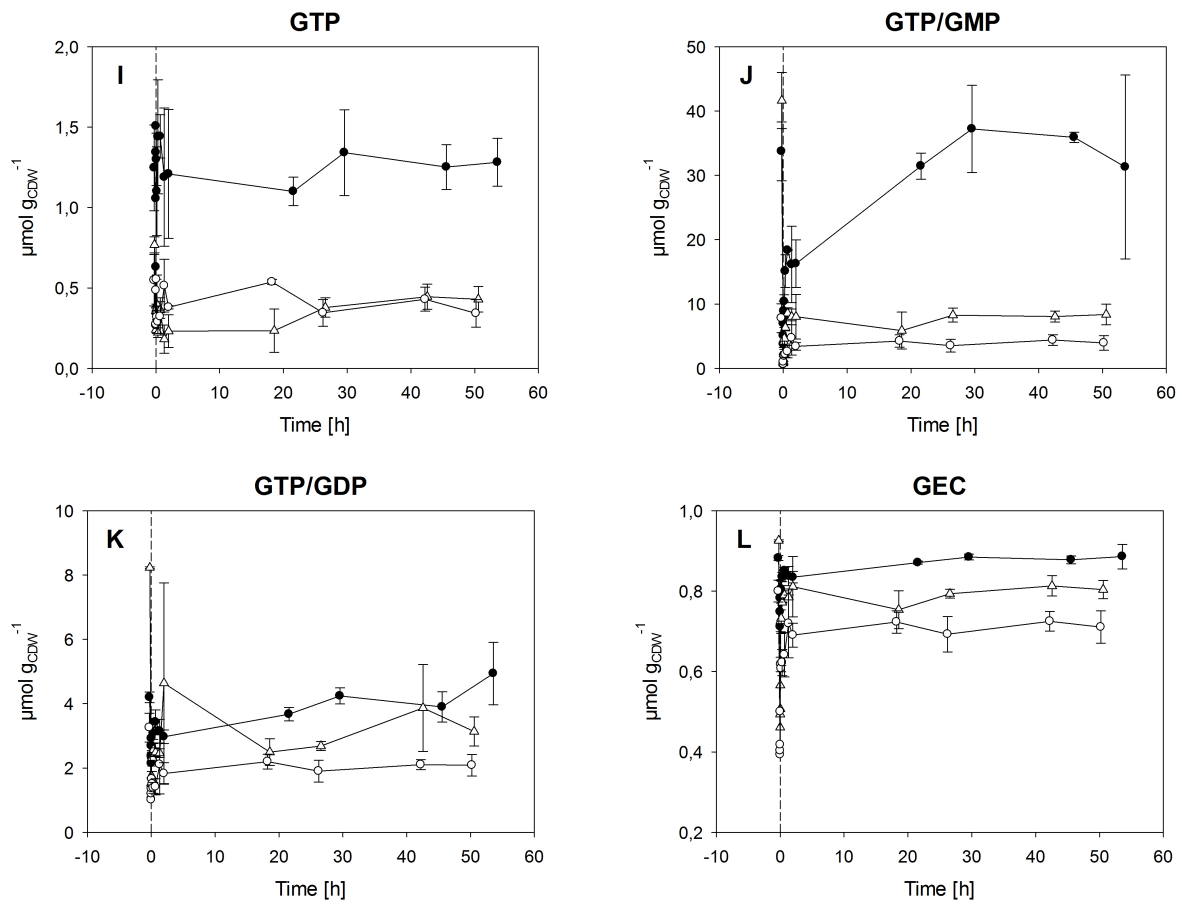


Figure 7-14: Intracellular metabolite time profiles whole fermentation - energy metabolites. Empty circles, *C. tenuis*; full circles, IBB10B05; empty triangles, *S. stipitis*. Dotted lines represent time point of switch from aerobic to anaerobic conditions. Same panel numbering used as in Figure 7-7. For *S. stipitis* fermentation 2 no physiological data recorded.

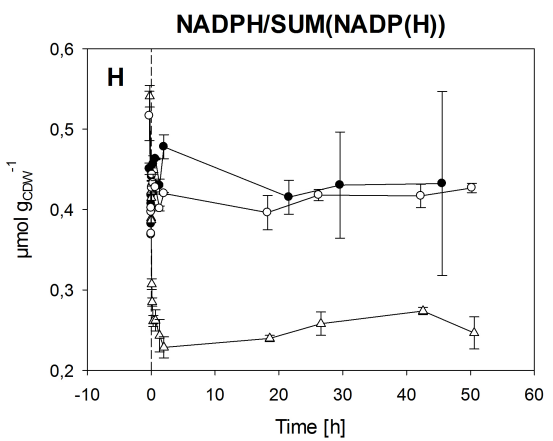
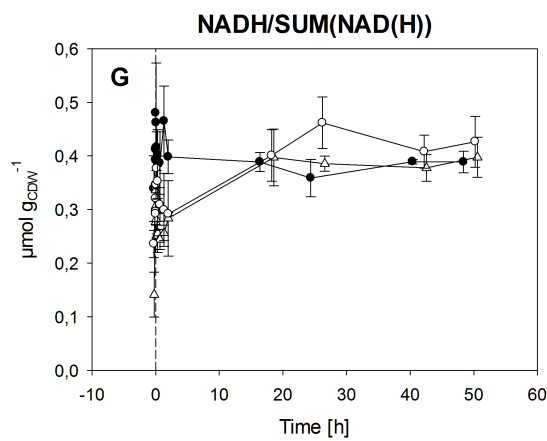
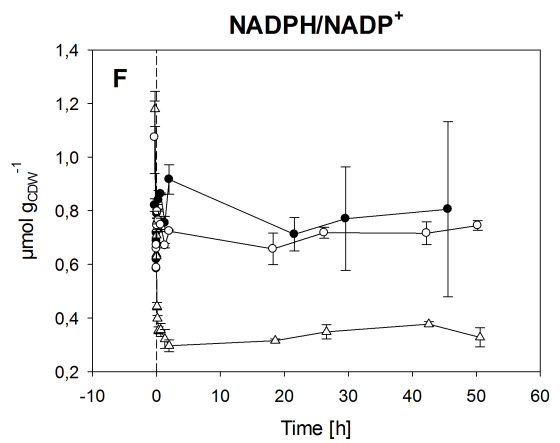
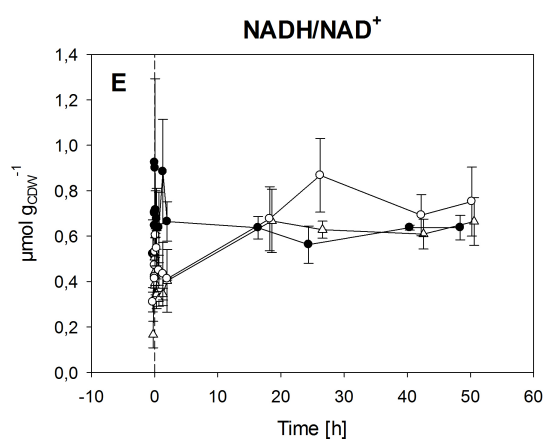
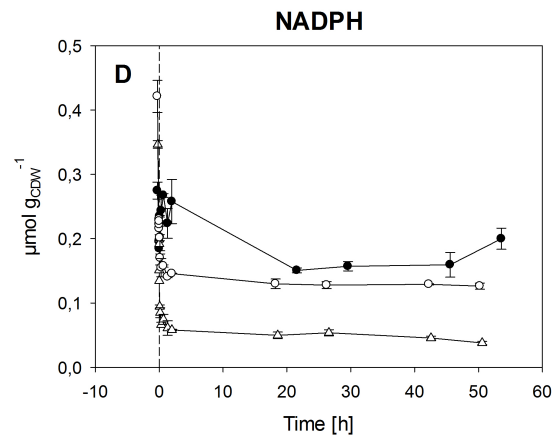
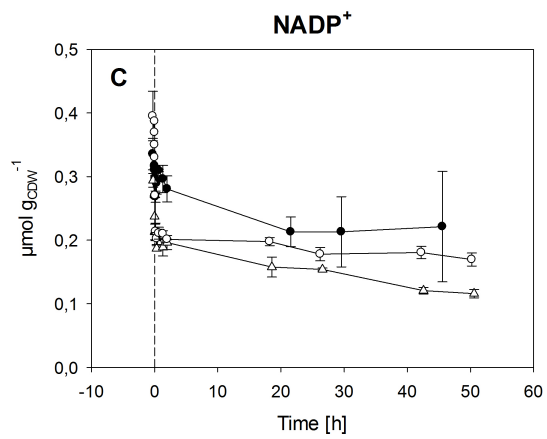
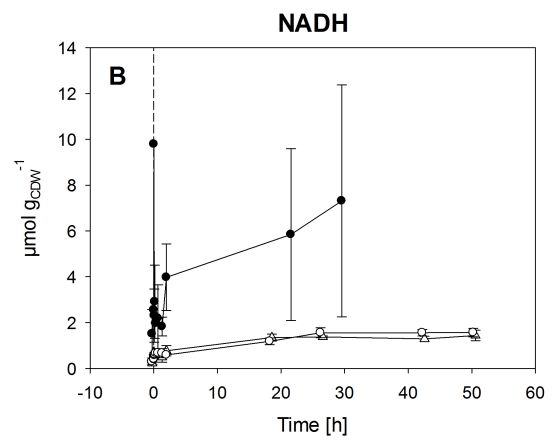
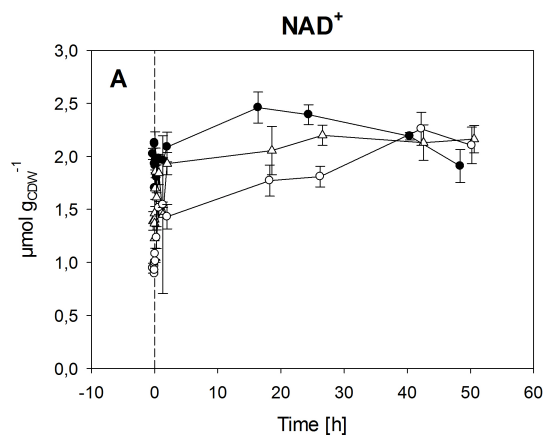


Figure 7-15: Intracellular metabolite time profiles whole fermentation - redox cofactors. Empty circles, *C. tenuis*; full circles, IBB10B05; empty triangles, *S. stipitis*. Dotted lines represent time point of switch from aerobic to anaerobic conditions. Same panel numbering used as in Figure 7-8. For *S. stipitis* fermentation 2 no physiological data recorded.

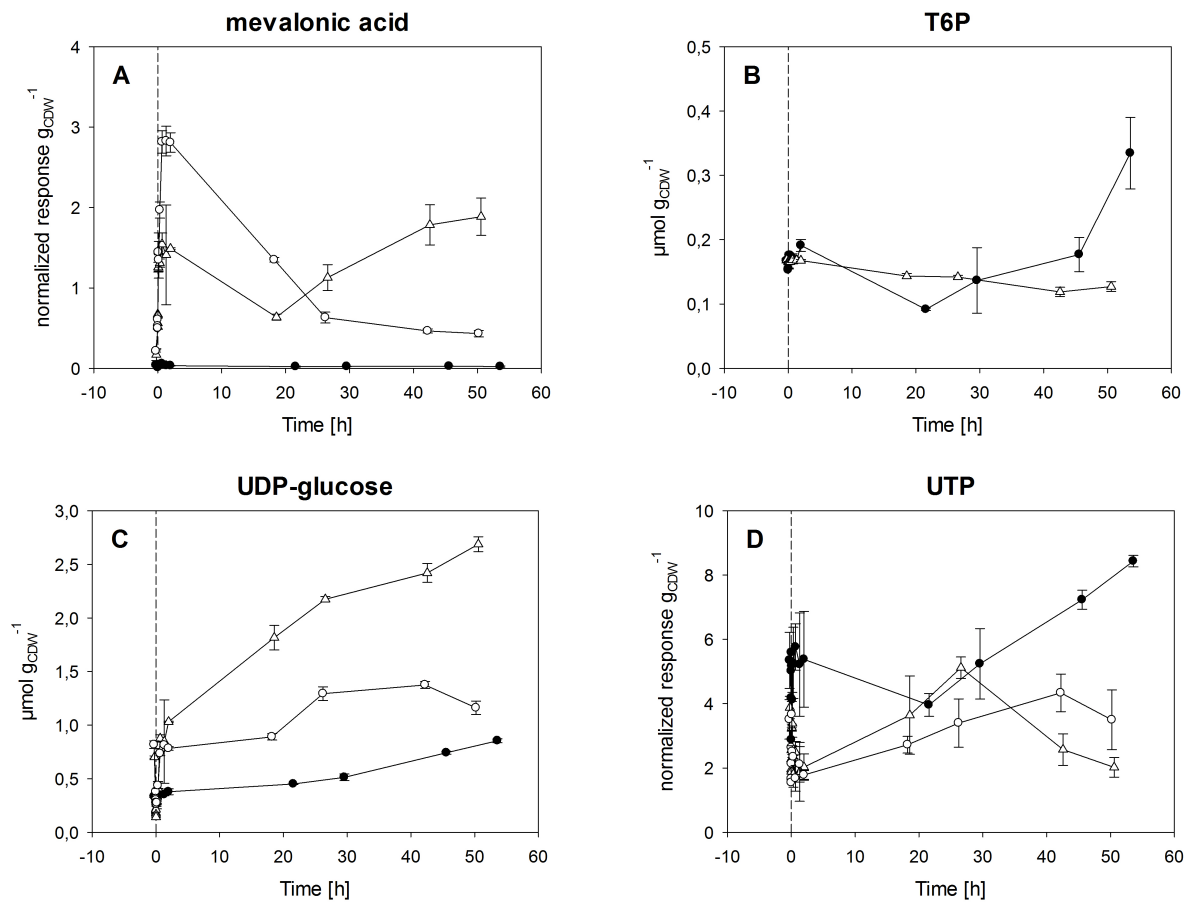


Figure 7-16: Intracellular metabolite time profiles whole fermentation - others. Empty circles, *C. tenuis*; full circles, IBB10B05; empty triangles, *S. stipitis*. Dotted lines represent time point of switch from aerobic to anaerobic conditions. Same panel numbering used as in Figure 7-9. For *S. stipitis* fermentation 2 no physiological data recorded.

To analyze the reproducibility of time-dependent dynamics of intracellular metabolites, two independent fermentations were carried out for each strain and compared. Results are listed in Table 7-6. Metabolite time profiles of 33 metabolites (out of 54 individually detected metabolites) could be reproduced for each of the strains. Among the remaining 21 metabolites, are some, for which data is either lacking or for which a different metabolite pattern was observed when comparing two independent fermentations. For fermentations with *C. tenuis*, 3 metabolite profiles could not be reproduced (GLY, HIS and pyruvic acid), while data of 2 other metabolites were lacking (SER and T6P). For cultivations with IBB10B05, 8 metabolite profiles were not reproducible (AcCoA, CYS, GADP, HXP, LYS, PRO, SER and TRP) and the data of PEP was missing. For fermentations with *S. stipitis*, 8 metabolite profiles could not be reproduced (ASN, GADP, GLU, HIS, PRO, pyruvic acid, SER and T6P), while data of 4 metabolites were lacking (CYS, GLY, PXP and TRP).

Table 7-6: Reproducibility of intracellular metabolite time profiles.

Metabolite	<i>C. tenuis</i>	IBB10B05	<i>S. stipitis</i>
23BPG	✓	✓	✓
3PG	✓	✓	✓
6PG	✓	✓	✓
AcCoA	✓	X	✓
ADP	✓	✓	✓
AMP	✓	✓	✓
ARG	✓	✓	✓
ASN	✓	✓	X
ASP	✓	✓	✓
ATP	✓	✓	✓
Citrulline	✓	✓	✓
CYS	✓	X	-
DHAP	✓	✓	✓
FBP	✓	✓	✓
GADP	✓	X	X
GDP	✓	✓	✓
GLN	✓	✓	✓
GLU	✓	✓	X
GLY	X	✓	-
Glyc3P	✓	✓	✓
GMP	✓	✓	✓
GTP	✓	✓	✓
HIS	X	✓	X
HXP ^a	✓	X	✓
LYS	✓	X	✓
Malate	✓	✓	✓
MET	✓	✓	✓
Mevalonic acid	✓	✓	✓
NAD ⁺	✓	✓	✓
NADH	✓	✓	✓
NADP ⁺	✓	✓	✓
NADPH	✓	✓	✓
Ornithine	✓	✓	✓
Oxoglutaric acid	✓	✓	✓
PEP	✓	-	✓
PHE	✓	✓	✓
PRO	✓	X	X
PXP ^b	✓	✓	-
Pyruvic acid	X	✓	X

S7P	✓	✓	✓
SER	-	X	X
T6P	-	✓	X
THR	✓	✓	✓
TRP	✓	X	-
TYR	✓	✓	✓
UDP-glucose	✓	✓	✓
UTP	✓	✓	✓
VAL	X	X	✓
XLEU^c	✓	✓	✓

-
- ✓ Reproducible.
 - X Not reproducible.
 - Not given.
 - ^a G6P, F6P, G1P, F1P
 - ^b R5P, Ru5P
 - ^c LEU, ILE

8 DISCUSSION

8.1 Macroscopic analysis of investigated yeasts

8.1.1 Growth behaviour

Under aerobic conditions native xylose-fermenting yeasts displayed a ~3.7-fold (*C. tenuis* = 0.26-0.32 h⁻¹) or ~4.9-fold (*S. stipitis* = 0.28-0.48 h⁻¹) higher μ than recombinant yeast strain IBB10B05 (0.054-0.102 h⁻¹). The exact opposite was the case under anaerobic conditions. Here IBB10B05 displayed the highest μ (= 0.015-0.021 h⁻¹) and doubled ~2.4-fold until it ceases growth, while *S. stipitis* displayed significantly slower growth (μ = 0.010-0.011 h⁻¹) and underwent only ~1.4 duplications. On the contrary, *C. tenuis* showed nearly no growth (μ = 0.005 h⁻¹). These results are in reasonable agreement with data reported elsewhere ([43], [51], [69], [70]). Only the μ recorded for IBB10B05 were lower than values obtained from literature ([13]) (on average 50% lower under aerobic conditions and 70% lower under anaerobic conditions). This is because fermentations were, unlike previous studies ([13]), performed without addition of ergosterol and Tween 80. Ergosterol and Tween 80 are important additives to support growth of yeasts under anaerobic conditions [17]. However, ethanol, which is typically used to solve both ingredients prior addition to the medium is preferentially utilized by IBB10B05 under aerobic conditions when both ethanol and xylose are present. With the aim to record the immediate metabolic response of cells growing aerobically on xylose to oxygen deprivation, both ergosterol and Tween 80 were not considered in the medium formulation. Nevertheless, IBB10B05 and *S. stipitis* could increase their biomass by a factor of ~2.4 and ~1.4, respectively, even without addition of ergosterol and Tween 80.

Furthermore IBB10B05 and *S. stipitis*, but not *C. tenuis*, displayed ~1.7-fold higher values of μ in aerobic bioreactor cultivations compared to aerobic shake flask cultivations. This is most likely due to controlled reaction conditions like pO₂, pH and temperature in bioreactor fermentations. As only the growth velocity under aerobic conditions was affected, an oxygen limitation in shake flasks seems to be the most likely explanation for that. However, *C. tenuis* and *S. stipitis* have higher values of q_{O_2} (= 3.23-3.78 mmol_{O₂} g_{BM}⁻¹ h⁻¹ and 5.42-8.61 mmol_{O₂} g_{BM}⁻¹ h⁻¹, respectively) than IBB10B05 (= 0.83-2.87 mmol_{O₂} g_{BM}⁻¹ h⁻¹). Consequently, this presumption could not explain why the growth velocity of *C. tenuis* was not affected.

8.1.2 Substrate consumption and product formation

In accordance with the higher μ of native xylose-fermenting yeasts under aerobic conditions [72], the Y_{XS} was also ~1.4-fold higher in *C. tenuis* (= 0.40-0.64 g g⁻¹) and ~1.5-fold higher in *S. stipitis* (= 0.47-0.63 g g⁻¹) than in IBB10B05 (= 0.29-0.46 g g⁻¹). This corresponded in turn with a faster oxygen and xylose consumption in native xylose-utilizing yeasts (*C. tenuis*: q_{O_2} = 3.23-3.78 mmol_{O₂} g_{BM}⁻¹ h⁻¹, q_{xylose} = 0.48-0.64 g g_{BM}⁻¹ h⁻¹; *S. stipitis*: q_{O_2} = 5.42-8.61 mmol_{O₂} g_{BM}⁻¹ h⁻¹, q_{xylose} = 0.61-0.75 g g_{BM}⁻¹ h⁻¹) compared to IBB10B05 (q_{O_2} = 0.83-2.87 mmol_{O₂} g_{BM}⁻¹ h⁻¹, q_{xylose} = 0.15-0.22 g g_{BM}⁻¹ h⁻¹). In addition, *C. tenuis* and *S. stipitis* produced, besides carbon dioxide and small amounts of glycerol, no by-products under aerobic conditions, while IBB10B05 formed significant amounts of glycerol ($Y_{glycerol}$ = 0.14-0.34 g g⁻¹). A possible reason for this is that not all excess NADH from the XDH reaction can be recycled with oxygen as terminal electron acceptor and thus some NADH is recycled via production of glycerol. The aerobic production of glycerol demonstrates a completely new finding, as previous studies of IBB10B05 focused only on anaerobic fermentation of xylose ([13], [22]). Therefore also no reference values were available for q_{xylose} and Y_{XS} of IBB10B05 under oxic conditions. Nevertheless, q_{xylose} and Y_{XS} for *S. stipitis* were in reasonable agreement with the ones reported elsewhere ([70]). On the contrary, Y_{XS} for *C. tenuis* was lower and q_{xylose} for *C. tenuis* was higher than previously published values ([69]). This is most likely due to differences in cultivation conditions.

Under anoxic conditions, *C. tenuis* and *S. stipitis* showed, relative to their recombinant opponent IBB10B05, a ~1.2-fold higher $Y_{ethanol}$ (0.35-0.49 g g⁻¹ and 0.41-0.46 g g⁻¹, respectively) and lower by-product formation (*C. tenuis*: $Y_{xylitol}$ = 0.02-0.103 g g⁻¹, $Y_{glycerol}$ = 0.022-0.052 g g⁻¹, $Y_{acetate}$ = 0.007 g g⁻¹; *S. stipitis*: $Y_{xylitol}$ = 0.063-0.10 g g⁻¹, $Y_{glycerol}$ = 0.007-0.008 g g⁻¹, $Y_{acetate}$ = 0.015-0.028 g g⁻¹). Results are in good agreement with former physiological studies ([43], [51]) and indicate an efficient oxygen-independent ability of coenzyme regeneration of native xylose-fermenting yeasts [22], [42], [43]. Furthermore the high $Y_{ethanol}$ explain, why these yeasts can be ranked among the best native xylose-to-ethanol converters. Recombinant strain IBB10B05, in contrast, displayed lower $Y_{ethanol}$ (= 0.33-0.39 g g⁻¹) and higher formation of by-products ($Y_{xylitol}$ = 0.074-0.19 g g⁻¹, $Y_{glycerol}$ = 0.043-0.08 g g⁻¹, $Y_{acetate}$ = 0.056-0.07 g g⁻¹), though expressing a similar xylose assimilation pathway with balanced coenzyme utilization. Results were in reasonable agreement with those reported elsewhere ([13]). Apart from its lower $Y_{ethanol}$, IBB0B05 showed according to its high μ under anaerobic conditions, the fastest conversion of xylose (q_{xylose} = 0.36-0.61 g g_{BM}⁻¹ h⁻¹), while xylose consumption was ~2.6-fold slower in *C. tenuis* (q_{xylose} = 0.19 g g_{BM}⁻¹ h⁻¹) and ~1.9-fold slower in *S. stipitis* (q_{xylose} = 0.25-0.27 g g_{BM}⁻¹ h⁻¹). The q_{xylose} values obtained for all three strains were in good agreement with previously published data ([13], [43], [51]).

To sum up, the general macroscopic response to the transition from aerobic (respirofermentative metabolism) to anaerobic conditions (fermentative metabolism) was accumulation of ethanol and other by-products like xylitol and glycerol. In addition, also a fundamental effect on the q_{xylose} was observed. When the oxygen saturation changed from 40% to 0%, q_{xylose} decreased ~3.4-fold in *C. tenuis* and 2.7-fold in *S. stipitis*, while it increased ~2.5-fold in IBB10B05. This is one possible reason why IBB10B05 is capable of anaerobic growth on xylose [13], while *C. tenuis* and *S. stipitis* are not. However, a recent study ([74]) revealed that a low q_{xylose} is not the main reason for growth absence on xylose and other unknown factors are also thought to play a role [15].

Anyway, q_{xylose} is closely related to the formation rate of precursor metabolites required for biosynthesis of macromolecules [15]. As these metabolites are produced in glycolysis, PPP and TCA, investigation of these pathways should reveal clear differences between native xylose-fermenting yeasts and IBB10B05 [15]. To identify them and thus also possible reasons for phenotype differentiations in terms of anaerobic growth on xylose as well as ethanol productivity, metabolite profiling was used. Results thereof are discussed in the following Section.

8.2 Intracellular metabolite pattern of xylose metabolization

Metabolite profiling was used to analyze the dynamic response of 54 metabolites on changing oxygen concentrations from fully aerobic to completely anaerobic conditions in recombinant *S. cerevisiae* IBB10B05 and native xylose-utilizing yeast strains during batch fermentation of xylose. The transition went along with massive changes in cell metabolism. Thereby metabolites belonging to PPP, glycolysis and TCA as well as AA, redox cofactors and energy metabolites were affected.

8.2.1 PPP

Tremendous effects were obvious in the PPP, where transition from aerobic to anaerobic conditions went along with decreased levels of PXP (R5P, Ru5P) in native xylose-fermenting yeasts, but increased levels of PXP in IBB10B05. Concentrations of PXP were ~3-18-fold higher in IBB10B05 compared to native yeasts. In addition, pools of S7P declined in all three strains when switching from aerobic to anaerobic conditions. However, levels thereof were ~30-50-fold higher in IBB10B05. The significantly higher flux through the PPP in IBB10B05, compared to native xylose-fermenting yeasts, goes together with its ability to grow anaerobically, as the PPP provides precursor metabolites (E4P, R5P) required for the cells anabolism [22], [75]. Furthermore there is a correlation between q_{xylose} and the concentration of PPP-metabolites [15]. Enhanced q_{xylose} under anoxic conditions in IBB10B05 was

accompanied by high concentrations of PPP-metabolites, while reduced q_{xylose} in native xylose-utilizing yeasts went along with low concentrations of PPP-metabolites.

The transition from oxic to anoxic conditions was further accompanied by a depletion of 6PG in all three strains. This indicates a lower flux through the oxidative PPP (ox-PPP). The flux through the ox-PPP depends on the G6P formation, which can during assimilation of xylose only take place via the PPP and the subsequent conversion of F6P by phosphoglucosomerase (PGI (EC 5.3.1.9)) [15]. Hence, the depletion of 6PG is probably due to a decreased flux through the PPP. This is most likely the case in native yeasts, where levels of PPP-metabolites were low. On the contrary, levels of PPP-metabolites were high in IBB10B05. This suggests sufficient flux through the ox-PPP in IBB10B05, though levels of 6PG likewise decreased. This corresponds in turn with higher xylitol formation in IBB10B0, as high flux through the ox-PPP leads to increased xylitol production, while low flux through the ox-PPP is associated with more efficient ethanol production and is thus beneficial [22].

8.2.2 Glycolysis

The concentration of all glycolytic metabolites except for FBP, DHAP and Glyc3P decreased notably in all three strains during the switch from oxic to anoxic conditions. In contrast, levels of FBP, DHAP and Glyc3P rose for all three strains, though the increase was substantially higher in native xylose-utilizing yeasts, especially in *C. tenuis*. This was already reported by Trausinger ([22]) and suggests an alternative way of NADH reoxidation, besides ethanol formation. This way involves the reduction of DHAP to Glyc3P by G3PDH, which was displayed by ~3-8-fold higher Glyc3P levels in *C. tenuis* compared to IBB10B05. The reason for this, is most likely a bottleneck in the reaction from Glyc3P to glycerol due to low or absent activity of GPP (EC 3.1.3.21) [22]. Moreover this could relocate the carbon flux towards ethanol formation and is therefore a potential explanation for higher Y_{ethanol} and lower Y_{glycerol} in native xylose-utilizing yeasts [22].

8.2.3 TCA

TCA is required for energy generation and synthesis of AA and NADH [76]. When switching to anaerobic conditions, TCA enzymes in yeasts become inhibited by high concentrations of NADH [76]. As a result, the concentration of all TCA intermediates (AcCoA and oxoglutaric acid), except for malate, declined significantly in all three strains, which led in turn to reduced amounts of ATP. The level of malate increased instead during the first 15 min after switching off the oxygen supply. This is probably due to enzyme inhibition through NADH and consequent accumulation of TCA-reactants.

8.2.4 Amino acids

AA showed a delayed response on oxygen depletion. This is because they have, in contrast to energy metabolites and metabolites from catabolic reactions, much longer turnover times [57]. However, after several minutes or even hours depending on the AA itself, a significant increase in aromatic AA (PHE, TRP, TYR) and AA from TCA (ARG, ASN, ASP, HIS, GLN, GLU, PRO, THR) as well as in VAL and XLEU was observable in IBB10B05. Increased concentrations of ASN, GLY, HIS, PHE, TYR, XLEU were also visible in *C. tenuis*. The accumulation of these AA was in good agreement with previously observed responses to carbon starvation in yeast, where concentrations of ASN and aromatic AA increased under oxic conditions [77] and concentrations of GLU, PHE and TRP rose under anoxic conditions [47]. As synthesis of aromatic AA requires massive amounts of ATP [78], it is unlikely that the observed accumulation is due to synthesis [15]. More likely, it is the result of protein degradation and consequent accumulation of aromatic AA, whose aromatic ring is energetically too expensive to break [15]. This goes also together with the decreasing AEC in IBB10B05 at the end of the fermentation. To analyze if accumulation of aromatic AA results whether from protein degradation or synthesis, an isotope labeling approach that investigates AA during growth on ^{13}C -labeled xylose would be suited.

8.2.5 Redox cofactors

Redox cofactors are electron carriers that play, as the name suggests, major roles in redox reactions [79]. When switching to anaerobic conditions, massive changes in their levels could be observed. Levels of NAD^+ increased in *C. tenuis* and *S. stipitis*, while they stayed relatively stable in IBB10B05. In addition, an accumulation of NADH could be observed in all yeasts, but especially in native xylose-fermenting yeasts. This is because oxidative phosphorylation and thus ATP synthesis is blocked under anoxic conditions [76]. Furthermore transition went along with a ~2-fold and ~1.5-fold decrease of NADP^+ levels in *C. tenuis* and *S. stipitis*, respectively. IBB10B05 showed a similar response, however, after a transient decline, its NADP^+ levels increased again. Oxygen deprivation went also along with decreased concentrations of NADPH in all three strains, especially in *C. tenuis* (~4-fold) and *S. stipitis* (~3-fold). This is most likely due to a reduced flux through ox-PPP and correlates with the depletion of 6PG. Moreover, it corroborates with the above-stated assumption of low flux through PPP in native xylose-utilizing yeasts, as the PPP is required for formation of G6P [15].

To sum up, it can be said that the transition to anaerobic conditions went along with permanent changes in redox cofactors of native yeasts, while redox cofactor changes in IBB10B05 were only temporary. This clearly indicates a better adaptation of IBB10B05 to anoxic conditions.

8.2.6 Energy charges

The energy status of biological cells is usually assessed by the AEC ($= \frac{\text{ATP} + \frac{1}{2}\text{ADP}}{\text{ATP} + \text{ADP} + \text{AMP}}$) [80]. It plays an important role in controlling the energy balance by adapting enzyme activities [81], [82]. In yeast the AEC amounts to ~ 0.1 ([83]) for starving, ~ 0.7 ([47]) for metabolizing and $\sim 0.8-0.9$ ([47], [83]) for growing cells.

In response to oxygen depletion the AEC dropped sharply from ~ 0.9 to ~ 0.4 in *C. tenuis*, to ~ 0.5 in *S. stipitis* and to ~ 0.7 in IBB10B05 (due to higher AMP and lower ATP concentrations). This suggests a better physiological adaptation of IBB10B05 to anoxic conditions and coincides with μ , as IBB10B05 displayed followed by *S. stipitis* and finally by *C. tenuis* the highest μ under anoxic conditions. Immediately after switch, cells adapted to anoxic conditions, which is exemplified by an increase in the AEC to ~ 0.6 in *C. tenuis*, to ~ 0.7 in *S. stipitis* and to ~ 0.8 in IBB10B05 within the first 5 min after oxygen exhaustion. After reaching this level, the AEC in native xylose-fermenting yeasts remained constant over the whole fermentation, while the one of IBB10B05 decreased at the end of the fermentation. Interestingly, *C. tenuis* and *S. stipitis* managed to keep AEC relatively high and stable, despite of their slow q_{xylose} under anoxic conditions. This implies that cells rather respond with carbon starvation than energy starvation on oxygen deprivation and that the AEC is not the needed signal for growth on xylose [15].

The GECs were calculated similarly to the AECs and showed the exact same response on oxygen deprivation. This confirmed that the nucleoside diphosphokinase reactions that use GTP as a phosphate donor for ATP synthesis and vice versa [15], [84], are equilibrated [22]. However, the function of guanine nucleotides in yeasts is, in contrast to adenine nucleotides, still largely unknown [15], [85], [86]. It is only known that guanine nucleotides play roles in biochemical reactions that are necessary for survival and growth [15], [85], [86].

In summary, it can be said that the ECs (AEC and GEC) were in the first 20 h of fermentation significantly higher in IBB10B05, compared to *C. tenuis* and *S. stipitis*, and resemble those for *S. cerevisiae* when growing on glucose under anoxic conditions [47]. This indicates good adaptation of IBB10B05 to both xylose as substrate and anaerobic conditions.

8.2.7 Mevalonic acid

Oxygen depletion went along with increased concentrations of mevalonic acid in native xylose-fermenting yeasts, while concentrations in IBB10B05 were not affected. Mevalonic acid is a precursor for production of ergosterol in the so-called mevalonate pathway and is within several steps converted to squalene [87]. Further oxidation of squalene to 2,3-oxidosqualene is catalyzed by squalene epoxidase (SQLE (EC 1.14.99.7), encoded by ERG1) [87]. As this enzyme is dependent on oxygen [19], [76], most likely a bottleneck in this

reaction leads to the observed accumulation of mevalonic acid in native xylose-utilizing yeasts. Likewise an accumulation of mevalonic acid was also expected in IBB10B05. Reasons why this was not the case are not known yet and request further investigations.

9 ABBREVIATIONS

^{13}C -ISTD	^{13}C -labeled internal standard
<i>a</i>	Oxygen demand
AA	Amino acids
AEC	Adenylate energy charge
BE	Boiling ethanol
BEF	Baffled Erlenmeyer flask
BL	Blank
BM	Biomass
CDW	Cell dry weight
CE	Capillary electrophoresis
CS	Calibration standards
<i>CtXR</i>	Xylose reductase from <i>Candida tenuis</i>
EC	Energy charge
ES	Extraction solution
GC	Gas chromatography
GEC	Guanylate energy charge
GF	Gasflow
GPP	Glycerol 3-phosphatase
GT	Dipl.-Ing. Gert Trausinger Bakk.techn.
HESI	Heated electrospray ionization
HPLC	High performance liquid chromatography
I.B.B.	Institute of Biotechnology and Biochemical Engineering
ISTD	Internal standard
LC	Liquid chromatography
LC-MS	Liquid chromatography-mass spectrometry
MC	Mainculture
MM	Mineral Medium
MS	Mass spectrometry
MW	Molecular weight
n.a.	Not available
n.d.	Not determined / not determinable
NMR	Nuclear magnetic resonance
OD ₆₀₀	Optical density at 600 nm
Ox-PPP	Oxidative pentose phosphate pathway
PC	Preculture
PFK	Phosphofructokinase
PGI	Phosphoglucoisomerase

PPP	Pentose phosphate pathway
QC	Quality control
q_{ethanol}	Specific ethanol formation rate
q_{O_2}	Specific oxygen uptake rate
QS	Quenching solution
q_{xylose}	Specific xylose uptake rate
RPM	Revolutions per minute
S.D.	Standard deviation
ScURA1	Dihyoorotate dehydrogenase from <i>Saccharomyces cerevisiae</i>
SQLE	Squalene epoxidase
SV	Sample volume
TCA	Citric acid cycle
XDH	Xylitol dehydrogenase
XI	Xylose isomerase
XK	Xylulose kinase
XR	Xylose reductase
Y	Yield
YPD	Yeast Peptone Dextrose
μ	Specific growth rate

Metabolites

23BPG	2,3-Bisphosphoglyceric acid
3PG	3-Phosphoglyceric acid
6PG	6-Phosphogluconic acid
AcCoA	Acetyl-CoA
ADP	Adenosine 5-diphosphate
AMP	Adenosine 5-monophosphate
ARG	Arginine
ASN	Asparagine
ASP	Aspartic acid
ATP	Adenosine 5-triphosphate
CYS	Cysteine
DHAP	Dihydroxyacetone phosphate
F1P	Fructose 1-phosphate
F6P	Fructose 6-phosphate
FBP	Fructose 1,6-bisphosphate
G1P	Glucose 1-phosphate
G6P	Glucose 6-phosphate
GADP	Glyceraldehyde 3-phosphate

GDP	Guanosine 5-diphosphate
GLN	Glutamine
GLU	Glutamic acid
GLY	Glycine
Glyc3P	Glycerol 3-phosphate
GMP	Guanosine 5-monophosphate
GTP	Guanosine 5-triphosphate
HIS	Histidine
HXP	Hexose phosphates
LYS	Lysine
MET	Methionine
NAD(P) ⁺	β-Nicotineamide adenine dinucleotide (phosphate) - oxidized form
NAD(P)H	β-Nicotineamide adenine dinucleotide (phosphate) - reduced form
PEP	Phosphoenolpyruvic acid
PHE	Phenylalanine
PRO	Proline
PXP	Pentose phosphates
R5P	Ribose 5-phosphate
Ru5P	Ribulose 5-phosphate
S7P	Sedoheptulose 7-phosphate
SER	Serine
T6P	Trehalose 6-phosphate
THR	Threonine
TRP	Tryptophan
TYR	Tyrosine
UDP	Uridine diphosphate
UTP	Uridine triphosphate
VAL	Valine
X5P	Xylulose 5-phosphate
XLEU	Leucine and Isoleucine

10 REFERENCES

- [1] L. Olsson, *Biofuels*, vol. 108. Springer Berlin Heidelberg, 2007, pp. 1–372.
- [2] B. Hahn-Hägerdal, M. Galbe, M. F. Gorwa-Grauslund, G. Lidén, and G. Zacchi, “Bio-ethanol--the fuel of tomorrow from the residues of today,” *Trends Biotechnol.*, vol. 24, no. 12, pp. 549–556, Dec. 2006.
- [3] G. Scalcinati, J. M. Otero, J. R. H. van Vleet, T. W. Jeffries, L. Olsson, and J. Nielsen, “Evolutionary engineering of *Saccharomyces cerevisiae* for efficient aerobic xylose consumption,” *FEMS Yeast Res.*, vol. 12, no. 5, pp. 582–597, Aug. 2012.
- [4] A. Aristidou and M. Penttilä, “Metabolic engineering applications to renewable resource utilization,” *Curr. Opin. Biotechnol.*, vol. 11, no. 2, pp. 187–198, 2000.
- [5] B. Hahn-Hägerdal, C. F. Wahlbom, M. Gárdony, W. H. van Zyl, R. R. Cordero Otero, and L. J. Jönsson, “Metabolic engineering of *Saccharomyces cerevisiae* for xylose utilization,” *Adv. Biochem. Eng. Biotechnol.*, vol. 73, pp. 53–84, 2001.
- [6] T. K. Rout, “Pyrolysis of coconut shell,” *Master thesis*, pp.1-58, 2013.
- [7] L. J. Jönsson, B. Alriksson, and N. Nilvebrant, “Bioconversion of lignocellulose: inhibitors and detoxification,” *Biotechnol. Biofuels*, vol. 6, no. 1, p. 16, 2013.
- [8] B. C. Saha, “Hemicellulose bioconversion,” *J. Ind. Microbiol. Biotechnol.*, vol. 30, no. 5, pp. 279–291, 2003.
- [9] B. C. H. Chu and H. Lee, “Genetic improvement of *Saccharomyces cerevisiae* for xylose fermentation,” *Biotechnol. Adv.*, vol. 25, no. 5, pp. 425–441, 2007.
- [10] V. Menon, G. Prakash, and M. Rao, “Value added products from hemicellulose: Biotechnological perspective”, *Glob. J. Biochem.*, vol. 1, no. 1, pp. 36-67, 2010.
- [11] A. J. A. van Maris, A. A. Winkler, M. Kuyper, W. T. A. M. de Laat, J. P. van Dijken, and J. T. Pronk, “Development of efficient xylose fermentation in *Saccharomyces cerevisiae*: xylose isomerase as a key component,” *Biofuels*, pp. 179–204, 2007.
- [12] G. Sorda, M. Banse, and C. Kemfert, “An overview of biofuel policies across the world,” *Energy Policy*, vol. 38, no. 11, pp. 6977–6988, Nov. 2010.
- [13] M. Klimacek, E. Kirl, S. Krahulec, K. Longus, V. Novy, and B. Nidetzky, “Stepwise metabolic adaption from pure metabolization to balanced anaerobic growth on xylose explored for recombinant *Saccharomyces cerevisiae*,” *Microb. Cell Fact.*, vol. 13, no. 1, p. 37, 2014.
- [14] B. Petschacher and B. Nidetzky, “Altering the coenzyme preference of xylose reductase to favor utilization of NADH enhances ethanol yield from xylose in a metabolically engineered strain of *Saccharomyces cerevisiae*,” *Microb. Cell Fact.*, vol. 7, p. 9, Jan. 2008.
- [15] B. Bergdahl, D. Heer, U. Sauer, B. Hahn-Hägerdal, and E. W. van Niel, “Dynamic metabolomics differentiates between carbon and energy starvation in recombinant *Saccharomyces cerevisiae* fermenting xylose,” *Biotechnol. Biofuels*, vol. 5, no. 1, p. 34, Jan. 2012.
- [16] T. Jeffries, “Engineering yeasts for xylose metabolism,” *Curr. Opin. Biotechnol.*, vol. 17, pp. 320–326, 2006.
- [17] A. A. Andreasen and T. J. B. Stier, “Anaerobic nutrition of *Saccharomyces cerevisiae*. I. Ergosterol requirement for growth in a defined medium,” *J. Cell. Comp. Physiol.*, vol. 41, no. 1, pp. 23–36, 1953.
- [18] N. Q. Shi and T. W. Jeffries, “Anaerobic growth and improved fermentation of *Pichia stipitis* bearing a URA1 gene from *Saccharomyces cerevisiae*,” *Appl. Microbiol. Biotechnol.*, vol. 50, pp. 339–345, 1998.
- [19] I. S. I. Snoek and H. Y. Steensma, “Factors involved in anaerobic growth of *Saccharomyces cerevisiae*,” *Yeast*, vol. 24, no. 1, pp. 1–10, 2007.
- [20] M. Nagy, F. Lacroute, and D. Thomas, “Divergent evolution of pyrimidine biosynthesis between anaerobic and aerobic yeasts,” *Proc. Natl. Acad. Sci. U. S. A.*, vol. 89, no. 19, pp. 8966–8970, 1992.

- [21] S. R. Kim, Y. C. Park, Y. S. Jin, and J. H. Seo, "Strain engineering of *Saccharomyces cerevisiae* for enhanced xylose metabolism," *Biotechnol. Adv.*, vol. 31, no. 6, pp. 851–861, Nov. 2013.
- [22] G. R. Trausinger, "Mass spectrometry-based quantitative analysis of intracellular metabolites of yeasts converting xylose to ethanol," *Master thesis*, pp. 1–100, 2015.
- [23] U. Johnsen, M. Dambeck, H. Zaiss, T. Fuhrer, J. Soppa, U. Sauer, and P. Schönheit, "D-xylose degradation pathway in the halophilic archaeon *Haloferax volcanii*," *J. Biol. Chem.*, vol. 284, no. 40, pp. 27290–27303, Oct. 2009.
- [24] P. Bruinenberg and P. H. M. de Bot, J. P. van Dijken, and W. A. Scheffers, "NADH-linked aldose reductase: the key to anaerobic alcoholic fermentation of xylose by yeasts," *Appl. Microbiol. Biotechnol.*, vol. 19, pp. 256–260, 1984.
- [25] J. P. van Dijken and W. A. Scheffers, "Redox balances in the metabolism of sugars by yeasts," *FEMS Microbiol Rev*, vol. 32, pp. 199–224, 1986.
- [26] P. Bruinenberg, J. P. van Dijken, and W. A. Scheffers, "An Enzymic Analysis of NADPH Production and Consumption in *Candida utilis*," *J. Gen. Microbiol*, vol. 129, no. 4, pp. 965–971, 1983.
- [27] M. Jeppsson, O. Bengtsson, K. Franke, H. Lee, B. Hahn-Hägerdal, and M. F. Gorwa-Grauslund, "The expression of a *Pichia stipitis* xylose reductase mutant with higher K(M) for NADPH increases ethanol production from xylose in recombinant *Saccharomyces cerevisiae*," *Biotechnol. Bioeng.*, vol. 93, no. 4, pp. 665–673, Mar. 2006.
- [28] M. Walfridsson, X. Bao, M. Anderlund, G. Lilius, L. Bülow, and B. Hahn-Hägerdal, "Ethanol fermentation of xylose with *Saccharomyces cerevisiae* harboring the *Thermus thermophilus* xylA gene, which expresses an active xylose (glucose) isomerase," *Appl. Environ. Microbiol.*, vol. 62, no. 12, pp. 4648–4651, 1996.
- [29] A. V. Sarthy, B. L. McConaughy, Z. Lobo, J. A. Sundstrom, C. E. Furlong, and B. D. Hall, "Expression of the *Escherichia coli* xylose isomerase gene in *Saccharomyces cerevisiae*," *Appl. Environ. Microbiol.*, vol. 53, no. 9, pp. 1996–2000, 1987.
- [30] M. Kuyper, H. R. Harhangi, A. K. Stave, A. A. Winkler, M. S. M. Jetten, W. T. A. M. de Laat, J. J. J. den Ridder, H. J. M. Op den Camp, J. P. van Dijken, and J. T. Pronk, "High-level functional expression of a fungal xylose isomerase: the key to efficient ethanol fermentation of xylose by *Saccharomyces cerevisiae*," *FEMS Yeast Res.*, vol. 4, no. 1, pp. 69–78, Oct. 2003.
- [31] K. Karhumaa, R. Garcia Sanchez, B. Hahn-Hägerdal, and M. F. Gorwa-Grauslund, "Comparison of the xylose reductase-xylitol dehydrogenase and the xylose isomerase pathways for xylose fermentation by recombinant *Saccharomyces cerevisiae*," *Microb. Cell Fact.*, vol. 6, p. 5, Jan. 2007.
- [32] B. Petschacher, S. Leitgeb, and K. Kavanagh, "The coenzyme specificity of *Candida tenuis* xylose reductase (AKR2B5) explored by site-directed mutagenesis and X-ray crystallography," *Biochem. J*, vol. 83, no. 1, pp. 75–83, 2005.
- [33] E. Kirl, "Physiological characterisation of recombinant *Saccharomyces cerevisiae* strain evolved for anaerobic growth on xylose," *Master thesis*, pp. 1–69, 2011.
- [34] M. Sonderegger, M. Jeppsson, B. Hahn-Hägerdal, and U. Sauer, "Molecular Basis for Anaerobic Growth of *Saccharomyces cerevisiae* on Xylose, Investigated by Global Gene Expression and Metabolic Flux Analysis," *Appl. Environ. Microbiol.*, vol. 70, no. 4, pp. 2307–2317, 2004.
- [35] C. F. Wahlbom and B. Hahn-Hägerdal, "Furfural, 5-hydroxymethyl furfural, and acetoin act as external electron acceptors during anaerobic fermentation of xylose in recombinant *Saccharomyces cerevisiae*," *Biotechnol. Bioeng.*, vol. 78, no. 2, pp. 172–178, 2002.
- [36] V. Novy, S. Krahulec, M. Wegleiter, G. Müller, K. Longus, M. Klimacek, and B. Nidetzky, "Process intensification through microbial strain evolution: mixed glucose-xylose fermentation in wheat straw hydrolyzates by three generations of recombinant *Saccharomyces cerevisiae*," *Biotechnol. Biofuels*, vol. 7, no. 1, p. 49, Jan. 2014.
- [37] M. I. González-Siso, E. Ramil, M. E. Cérdan, and M. A. Freire-Picos, "Respirofermentative metabolism in *Kluyveromyces lactis*: ethanol production and the Crabtree effect," *Enzyme Microb. Technol.*, vol. 18, no. 8, pp. 585–591, 1996.

- [38] T. Lindén and B. Hahn-Hägerdal, "Fermentation of lignocellulose hydrolysates with yeasts and xylose isomerase," *Enzyme Microb. Technol.*, vol. 11, no. 9, pp. 583–589, 1989.
- [39] M. Jeppsson, B. Johansson, B. Hahn-Hägerdal, and M. F. Gorwa-Grauslund, "Reduced oxidative pentose phosphate pathway flux in recombinant xylose-utilizing *Saccharomyces cerevisiae* strains improves the ethanol yield from xylose," *Appl. Environ. Microbiol.*, vol. 68, no. 4, pp. 1604–1609, 2002.
- [40] K. Skoog and B. Hahn-Hägerdal, "Effect of oxygenation on xylose fermentation by *Pichia stipitis*," *Appl. Environ. Microbiol.*, vol. 56, no. 11, pp. 3389–3394, 1990.
- [41] F. Lutzoni and F. Kauff, "Assembling the fungal tree of life: progress, classification, and evolution of subcellular traits," *Am. J. Bot.*, vol. 91, no. 10, pp. 1446–1480, 2004.
- [42] C. Gruber, "The yeast *Candida tenuis*: assessment of the organism for xylose fermentation and stereospecific reduction of ketones," *Master thesis*, pp. 4–69, 2011.
- [43] S. Krahulec, R. Kratzer, K. Longus, and B. Nidetzky, "Comparison of *Scheffersomyces stipitis* strains CBS 5773 and CBS 6054 with regard to their xylose metabolism: implications for xylose fermentation," *Microbiologyopen*, vol. 1, no. 1, pp. 64–70, Mar. 2012.
- [44] M. Papini, I. Nookaew, M. Uhlén, and J. Nielsen, "*Scheffersomyces stipitis*: a comparative systems biology study with the Crabtree positive yeast *Saccharomyces cerevisiae*," *Microb. Cell Fact.*, vol. 11, p. 136, Jan. 2012.
- [45] B. Hahn-Hägerdal and N. Pamment, "Microbial pentose metabolism." *Appl. Biochem. Biotechnol.*, vol. 113–116, pp.1207–1209, 2004.
- [46] I. Humphery-Smith and M. Hecker, *Microbial Proteomics: Functional Biology of Whole Organisms*. John Wiley & Sons, 2006, pp. 1–448.
- [47] M. Klimacek, S. Krahulec, U. Sauer, and B. Nidetzky, "Limitations in xylose-fermenting *Saccharomyces cerevisiae*, made evident through comprehensive metabolite profiling and thermodynamic analysis," *Appl. Environ. Microbiol.*, vol. 76, no. 22, pp. 7566–7574, Nov. 2010.
- [48] A. Toivola, D. Yarrow, and E. van den Bosch, "Alcoholic fermentation of D-xylose by yeasts," *Appl. Environ. Microbiol.*, vol. 47, no. 6, pp. 1221–1223, 1984.
- [49] K. Skoog, H. Jeppsson, and B. Hahn-Hägerdal, "The effect of oxygenation on glucose fermentation with *Pichia stipitis*," *Appl. Biochem. Biotechnol.*, vol. 34, no. 1, pp. 369–375, 1992.
- [50] J. C. du Preez, "Process parameters and environmental factors affecting D-xylose fermentation by yeasts," *Enzyme Microb. Technol.*, vol. 16, no. 11, pp. 944–956, 1994.
- [51] G. Trausinger, C. Gruber, S. Krahulec, C. Magnes, B. Nidetzky, and M. Klimacek, "Identification of novel metabolic interactions controlling carbon flux from xylose to ethanol in natural and recombinant yeasts," *Biotechnol. Biofuels*, vol. 8, p. 157, Jan. 2015.
- [52] S. B. Milne, T. P. Mathews, D. S. Myers, P. T. Ivanova, and H. A. Brown, "Sum of the parts: Mass spectrometry-Based metabolomics," *Biochemistry*, vol. 52, no. 22, pp. 3829–3840, 2013.
- [53] R. Ramautar, R. Berger, J. van der Greef, and T. Hankemeier, "Human metabolomics: strategies to understand biology," *Curr. Opin. Chem. Biol.*, vol. 17, no. 5, pp. 841–846, Oct. 2013.
- [54] O. Fiehn, "Metabolomics—the link between genotypes and phenotypes," *Plant Mol. Biol.*, vol. 48, pp. 155–171, 2002.
- [55] M. Oldiges, S. Lütz, S. Pflug, K. Schroer, N. Stein, and C. Wiendahl, "Metabolomics: current state and evolving methodologies and tools," *Appl. Microbiol. Biotechnol.*, vol. 76, no. 3, pp. 495–511, Sep. 2007.
- [56] S. Noack and W. Wiechert, "Quantitative metabolomics: a phantom?," *Trends Biotechnol.*, vol. 32, no. 5, pp. 238–244, Apr. 2014.
- [57] M. Klimacek, "Quantitative Metabolomics and Its Application in Metabolic Engineering of Microbial Cell Factories Exemplified by the Baker's Yeast," *Metabolomics*, InTech, 2012, pp. 19–44.
- [58] W. M. van Gulik, "Fast sampling for quantitative microbial metabolomics," *Curr. Opin. Biotechnol.*, vol. 21, no. 1, pp. 27–34, Mar. 2010.

- [59] A. B. Canelas, C. Ras, A. ten Pierick, J. C. van Dam, J. J. Heijnen, and W. M. van Gulik, "Leakage-free rapid quenching technique for yeast metabolomics," *Metabolomics*, vol. 4, no. 3, pp. 226–239, Jun. 2008.
- [60] S. G. Villas-Bôas, U. Roessner, M. A. E. Hansen, J. Smedsgaard, and J. Nielsen, *Metabolome Analysis: An Introduction*. John Wiley & Sons, 2006, pp. 1–319.
- [61] J. M. Büscher, S. Moco, U. Sauer, and N. Zamboni, "Ultrahigh Performance Liquid Chromatography - Tandem Mass Spectrometry Method for Fast and Robust Quantification of Anionic and Aromatic Metabolites," *Anal. Chem.*, vol. 82, no. 11, pp. 4403–4412, 2010.
- [62] W. Lu, M. F. Clasquin, E. Melamud, D. Amador-Noguez, A. A. Caudy, and J. D. Rabinowitz, "Metabolomic analysis via reversed-phase ion-pairing liquid chromatography coupled to a stand alone orbitrap mass spectrometer," *Anal. Chem.*, vol. 82, no. 8, pp. 3212–3221, Apr. 2010.
- [63] D. A. Volmer and L. L. Jessome, "Ion Suppression: A Major Concern in Mass Spectrometry," *LCGC*, vol. 24, no. 5, pp. 498–510, 2006.
- [64] J. M. Büscher, D. Czernik, J. Ewald, U. Sauer, and N. Zamboni, "Cross-Platform Comparison of Methods for Quantitative Metabolomics of Primary Metabolism," *Anal. Chem.*, vol. 81, pp. 2135–2143, 2009.
- [65] L. Wu, M. R. Mashego, J. C. van Dam, A. M. Proell, J. L. Vinke, C. Ras, W. A. van Winden, W. M. van Gulik, and J. J. Heijnen, "Quantitative analysis of the microbial metabolome by isotope dilution mass spectrometry using uniformly ^{13}C -labeled cell extracts as internal standards," *Anal. Biochem.*, vol. 336, no. 2, pp. 164–171, Jan. 2005.
- [66] A. B. Canelas, A. ten Pierick, C. Ras, R. M. Seifar, J. C. van Dam, W. M. van Gulik, and J. J. Heijnen, "Quantitative evaluation of intracellular metabolite extraction techniques for yeast metabolomics," *Anal. Chem.*, vol. 81, no. 17, pp. 7379–7389, Sep. 2009.
- [67] M. R. Mashego, L. Wu, J. C. van Dam, C. Ras, J. L. Vinke, W. A. van Winden, W. M. van Gulik, and J. J. Heijnen, "MIRACLE: mass isotopomer ratio analysis of U- ^{13}C -labeled extracts. A new method for accurate quantification of changes in concentrations of intracellular metabolites," *Biotechnol. Bioeng.*, vol. 85, no. 6, pp. 620–628, Mar. 2004.
- [68] L. Werzer, "Improving the yield and coverage of metabolites in the production of internal ^{13}C labeled standard used for absolute quantification of metabolic analysis," *Proj. Lab. Report*, pp. 1–26, 2013.
- [69] M. Kern, B. Nidetzky, K. D. Kulbe, and D. Haltrich, "Effect of Nitrogen Sources on the Levels of Aldose Reductase and Xylitol Dehydrogenase Activities in the Xylose-Fermenting Yeast *Candida tenuis*," *J. Ferment. Bioeng.*, vol. 85, no. 2, pp. 196–202, 1998.
- [70] C. F. Wahlbom, W. H. van Zyl, L. J. Jönsson, B. Hahn-Hägerdal, and R. R. Cordero Otero, "Generation of the improved recombinant xylose-utilizing *Saccharomyces cerevisiae* TMB 3400 by random mutagenesis and physiological comparison with *Pichia stipitis* CBS 6054," *FEMS Yeast Res.*, vol. 3, no. 3, pp. 319–326, May 2003.
- [71] P. M. Doran, *Bioprocess Engineering Principles*, 2nd ed. Elsevier Ltd, 2013, pp. 1–903.
- [72] D. W. Tempest, J. R. Norris, and M. H. Richmond, *Dynamics of microbial growth*, No. Bd. 7. John Wiley & Sons Australia, Limited, 1978, pp. 1–32.
- [73] S. A. Rounds, F. D. Wilde, and G. F. Ritz, "National Field Manual for the Collection of Water-Quality Data Chapter A6 Field Measurements Section 6.2 Dissolved oxygen," *U.S. Geol. Surv.*, pp. 1–59, 2013.
- [74] C. Fonseca, K. Olofsson, C. Ferreira, D. Runquist, L. L. Fonseca, B. Hahn-Hägerdal, and G. Lidén, "The glucose/xylose facilitator Gxf1 from *Candida intermedia* expressed in a xylose-fermenting industrial strain of *Saccharomyces cerevisiae* increases xylose uptake in SSCF of wheat straw," *Enzyme Microb. Technol.*, vol. 48, no. 6–7, pp. 518–525, May 2011.
- [75] S. Vaseghi, A. Baumeister, M. Rizzi, and M. Reuss, "In vivo dynamics of the pentose phosphate pathway in *Saccharomyces cerevisiae*," *Metab. Eng.*, vol. 1, no. 2, pp. 128–140, Apr. 1999.
- [76] J. M. Berg, J. L. Tymoczko, and L. Stryer, *Biochemistry*, 5th ed. W. H. Freeman, 2002, pp. 1–1050.

- [77] M. J. Brauer, J. Yuan, B. D. Bennett, W. Lu, E. Kimball, D. Botstein, and J. D. Rabinowitz, "Conservation of the metabolomic response to starvation across two divergent microbes," *Proc. Natl. Acad. Sci. U. S. A.*, vol. 103, no. 51, pp. 19302–19307, Dec. 2006.
- [78] G. H. Braus, "Aromatic Amino Acid Biosynthesis in the Yeast *Saccharomyces cerevisiae*: a Model System for the Regulation of a Eukaryotic Biosynthetic Pathway," *Microbiol. Rev.*, vol. 55, no. 3, pp. 349–370, 1991.
- [79] K. H. Roehm, "Electron Carriers: Proteins and Cofactors in Oxidative Phosphorylation," *eLS*, John Wiley & Sons, 2001, pp. 1–8.
- [80] D. E. Atkinson, "Energy charge of the adenylate pool as a regulatory parameter. Interaction with feedback modifiers," *Biochemistry*, vol. 7, no. 11, pp. 4030–4034, Nov. 1968.
- [81] K. M. Dombek and L. O. Ingram, "Intracellular Accumulation of AMP as a Cause for the Decline in Rate of Ethanol Production by *Saccharomyces cerevisiae* during Batch Fermentation," vol. 54, no. 1, pp. 98–104, 1988.
- [82] A. G. Chapman and D. E. Atkinson, "Adenine nucleotide concentrations and turnover rates. Their correlation with biological activity in bacteria and yeast," *Adv. Microb. Physiol.*, vol. 15, pp. 253–306, 1977.
- [83] W. J. Ball and D. E. Atkinson, "Adenylate energy charge in *Saccharomyces cerevisiae* during starvation," *J. Bacteriol.*, vol. 121, no. 3, pp. 975–82, Mar. 1975.
- [84] J. Henderson and A. R. P. Paterson, *Nucleotide metabolism: An Introduction*. Academic Press, 1973, pp. 1–322.
- [85] F. M. Thompson and D. E. Atkinson, "Response of nucleoside diphosphate kinase to the adenylate energy charge," *Biochem. Biophys. Res. Commun.*, vol. 45, no. 6, pp. 1581–1585, Dec. 1971.
- [86] A. Varma, E. B. Freese, and E. Freese, "Partial deprivation of GTP initiates meiosis and sporulation in *Saccharomyces cerevisiae*," *Mol. Gen. Genet. MGG*, vol. 201, no. 1, pp. 1–6, 1985.
- [87] J. R. Dickinson and M. Schweizer, *The Metabolism and Molecular Physiology of Saccharomyces cerevisiae*, 2nd ed. CRC Press, 2004, pp. 1–480.